

**Synthesis and Characterization  
of Cationic  
Spherical Polyelectrolyte Brushes**

**DISSERTATION**

Zur Erlangung des akademischen Grades  
eines Doktors der Naturwissenschaften (Dr. rer. nat.)  
im Fach Chemie der Fakultät für Biologie, Chemie und Geowissenschaften  
der Universität Bayreuth

vorgelegt von  
**Yu Mei**  
aus Hunan, VR China

**Bayreuth, 2005**

Die vorliegende Arbeit wurde in der Zeit von Juni 2001 bis Dezember 2003 am Polymer-Institut der Universität Karlsruhe (TH) durchgeführt und von Januar 2004 bis Juni 2005 am Lehrstuhl für Physikalische Chemie I der Universität Bayreuth fortgesetzt.

Vollständiger Abdruck der von der Fakultät für Biologie, Chemie und Geowissenschaften der Universität Bayreuth zur Erlangung des akademischen Grades eines Doktors der Naturwissenschaften genehmigten Dissertation.

Dissertation eingereicht am: 08.06.2005

Zulassung durch die Promotionskommission: 15.06.2005

Wissenschaftliches Kolloquium: 18.11.2005

Amtierender Dekan: Prof. Dr. O. Meyer

Prüfungsausschuss:

Prof. Dr. M. Ballauff (Erstgutachter)

Prof. Dr. A. H. E. Müller (Zweitgutachter)

Prof. Dr. G. Platz (Vorsitzender)

Prof. Dr. J. Breu

## Contents

<b>Chapter 1 Introduction</b> .....	3
1.1 Definition of Polymer Brush.....	3
1.2 Synthesis of Polymer Brushes.....	5
1.2.1 Physical Adsorption.....	6
1.2.2 “Grafting to” Technique.....	6
1.2.3 “Grafting from” Technique.....	7
1.3 Theory for Spherical Polymer Brushes.....	8
1.3.1 Kuhn Length of Polyelectrolyte.....	10
1.3.2 Excluded Volume of Polyelectrolyte.....	12
1.3.3 Ionic Strength inside Polymer Brushes.....	13
1.4 References.....	18
<b>Chapter 2 Overview of this Thesis</b> .....	20
2.1 Overview.....	20
2.2 Individual Contribution to Joint Publications.....	23
2.3 References.....	24
<b>Chapter 3 Publications</b> .....	25
3.1 Engineering the Interaction of Latex Spheres with Charged Surfaces: AFM Investigation of Spherical Polyelectrolyte Brushes on Mica.....	25
3.2 Effect of Counterions on the Swelling of Spherical Polyelectrolyte Brushes.....	30
3.3 Interaction of spherical polyelectrolyte brushes with CaCO <sub>3</sub> and cellulose fibers. Mechanistic studies and their application in papermaking.....	39
<b>Summary</b> .....	57
<b>Zusammenfassung</b> .....	60
<b>Appendix</b> .....	63
<b>Experiments and Methods</b> .....	63
1 Synthesis of SPB Latices.....	63

1.1 Chemicals.....	64
1.2 Synthesis of Photo Initiator HMEM.....	64
1.3 Synthesis of Anionic PS-co-HMEM Core Latices.....	65
1.4 Synthesis of Modified Anionic PS-co-HMEM Core Latices.....	65
1.5 Synthesis of Cationic PS-co-HMEM Core Latices.....	66
1.6 Preparation of SPB by Photo Polymerization.....	67
1.7 Purification of Latices.....	69
2 Characterization of SPB Latices.....	70
2.1 Determination of Particle Size Distribution of Latices.....	71
2.2 Cleavage of Polyelectrolyte Brushes Grafted on PS Cores.....	72
3 Instruments and Methods.....	73
3.1 Disc Centrifuge Photosedimentometer (DCP) .....	73
3.2 Transmission Electron Microscope (TEM) .....	75
3.3 Field Emission Scanning Electron Microscope (FESEM) .....	76
3.4 Atomic Force Microscope (AFM / SFM) .....	77
3.5 Dynamic Light Scattering (DLS) .....	80
3.6 Dynamic Drainage Jar (DDJ) .....	85
3.7 Other Instruments and Methods.....	87
4 Survey of the Experimental Data.....	87
5 References.....	88
<b>Glossary</b> .....	90
<b>Publications</b> .....	94
<b>Curriculum Vitae</b> .....	96
<b>Danksagung</b> .....	97
<b>Erklärung</b> .....	99

# Chapter 1

## Introduction

### 1.1 Definition of Polymer Brush

Polymer brushes can be described as polymer chains tethered on a surface or interface with a sufficient high grafting density that the chains are forced to stretch away from the tethering site [1]. Ever since the first seminal papers of de Gennes and Alexander on polymer brushes, the preparation, properties and application of tethered polymers chains have excited both fundamental science and application-oriented research [2, 3]. Polymer brushes have significantly different properties from bulk polymers. They have thus many potential applications in surface related technologies such as stabilization of colloids, improved biosurface protein-resistance, and generation of nano-scale patterned surfaces [4].

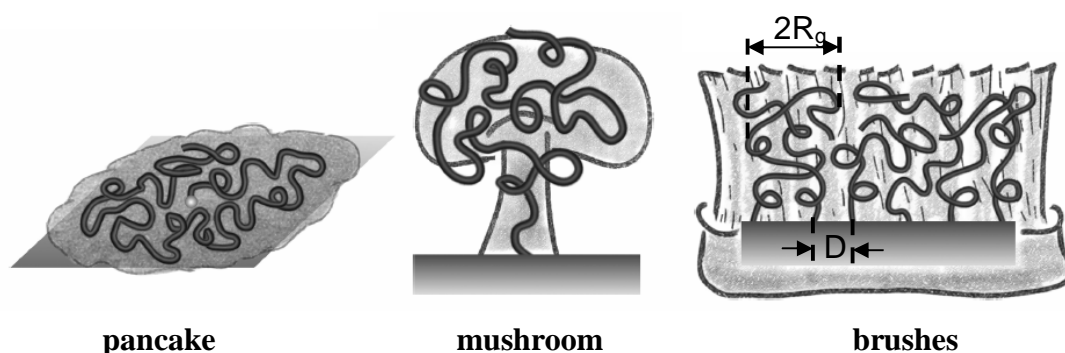


**Figure 1** Artist's perception of the terms “mushroom”, “pancake” and “brush” used for the different possible conformations of surface-attached polymers [5].

At low reduced grafting density, i.e., if the distance between two neighboring polymer chains ( $D$ ) is greater than the radius of gyration of free polymer chains ( $R_g$ ), two tethered chains feel no interaction. If polymer chains are poorly soluble in the solvent, it is favorable for them to lie flat on the surfaces. This is the so-called “pancake” conformation. Suspensions of such particles are not sterically stabilized. However, if polymer chains are well soluble in the solvent, they form a “mushroom” structure. Suspensions of particles with polymer chains assuming a “mushroom” conformation are usually unstable. Polymer chains stick together because of van der Waals attractions when they approach each other.

However, as the grafting density increases, the tethered polymer chains get more and more crowded and feel more and more interaction, and this forces the polymer chains into strongly stretched conformations due to steric constraints. If the average distance between two neighboring polymer chains is distinctly smaller than two times of gyration radius of polymer coils, the polymer molecules feel each other and stretch themselves away from the surfaces forming brush-like structures. The polymer layer is much thicker than in the other two cases and also larger forces are needed to compress the layer. Therefore particles in polymerically stabilized suspensions contain almost a brush-like layer.

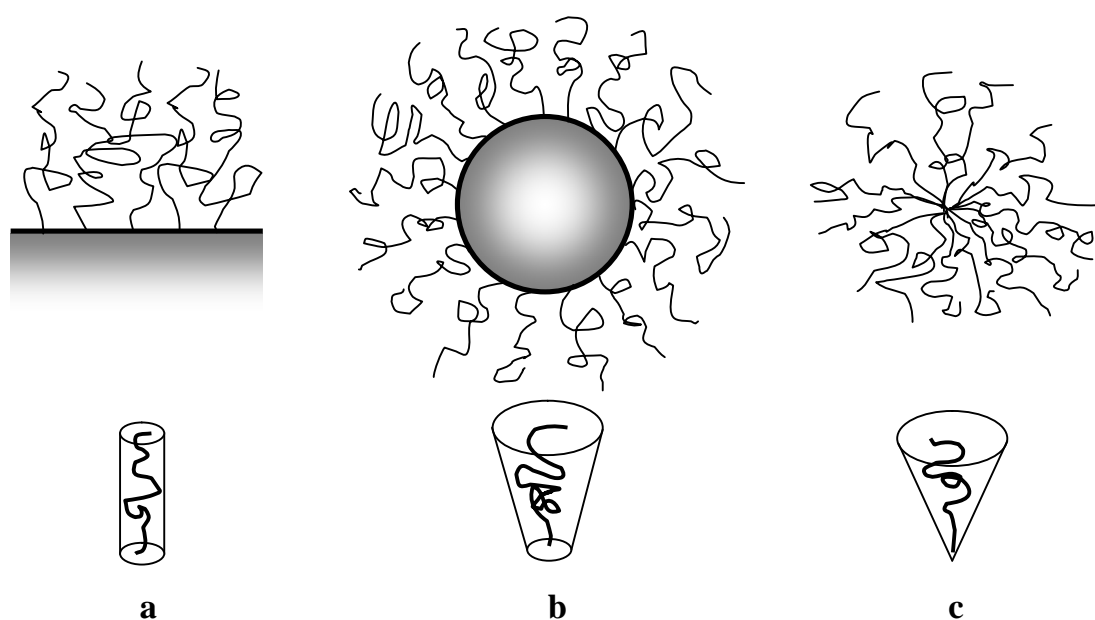


**Figure 2** The effect of substrate curvature. The average shape of the space a polymer molecule occupies in a layer depends on the curvature of the core surface. The shape is cylindrical for a giant core (planar surface) and becomes conical when core reduces to a point curvature [6].

- a) Planar polymer brush;
- b) Spherical polymer brush;
- c) Star-polymer.

Besides the grafting density and the solvent quality, the curvature of the surface is also important. The average lateral distance between polymer chains grafted on a flat surface is independent of the distance from the surface. This is in contrast to strongly curved substrate surfaces, that is, with a curvature radius comparable to the polymer layer thickness, which is demonstrated in figure 2. Due to the curvature the lateral distance between the molecules close to the core is much smaller than at the periphery

of the particle. The average shape of the space that a molecule occupies is thus a function of the curvature. It is cylindrical for polymers at flat surfaces and it becomes conical when the radius of curvature goes to zero. This has important implications for the structure of the polymer layer. This can be demonstrated by comparing two suspensions that consist of particles with different core radius but with molecules of the same molecular weight and the same number of molecules per area. The polymer layer of the particles with the larger core is thicker than the one on the particle with the smaller core [6].

When polyelectrolyte chains are densely grafted on a planar surface, planar polyelectrolyte brushes (PPB) are formed. Electrostatic interactions between polyelectrolyte chains and the osmotic pressure can become the dominant force in this case. This fact is clear to see for the limiting case of the so-called osmotic brush- that is for a polyelectrolyte brush in the absence of added salt. Star-polymers consist of polymer chains (arms) of equal length that are joined at a central “branching point”. It will not be further discussed since it is not the interest of this study. Grafting linear polyelectrolyte chains densely to colloidal core latex particles leads to spherical polyelectrolyte brushes (SPB) [5, 7, 8]. Spherical latex particles are equally interesting from the viewpoint of fundamental colloid science. Since the particles have typical diameters of a few 100 nm only, the entire surface created by a few grams of polymer may be of the order of 100 m<sup>2</sup>. Hence, the properties of the suspension such as its stability or its flow behaviour are almost fully determined by the surface of the particles. Latex suspensions are therefore good model systems for the study of surface-related problems such as the adsorption of proteins to surfaces [9, 10]. At the same time the stability and the resistance to coagulation of the particles can be modified by suitable surface layers [11, 12]. Furthermore, the specific surface area and cation exchange capacity of latex particles can evidently be enlarged by attached polyelectrolyte brushes. The grafting density, charge density and particle size can easily be varied by different synthesis conditions.

## **1.2 Synthesis of Polymer Brushes**

In recent years, the synthesis of polymer brushes has received significant attention, due to their unique properties and application possibilities, such as adhesion [13], lubrication [14], wettability [15], friction [16] and biocompatibility [17] etc.

Polymer brushes are typically synthesized by two different methods, physisorption and chemical bonding. The chemical bonding of polymer brushes can further be classified as “grafting to” and “grafting from” techniques.

### 1.2.1 Physisorption

Typically, polymer brushes synthesized using a physisorption approach consists of two-component polymer chains, where one part strongly adheres to the interface and the second part extends to generate the polymer layer [18]. This tethering point can be a single point, in the case of a functionalized polymer chain, or a diblock-copolymer chain. However, the interaction between polymer brushes and surface is mostly caused by van der Waals forces or hydrogen bonding. Brush layers are thus thermal and solvolytic instable due to desorption or displacement by other polymer or small molecules. The polyelectrolyte brushes have been prepared mostly by physical adsorption of block copolymers containing polyelectrolyte blocks [19, 20] or by micellization of the block copolymers [21, 22]. But for micellar systems, it is difficult to obtain a sharp core-corona interface, and the aggregation number can be influenced by free chains in solution. In the case of physical adsorption, the amount of adsorbed polyelectrolytes is controlled by the charge density of the polymer, the sign of the surface charge and the ionic strength of the solution [23, 24]. The electrostatic repulsion opposes the accumulation of polyelectrolytes at the surface, besides the possibility of desorption. Therefore, the grafting density obtained by this method is relative low and can be poorly controlled. This problem can partially be overcome by decreasing the electrostatic interaction by adding salt. But some other disadvantages may be brought by the addition of salt, such as strong desorption in the case of physisorption and unexpectedly by-reactions by chemisorption.

### 1.2.2 “Grafting to” Technique

A much stronger bonding between polymer chains and substrate can be achieved by the “grafting to” technique [13, 25, 26]. A preformed macromolecule possessing a suitable end-functionality with a reactive substrate is utilized to generate the polymer brush in the “grafting to” technique. The synthesis of the polymer chains has been performed using several techniques such as anionic, cationic, living free radical, and ring-opening metathesis polymerization. These techniques in particular allow the facile conversion of the chain ends to any number of desired functionalities (hydroxyl, carboxyl, amino, thiol, etc.). The polymerization methods also present advantage of synthesizing polymer chains possessing narrow molecular weight distributions, which allows a uniform brush layer thickness [5]. The substrate surface also plays an important role in

the synthesis of the polymer brush layers. Silica and gold surfaces possess surface functionalities that can undergo condensation reactions with polymer chains containing thiol, hydroxyl, and carboxyl functionalities. Furthermore, these and other surfaces can be modified by the use of self-assembled monolayers (SAMs) and other coupling agents to introduce various other surface functionalities.

Mir et al. prepared polyelectrolyte brushes of poly(sodium styrenesulfonate) using the “grafting to” technique for the first time [28]. They immobilized perdeuterated PS chains, which had been functionalized with a reactive monochloro- or trichlorosilane end group, to the surface of porous silica. The PS chains were sulfonated subsequently with  $\text{SO}_3$  and turned into PNaSS. However, this route is confronted with several difficulties, such as the harsh conditions for sulfonation, and the incomplete sulfonation. The degree of ionization is not easy to control exactly. Such a “grafting to” approach is generally limited as only moderate molecular weight polymers can be used. The anchor groups in polymer chains with high molecular weight are more difficult to reach the surface. The disadvantage of this technique is that it often leads to low grafting densities and low film thickness, as the polymer molecules must diffuse through the existing polymer film to reach the reactive sites on the surface [28].

### 1.2.3 “Grafting from” Technique

Steric hindrance for surface attachment increases as the thickness of tethered polymer film increases in the case of “grafting to”. To overcome this problem, the “grafting from” approach can be used and has generally become the most attractive way to prepare dense, covalently tethered polymer brushes with a high grafting density [15, 29-31]. The “grafting from” technique involves the immobilizing of initiators onto the substrate followed by in situ surface initiated polymerization to generate the tethered polymer brush. Surface immobilized initiators can be generated by either treating the substrate with plasma or glow discharge in the presence of a gas [32] or attaching initiator containing self-assembled monolayers on the substrates [33]. As the chains are growing from the surface, the only limit to propagation is diffusion of monomer to the chain ends, thus resulting in thick tethered polymer brushes with high grafting density.

Unlike the situation in the “grafting to” technique, the substrate surface must be modified to generate the initiator functionality suitable for the polymer brush synthesis from a surface in the “grafting from” technique. This surface modification can be performed using Langmuir-Blodgett techniques or SAM deposition. Furthermore,

depending on the polymerization method, the initiator can be a free radical, ionic, ring-opening metathesis, or controlled radical polymerization type. By varying the substrate (gold, silicon, nanoparticles, etc.), initiator deposition technique, and polymer synthesis route, virtually limitless possibilities present themselves for brush formation.

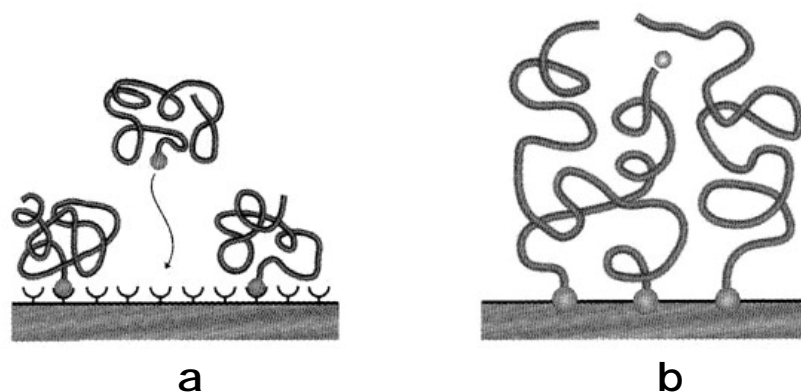


**Figure 3** Schematic illustration of different processes used for the attachment of polymers to surfaces [5]:

(a) “Grafting to” technique: The steric hindrance for surface attachment rises with increase of the thickness of tethered polymer film.

(b) “Grafting from” technique: All polymer chains grow simultaneously without steric hindrance.

The “grafting from” technique can be also used to synthesize polyelectrolyte brushes. Biesalski et al. have reported a preparation of polyelectrolyte brushes growing in situ on a planar silicon oxide surface for the first time [34]. At first, an azo radical chain initiator containing a monochlorosilane group was immobilized onto a planar silicon oxide surface by the chemical reaction between the hydroxyl group of substrate and the monochlorosilane group. The reaction was carried out in dry toluene at room temperature under argon for about 15 hours. Then, 4-vinylpyridine was polymerized in benzene or ethanol at 60 °C in Schlenk tubes initiated by the surface attached azo initiator. At last, poly(4-vinylpyridine) was quarternized by *n*-butylbromide in nitromethane at 65 °C to yield a poly(4-vinyl-*N*-*n*-butylpyridinium) bromide brush. Using this “grafting from” technique, the grafting density and molecular weight of the polyelectrolyte brushes can be easily controlled by adjusting the polymerization conditions.

### 1.3 Theory for Spherical Polyelectrolyte Brushes

Polymer brushes can be classified in planar brushes and spherical brushes according to geometries of substrate, neutral brushes and charged brushes according to their charges. During the last decades, several theoretic models for systems with neutral or charged polymer chains were developed by many authors [35-37, 20]. In the following, the modified Daoud-Cotton model will be introduced.

The geometry of the substrate surface may affect the behavior of polyelectrolyte brushes [38-40]. When a planar polyelectrolyte brush is bent to a spherical brush, the excluded volume interactions decrease as the volume occupied per chain increases with distance from the grafted surface. The chain density also decreases along the direction against the core surface. Hence, the counterion distribution and the local degree of ionization  $\alpha$  in the case of an annealed brush become functions of the distance from the grafting surface [41].

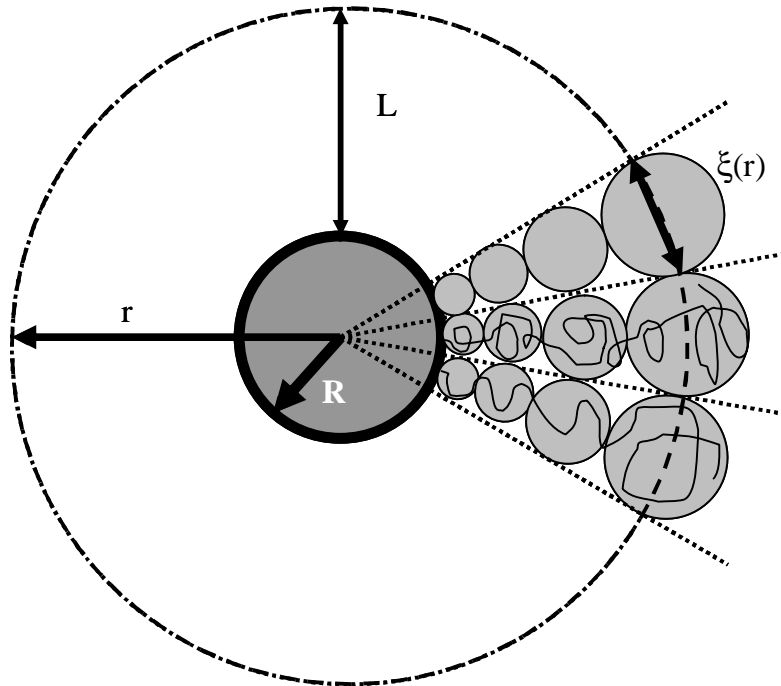


**Figure 3** Blob model for grafted polymer chains of thickness  $L$  on a sphere with core radius  $R$ .

For polyelectrolyte brushes a notable effect of the geometry of the surface on the scaling exponents in the neutral brush regime and salted brush regime will be expected due to the excluded volume interactions. While in the osmotic brush regime, there is a universal expression for the brush thickness independent of the brush morphology because the short-range steric hindrance becomes less important

compared with the long-range electrostatic interactions. In almost all geometries, the annealed polyelectrolyte brushes can exhibit a non-monotonic dependence of the brush thickness on the grafting density and salt concentration [42].

A suitable approach for spherical polyelectrolyte brushes is given by the modified Daoud-Cotton model [37] developed by Hariharan *et al.* [20, 43] to treat charged systems. In this model the spherical polyelectrolyte brushes are described by a sphere of radius  $R$  onto which linear chains are grafted with a grafting density  $\sigma$ . The average distance between the chains is much smaller than the contour length of the chains [20, 43], as shown in Figure 3.

### 1.3.1 Kuhn Length of Polyelectrolyte

According to OSF theory [44, 45], the local chain stiffening for polyelectrolyte arises from both steric hindrances and electrostatic repulsions. The former depends primarily on the molecular structure and determines the intrinsic persistence length ( $l_{p,0}$ ), and the latter, which is called the electrostatic persistence length ( $l_{p,e}$ ), is a function of the ionic strength and sometimes dominates the chain stiffness. Therefore, for neutral chains

$$l_p = l_{p,0}$$

While for charged chains the total persistence length

$$l_p = l_{p,0} + l_{p,e}$$

The range of the Coulombic repulsive interaction can be described by the Debye length  $k^{-1}$ , a screening length giving a measure of the range of the potential around a point charge. In an electrolyte solution the Debye length is given by:

$$k^{-1} = \left( \frac{\epsilon_0 \epsilon k T}{2 N_A e^2 I} \right)^{\frac{1}{2}} \quad (1)$$

where  $e$  denotes the elementary charge,  $\epsilon_0$  the dielectric constant of the solvent,  $\epsilon$  the dielectric constant of the solution,  $k$  Boltzmann constant,  $I$  the ionic strength,  $N_A$  the Avogadro constant, and  $T$  the temperature of electrons.

From the OSF theory [44, 45], one obtains the persistence length:

$$l_p = \frac{1}{4l_c k^{-2}} \quad (2)$$

where  $l_c$  is the distance between two charged points along the polymer chain.

According to the Manning condensation theory [46], when  $l_c < l_B$ , the counterions will condense on the backbone of the polyelectrolyte chain, and the charges are no longer effective. For charges spaced out farther than  $l_B$ , no condensation occurs. The brushes employed in our investigation are made of PAA and PNaSS, in which  $l_c = 0.252$  nm ( $l_c < l_B$ ). So  $l_c$  is replaced by  $l_B$ . Thus, equation (2) becomes [44]:

$$l_p = \frac{1}{4l_B k^{-2}} \quad (3)$$

When the real polyelectrolyte chain is replaced by an equivalent chain of  $N_k$  Kuhn statistical segments, each of length  $l_k$ , the same definition as for the persistence length can be made:

$$l_k = l_{k,0} = \frac{\langle R^2 \rangle}{L_c}$$

where  $l_{k,0}$  denotes the intrinsic Kuhn length, which only depends on the structural stiffness of the segments of polymer chains and can be considered as constant.  $\langle R^2 \rangle$  is the mean square end-to-end distance.

A second characteristic length for charged polymer is the Bjerrum length  $l_B$ , which is defined as the distance at which the Coulomb interaction between two unscreened elementary charges is equal to the thermal energy, i.e.

$$l_B = \frac{e^2}{4\pi\epsilon_0 ekT} \quad (4)$$

For electrolyte in water at 25 °C,  $l_B = 0.714$  nm. The relationship between the Debye length  $k^{-1}$  and the Bjerrum length  $l_B$  is given by:

$$k = \sqrt{8pl_B I} \quad (5)$$

For charged chains the total Kuhn length

$$l_k = l_{k,0} + l_{k,e} \quad (6)$$

where  $l_{k,e}$  denotes the electrostatic Kuhn length, which represents the contribution of electrostatic interaction to the chain stiffness. Substituting equation (3) and (5) into equation (6) the Kuhn length can be expressed as

$$l_{k,e} = \frac{1}{2l_B k^{-2}} \quad (7)$$

For the sake of simplicity, the treatment of Pincus [47] can be adopted in which only electrostatic interactions are considered. Thus

$$l_k \propto \frac{1}{l_B k^{-2}} \quad (8)$$

In a different model, Barrat and Joanny [48] used a variational theory to calculate the electrostatic persistence length for flexible chains. These authors found

$$l_p \propto k^{-1}$$

The Kuhn length therefore becomes

$$l_k \propto k^{-1} \quad (9)$$

### 1.3.2 Excluded Volume of Polyelectrolyte

Assuming the electrostatic repulsion to be the major effect on the conformation of polyelectrolytes, the excluded volume of polyelectrolyte can be estimated solely by considering the electrostatic contributions. Therefore, the excluded volume can adopt the simple scaling form of the electrostatic wormlike chain theory in which the electrostatic contribution is given by the excluded volume between two cylinders of length  $l_p$  and an effective repulsive diameter of the  $k^{-1}$  [44, 49-51]. Then

$$v \propto l_p^2 k^{-1}$$

namely

$$v \propto l_k^2 k^{-1} \quad (10)$$

Argillier and Tirrell [52] described the chain as a succession of segments of size  $l_p$ , which can be characterized by an excluded volume

$$v = l_p^3$$

Using the concept of the Kuhn segment, one obtains at once

$$v \propto l_k^3 \quad (11)$$

Pincus treated the effective excluded volume per segment of polyelectrolyte as follows [47]:

$$v = 4pl_B k^{-2}$$

or

$$v \propto l_B k^{-2} \quad (12)$$

Hence, the electrostatic excluded volume is modeled as a cylinder of length  $l_B$  and radius  $k^{-1}$ .

### 1.3.3 Ionic Strength inside Polymer Brushes

It is evident that all of the expressions of both Kuhn length  $l_k$  and excluded volume parameter  $v$  depend on ionic strength via the Debye length  $k^{-1}$ . As shown by equation (1), the Debye length depends on the local ionic strength within a blob in the brush which may obviously differ from that in the bulk at low salt concentration due to the Donnan effect. In the following the calculation of the local ionic strength in the brush will be discussed.

Let us consider the Donnan equilibrium between the polyelectrolyte brush layer and the solution in the case of quenched brush of PNaSS in NaCl solution. The original ionic strength of PNaSS inside the brush is assumed to be  $c_1$  and that of NaCl in solution is  $c_2$ . When the system reaches the Donnan equilibrium, inside the brush the concentrations of ions become:

$$\begin{aligned} [\text{PSS}^-] &= c_1 \\ [\text{Na}^+] &= c_1 + x \\ [\text{Cl}^-] &= x \end{aligned}$$

while in the bulk solution:

$$\begin{aligned} [\text{Na}^+] &= c_2 - x \\ [\text{Cl}^-] &= c_2 - x \end{aligned}$$

At equilibrium we have [53]:

$$(c_1 + x)x = (c_2 - x)^2$$

or

$$x = \frac{c_2^2}{c_1 + 2c_2}$$

Then, the ionic strengths inside  $c_s$  and outside the brush  $c_a$  can be expressed as

$$\frac{c_s}{c_a} = 1 + \frac{c_1}{c_2} \quad (13)$$

Therefore, the local ionic strength inside the brush  $c_s$  is always higher than that in the bulk  $c_a$ . The smaller the added salt concentration  $c_2$  is, the greater will be the deviation of  $c_s$  from  $c_a$ .

Assumed a Donnan equilibrium between the brush layer and the solution (Figure 4), Hariharan *et al.* [20] proposed a simple model to calculate the ionic strength in the brush  $c_s$ , in which the charge density and electrostatic potential in the brush are treated as uniform, and the brush as electrically neutral.

The volume-averaged fixed charge density in the brush is defined as

$$\overline{r_v} = \frac{1}{V} \int_V r_v dV = \frac{3eR^2 s L_c}{l_c [(R+L)^3 - R^3]} \quad (14)$$

where  $e$  denotes the unit charge,  $l_c$  the distance between two charge groups along the polyelectrolyte chain. As discussed above we chose  $l_c = l_B = 0.714$  nm (25 °C, in water) according to the counterion condensation theory [46].

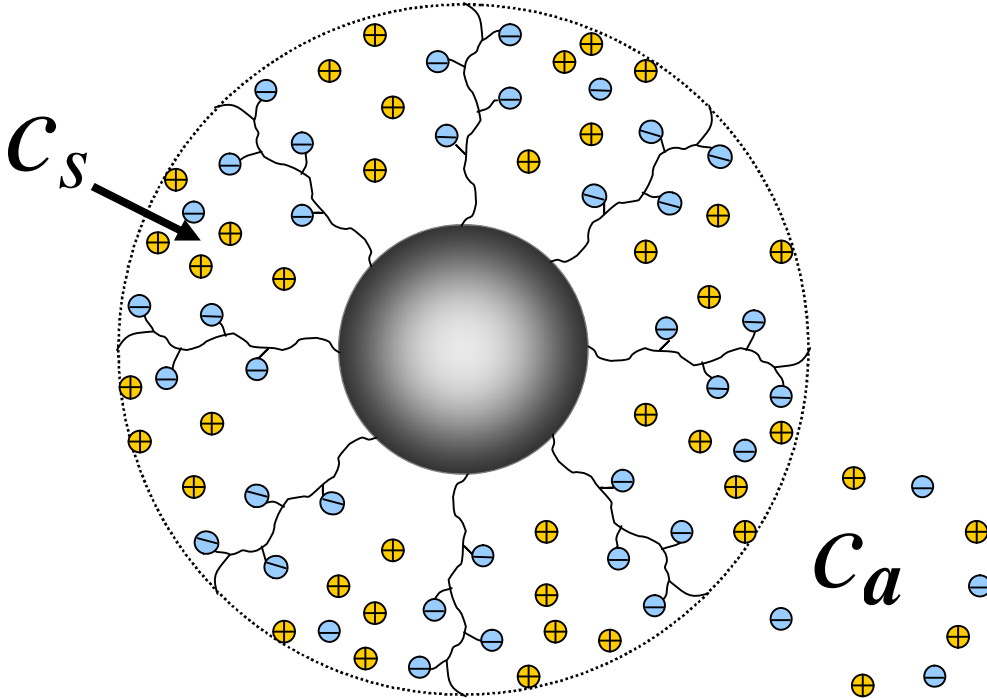


**Figure 4** Donnan equilibrium between the brush layer and the solution outside, where  $c_s$  is the local ionic strength inside brushes,  $c_a$  the ionic strength of the system.

The electrically neutral treatment implies that the negative charge in the chain should be equal to the positive charge from the counterions:

$$\overline{r_v} = -\sum_i e z_i n_i \quad (15)$$

where  $z_i$  is the valence of the ions,  $n_i$  the concentrations of the ions of species  $i$  in the brush, which can be related to the concentration of the ions in the bulk  $n_i^0$  using the Boltzmann distribution

$$n_i = n_i^0 \exp\left(-\frac{ez_i \bar{j}}{kT}\right)$$

where  $\bar{j}$  is the mean electrostatic potential,  $k$  the Boltzmann constant,  $T$  the absolute temperature. For symmetric electrolyte there are:

$$z_+ = -z_- = z$$

and

$$n_+^0 = n_-^0 = n^0$$

Thus equation (15) can be rewritten as:

$$\bar{r}_v = ezn^0 \left[ \exp\left(\frac{ez\bar{j}}{kT}\right) - \exp\left(-\frac{ez\bar{j}}{kT}\right) \right] \quad (16)$$

which has the solution

$$\exp\left(-\frac{ez\bar{j}}{kT}\right) = \left[ 1 + \left( \frac{\bar{r}_v}{2ezn^0} \right)^2 \right]^{\frac{1}{2}} - \frac{\bar{r}_v}{2ezn^0} \quad (17)$$

Using equation (14), (16) and (17), the ionic strength in the brush can be rewritten as:

$$c_s = \frac{1}{2} \sum_i \frac{n_i z_i^2}{N_A} = \frac{n^0 z^2}{N_A} \left[ 1 + \left( \frac{\bar{r}_v}{2ezn^0} \right)^2 \right]^{\frac{1}{2}} = c_a \left[ 1 + \left( \frac{z\bar{r}_v}{2eN_A c_a} \right)^2 \right]^{\frac{1}{2}} \quad (18)$$

where  $N_A$  is the Avogadro's number,  $c_a$  the ionic strength of added symmetric salt. Substituting equation (8) into (12), the ionic strength in the brush can be calculated from the concentration of added salt as:

$$c_s = c_a \left[ 1 + \frac{3z_s L_c}{2N_A c_a l_B R \left[ \left( 1 + \frac{L}{R} \right)^3 - 1 \right]} \right]^2 \right]^{\frac{1}{2}} \quad (19)$$

Hariharan *et al.* [20] followed Pincus in ignoring the local chain stiffening [47] but modified the excluded volume for interacting polyelectrolyte segments to the form derived by Odijk *et al.* [44]. The Daoud-Cotton model for a spherical polyelectrolyte brush reduces to [41]:

$$\left( \frac{L}{R} + 1 \right)^{\frac{5}{3}} = 1 + k \frac{L_c}{R} \left( \frac{l_k S}{k} \right)^{\frac{1}{3}} \quad (20)$$

A detailed discussion of equation (20) and its possible limitations were given by Hariharan, Biver and Russel [20]. It provides a good description for experimental data in case of neutral brushes [20, 43]. Moreover, it can be used for spherical polyelectrolyte brushes in the presence of high concentrations of added salt, that is, if the electrostatic interaction between the segments is strongly screened [20, 54, 55].

Following the suggestion of Hariharan *et al.*, equation (20) may be rearranged by elementary steps to yield [20]

$$\left( \frac{v}{l_k l^2} \right)^{1/3} \approx \frac{R}{L_c (l^2 S)^{1/3}} \left[ \left( \frac{L}{R} + 1 \right)^{5/3} - 1 \right] \quad (21)$$

if the constant  $k$  is equated to unity. Here  $l$  is the bare Kuhn length of the respective polyelectrolyte chains. For a high ionic strength,  $l_k = l$  and the reduced excluded-volume parameter  $v/l^3$  can be obtained directly from experimental data by use of equation (21). For low ionic strength,  $v$  and  $l_k$  depend on  $c_a$  and the evaluation of the data must include this effect.

The above-mentioned modified Daoud-Cotton model by Hariharan *et al.* [20] will be used in the Chapter 3.2 to evaluate swelling behavior of anionic and cationic SPB in different salt solutions.

## 1.4. References

1. Milner, S.T., *Science*, **1991**, *251*, 905-914.
2. Alexander, S., *J. Phys. France*, **1977**, *38*, 983.
3. de Gennes, P.G.; *Scaling Concepts in Polymer Physics*, **1979**, Cornell University Press, Ithaca, New York.
4. Habicht, J.; Schmidt, M.; Rhe, J.; Johannsmann, D., *Langmuir*, **1999**, *15*, 2460-2465.
5. Rhe J. *et al.*, *Adv. Polym. Sci.*, **2004**, *165*, 79.
6. Nommensen P.A., *Rheology of Polymer Coated Particle Suspension*, **2000**, University of Twente, Enschede.
7. Ballauff, M., *Macromol. Chem. Phys.*, **2003**, *204*, 220-234.
8. Ballauff, M., *Polymer Brushes*, **2004**, edited by K. Caster, Wiley-VCH, Weinheim.
9. Horbett, T.A.; Brash, J.L., *Proteins at Interfaces II, ACS Symposium Series 602*, **1995**, American Chemical Society, Washington DC.
10. Wittemann, A.; Haupt, B.; Ballauff, M., *Phys. Chem. Chem. Phys.*, **2003**, *5(8)*, 1671.
11. Russel, W.B.; Saville, D.A.; Schowalter, W.R., *Colloidal Dispersions*, **1989**, Cambridge University Press, Cambridge.
12. Napper, D.H., *Polymeric Stabilization of Colloidal Dispersions*, **1983**, Academic Press: London.
13. Norton, L.J.; Smiglova, V.; Pralle, M.U.; Hubenko, A.; Dai, K.H.; Kramer, E.J.; Hahn, S.; Begrlund, C.; Dekoven, B., *Macromolecules*, **1995**, *28*, 1999.
14. Uyama, Y.; Tadokoro, H.; Ikada, Y., *J. Appl. Polym. Sci.*, **1990**, *39*, 489.
15. Luzinov, I.A.; Voronov, S.A.; Minko, S.S.; Kraus, R.; Wilke, W.; Zhuk, A., *J. Appl. Polym. Sci.*, **1996**, *61*, 1101.
16. Leger, L.; Raphael, E.; Hervet, H., *Adv. Polym. Sci.*, **1999**, *138*, 185.
17. Kulik, E.; Ikada, Y., *J. Biomed. Mater. Res.*, **1996**, *30*, 295.
18. Belder, G. F.; ten Brinke, G.; Hadziioannou, G., *Langmuir*, **1997**, *13*, 4102-4105.
19. Biver, C.; Hariharan, R.; Mays, J.; Russel, W.B., *Macromolecules*, **1997**, *30*, 1787.
20. Hariharan, R.; Biver, C.; Mays, J.; Russel, W.B., *Macromolecules*, **1998**, *31*, 7506.
21. Marko, J.F.; Rabin, Y., *Macromolecules*, **1992**, *25*, 1503.
22. Wittmer, J.; Joanny, J.F., *Macromolecules*, **1993**, *26*, 2691.
23. Cohen Stuart, M.A.; Fleer, G.J.; Lyklema, J.; Norde, W.; Scheutjens, J.M.H.M., *Adv. Colloid Interface Sci.*, **1991**, *34*, 477.

24. Cohen Stuart, M.A., *J. Phys. (Paris)*, **1988**, 49, 1001.
25. Mansky, P.; Liu, Y.; Huang, E.; Russell, T.P.; Hawker, C.J., *Science*, **1997**, 275, 1458.
26. Luzinov, I.; Julthongpiput, D.; Malz, H.; Piontech, J.; Tsukruk, V.V., *Macromolecules*, **2000**, 33, 1043.
27. Mir, Y.; Auroy, P.; Auvray, L., *Phys. Rev. Lett.*, **1995**, 75, 2863.
28. Boyes, S.G.; Granville, A.M.; Baum, M.; Akgun, B.; Mirous, B.K.; Brittain W.J., *Surface Science*, **2004** 570, 1-12.
29. Meier, L.P.; Shelden, R.A.; Caseri, W.R.; Suter, U.W., *Macromolecules*, **1994**, 27, 1637.
30. Uchida, E.; Ikada, Y., *Macromolecules*, **1997**, 30, 5464.
31. Zhao, B.; Brittain, W.J., *Prog. Polym. Sci.*, **2000** 25 , 677.
32. Ito, Y.; Ochiai, Y.; Park, Y.S.; Imanishi, Y., *J. Am. Chem. Soc.*, **1997** 119, 1619.
33. Prucker, O.; Rhe, J., *Macromolecules*, **1998** 31, 592-602.
34. Biesalski, M.; Rhe, J.; Johannsmann, D., *J. Chem. Phys.*, **1999**, 111, 7029.
35. Alexander, S., *J. Phys. France*, **1977**, 38, 983.
36. de Gennes, P.G., *Macromolecules*, **1980** 13, 1069.
37. Daoud, M.; Cotton, J.P., *J. Phys. Paris*, **1982**, 43, 531.
38. Ross, R.; Pincus, P.A, *Macromolecules*, **1992**, 25, 2177.
39. Misra, S.; Mattice, W. L.; Napper, D. H., *Macromolecules*, **1994**, 27, 7090.
40. Zhulina, E.B.; Borisov, O.V.; Birshtein, T.M., *Macromolecules*, **1999**, 32, 8189.
41. Guo, X., *Synthesis and Study of the Colloidal Polyelectrolyte Brushes prepared by Photo-emulsion Polymerization*, **2001**, Logos Verlag Berlin.
42. Zhulina, E.B.; Borisov, O.V., *Macromolecules*, **1996**, 29, 2618.
43. Biver, C.; Hariharan, R.; Mays, J.; Russel, W.B., *Macromolecules*, **1997**, 30, 1787.
44. Odijk, T., *J. Polym. Sci., Polym. Phys. Ed.*, **1977**, 15, 477.
45. Skolnick, J; Fixman, M., *Macromolecules*, **1977**, 10, 944.
46. Manning, G.S., *J. Chem. Phys.*, **1969**, 51, 924.
47. Pincus, P., *Macromolecules*, **1991**, 24, 2912.
48. Barrat, J.L.; Joanny J.F., *Europhys. Lett.*, **1993**, 24, 333.
49. Fixman, M.; Skolnick, J., *Macromolecules*, **1978**, 11, 863.
50. Fixman, M., *J. Chem. Phys.*, **1990**, 92, 6283.
51. Davis, R.M.; Russel, W.B., *J. Polym. Sci., Polym. Phys. Ed.*, **1996**, 24, 511.
52. Argillier, J.F.; Tirrell, M., *Theoretica Chimica Acta*, **1992**, 82, 343.
53. Donnan, F.G., *Z. Elektrochem.*, **1911**, 17, 572.
54. Guo, X.; Ballauff, M., *Langmuir*, **2000**, 16, 8719.
55. Guo, X.; Ballauff, M., *Phys. Rev. E*, **2001**, 64, 051406.

## Chapter 2

# Overview of this Thesis

### 2.1 Overview

Polyelectrolyte brushes consist of polyelectrolyte chains attached to planar or curved surfaces. They have in the past decade been recognized as an exciting state of matter and attracted much attention [1]. The combination of short-range steric force, long-range electrostatic interactions, and conformational effects has yielded a large variety of predicted brush regimes in theoretical studies [2-10]. Compared to the advanced theoretical understanding of brushes, the number of experimental studies devoted to spherical polyelectrolyte brush system is much smaller [11-14]. A comprehensive study of anionic spherical polyelectrolyte brushes has recently been presented by Guo *et al.* [15-18]. These workers investigated anionic spherical polyelectrolyte brushes by dynamic light scattering and so on. Their results demonstrate that the entire set of brush length  $L$  as a function of core radius  $R$ , contour length  $L_c$ , and grafting density  $S$  can be fully explained in terms of a simple two-parameter theory developed by Hariharan *et al.* [19].

To achieve a better understanding of spherical polyelectrolyte brush system and study the effect of different charges on surface-particle interaction the method developed by Guo *et al.* [20] was modified to synthesize cationic SPB latex consisting of a poly(styrene) (PS) core and poly((2-(acryloyloxy)ethyl)-trimethylammonium chloride) (PATAC) brushes. The cationic SPB was characterized by methods such as transmission electron microscopy (TEM), dynamic light scattering (DLS), atomic force microscopy (AFM) and disc centrifugation (DCP). In order to obtain deeper insight into the interaction of spherical polyelectrolyte brushes with  $\text{CaCO}_3$  particles and cellulose fibers, cationic and anionic SPB were tested as dual retention-aid in papermaking. This thesis includes three publications which are presented in chapter 3, and is mainly related to the synthesis, characterization of cationic SPB, and all of their behaviors were compared with that of anionic SPB.

The interaction of charged SPB with negatively charged mica surfaces investigated by AFM was introduced in chapter 3.1. Anionic and cationic SPB exhibited totally different behavior on charged mica surfaces. It was demonstrated that the negative SPB forms two-dimensional aggregates of densely packed polymer particles, which can be explained by a particle-particle interaction dominating the repulsive interaction

of the particles with the substrate. While the cationic SPB exhibits a completely different particle-surface interaction behavior as expected. Network-like structure films of dried particles without long-range 2D order are formed due to the strong attractive particle-surface interaction of positively charged polyelectrolyte chains. The cationic polymer chains spread over the negative surface and anchor the particles. Hence, a shell of polyelectrolyte chains could be a highly efficient tool of adjusting the interaction of colloidal particles with charged solid substrates.

In chapter 3.2 the effect of ionic strength on swelling behavior of SPB was studied by DLS. The ionic strength of the whole system or inside brushes can be changed by adding of mono- and divalent counterions, which will lead to a strong shrinkage of the surface layer of the polyelectrolyte brushes. The interaction of the counterions with the cationic and the anionic brush layers may be classified as follows: At lowest ionic strength electrostatic interaction prevails and the brush layer is swollen in all cases by the osmotic pressure of the counterions. Intermediate salt concentrations lead to a partial screening of the electrostatic interaction and to a shrinkage of the brush layer. This effect can be well captured by the theory of Hariharan *et al.* [19]. In case of cationic brushes, however, the shrinkage becomes very pronounced around salt concentrations of 0.1 mol/l. In some cases there is even a collapse of the surface layer due to specific interactions between the polyion and the counterions. Cationic systems re-swell if immersed in concentrated salt solutions (“salting-in”). This is observed for monovalent as well as for divalent counterions. The analysis of the reduced excluded-volume parameter  $\nu/(l_K l^2)$  suggests that there is an adsorption of the counterions at high salt concentrations. The increase of  $\nu/(l_K l^2)$  thus affected leads to the re-swelling of the brush layer. The salting-in behavior thus finds an explanation in the increase of  $\nu$  due to the adsorption of salt ions. All data demonstrate that specific effects of different counterions lead to a behavior of the brush layer not expected from a purely electrostatic model.

Papermaking invented by Ts'ai-Lun in A.D. 105 promoted the development of civilization, and cultural exchange [21]. Nowadays, high speed papermaking machines were used to get high production efficiency; synthetic polymers were used as retention aids to improve paper qualities, productivities and runnabilities of papermaking machines. But both of natural and synthetic single-component retention aids show disadvantages, either in performance or in paper formation control. Dual-component retention system, on the contrary, combines high performance and uniform paper formation. In order to obtain deeper insight into retention systems, dual-component system consisting of anionic SPB and cationically modified polyacrylamide (CPAM) was used as a model system, different SPB in conjunction with cationically modified polyacrylamide (CPAM) as dual-component retention

system were tested, and compared with the traditional “microparticle” retention system in which bentonite acts as secondary flocculant in chapter 3.3. The dual-component retention system consisting of anionic SPB and CPAM showed high flocculation efficiency as tested under sheared conditions using a dynamic drainage jar. The high retention level of the anionic SPB dual-component retention system suggests that the flocculation efficiency can be attributed to a high cation exchange capacity of the anionic SPB in combination with a flexibility of grafted polyelectrolyte chains. The flocculation mechanism of anionic SPB and CPAM as dual-component retention system and deposition mechanism of  $\text{CaCO}_3$  particles were studied by means of field emission scanning electron microscopy (FESEM) and atomic force microscopy (AFM). Images obtained from FESEM and AFM support the model of anionic SPB’ acting as a particle bridge in between fibers and  $\text{CaCO}_3$  fillers.

All the experimental work and data used in this study were summarized in appendix. Furthermore, principles of all the instruments related to this study were briefly introduced.

## 2.2 Individual Contribution to Joint Publications

The results presented in the thesis were obtained in cooperation with other co-workers. In the following, my contributions to each publication are specified.

### Chapter 3.1

This work has been published under the name “**Engineering the Interaction of Latex Spheres with Charged Surfaces: AFM Investigation of Spherical Polyelectrolyte Brushes on Mica**” by Mei, Y.; Wittemann, A.; Sharma, G.; Ballauff, M.; Koch, Th.; Gliemann, H.; Horbach, J.; Schimmel, Th. in *Macromolecules* 2003, 36, 3452.

I performed all the chemical experiments.

H. Gliemann and J. Horbach from Institut für Angewandte Physik of Karlsruhe Universität measured the samples with AFM.

M. Ballauff, W. Alexander, G. Sharma, Th. Koch and Th. Schimmel from Institut für Angewandte Physik of Karlsruhe Universität contributed to the discussion.

### Chapter 3.2

This work has been published under the name “**Effect of counterions on the swelling of spherical polyelectrolyte brushes**” by Y. Mei; M. Ballauff in the *European Physical Journal E* 16, 341-349 (2005).

The cationic SPB were synthesized by me for the first time, I performed all the experiments and evaluated the data getting from dynamic light scattering.

M. Ballauff contributed to the discussion.

### Chapter 3.3

This work was submitted under the name “**Interaction of spherical polyelectrolyte brushes with CaCO<sub>3</sub> and cellulose fibers. Mechanistic studies and their application in papermaking**” by Y. Mei, C. Abetz, O. Birkert, V. Schädler, R.J. Leyrer, M. Ballauff to *Journal of Applied Polymer Science*.

I have prepared all the SPB samples. The retention testes were performed by me with the help of O. Koch and R. Barthel. I measured the samples with AFM.

C. Abetz has performed FESEM measurement.

M. Ballauff, O. Birkert, V. Schädler, R.J. Leyrer contributed to the discussion.

## 2.3 References

1. Dubreuil, F; Guenon, P., *Eur. Phys. J. E*, **2001**, 5, 59.
2. Zhulina, E.B.; Borisov, O.V.; Birshtein, T.M., *J. Phys. II*, **1991**, 1, 521.
3. von Goeler, F.; Muthukumar, M., *Macromolecules*, **1995**, 28, 6608.
4. Argiller, J.F.; Tirell M., *Theor. Chim. Acta*, **1992**, 82, 343.
5. Zhulina, E.B.; Borisov, O.V., *Macromolecules*, **1996**, 29, 2618.
6. Zhulina, E.B.; Borisov, O.V.; Birshtein, T.M., *Macromolecules*, **1999**, 32, 8189.
7. Pincus, P., *Macromolecules*, **1991**, 24, 2912.
8. Hariharan, R.; Biver, C.; Mays, J.; Russel, W.B., *Macromolecules*, **1998**, 31, 7506.
9. Biver, C.; Hariharan, R.; Mays, J.; Russel, W.B., *Macromolecules*, **1997**, 30, 1787.
10. Misra, S.; Mattice, W. L.; Napper, D. H., *Macromolecules*, **1994**, 27, 7090.
11. An, S.W.; Thirtle, P.N.; Thomas, R.K.; Baines, F.L.; Billingsham, N.C.; Armes, S.P. and Penfold, J., *Macromolecules*, **1999**, 32, 2731.
12. Biesalski, M.; Ruhe, J. and Johannsmann, D., *J. Chem. Phys.*, **1999**, 111, 7029.
13. Tran, Y. ; Auroy, P., *Eur. Phys. J. E*, **2001**, 5, 65.
14. Tran, Y.; Auroy, P.; Lee, L.T., *Macromolecules*, 1999, 32, 8951.
15. Guo, X.; Ballauff, M., *Langmuir*, **2000**, 16, 8719.
16. Guo, X.; Ballauff, M., *Phys. Rev. E*, **2001**, 64, 051406.
17. Guo, X., *Synthesis and Study of the Colloidal Polyelectrolyte Brushes prepared by Photo-emulsion Polymerization*, **2001**, Logos Verlag Berlin.
18. Guo, X.; Weiss, A.; Ballauff, M., *Macromolecules*, **1999**, 32, 6043.
19. Hariharan, R.; Biver, C.; Mays, J.; Russel, W.B., *Macromolecules*, **1998**, 31, 7506.
20. Guo, X.; Weiss, A.; Ballauff, M., *Macromolecules*, **1999**, 32, 6043
21. Michael, H., *Ts'ai Lun. In 100 A Ranking of the Most Influential Persons in History*, **1978**, 36-41, New York, Hart Publishing Co.

## Chapter 3

### Publications

### 3.1 Engineering the Interaction of Latex Spheres with Charged Surfaces: AFM Investigation of Spherical Polyelectrolyte Brushes on Mica.

#### Engineering the Interaction of Latex Spheres with Charged Surfaces: AFM Investigation of Spherical Polyelectrolyte Brushes on Mica

Y. Mei, A. Wittmann, G. Sharma, and M. Ballauff\*

*Polymer-Institut, Universität Karlsruhe,  
76128 Karlsruhe, Germany*

Th. Koch,<sup>†</sup> H. Ciemann,<sup>†</sup> J. Horbach,<sup>‡</sup> and  
Th. Schimmel\*<sup>†,‡</sup>

*Institut für Nanotechnologie, Forschungszentrum Karlsruhe  
GmbH, PO Box 3640, 76021 Karlsruhe, Germany, and  
Institut für Angewandte Physik, Universität Karlsruhe,  
76128 Karlsruhe, Germany*

Received November 15, 2002

Revised Manuscript Received April 7, 2003

**Introduction.** Colloidal particles are often stabilized by long polymeric chains grafted to their surface.<sup>1</sup> If two such particles are dispersed in a good solvent for the chains and these particles approach each other, a repulsive interaction results. The steric interaction thus effected has been studied for decades and is well understood by now.<sup>2,3</sup> It can be enhanced even more if the polymers attached to the surface carry charges. The resulting electrosteric interaction can be understood in terms of the increased osmotic pressure of the counterions if the polyelectrolyte chains attached to the surfaces of the particles are to share the same volume.<sup>4,5</sup> The great practical importance of electrosteric interaction is related to the fact that most industrial latexes are stabilized in this way.<sup>6</sup>

Application of latexes not only requires a fundamental understanding of mutual interaction, however. Controlling the interaction of the particles with solid shells is of comparable importance when considering latex particles as the base of paints and coatings.<sup>6</sup> A comprehensive investigation of these problems requires latex particles onto which the polyelectrolyte chains are firmly attached, i.e., by a chemical bond. Otherwise, the particles would disintegrate upon strongly interacting with a solid substrate. Moreover, the polyelectrolyte chains must be densely grafted to the particles. Colloidal objects carrying only a small number of chains can approach solid substrates so closely that their strong van der Waals interaction with the substrate becomes the leading effect.<sup>1,7</sup>

Recently, we demonstrated that colloidal particles with attached polyelectrolyte chains can conveniently be prepared by photoemulsion polymerization.<sup>8</sup> By this method the polyelectrolyte chains can be affixed rather densely to the surface of poly(styrene) latex particles so that the overall dimensions are much larger than their average distance on the surface of the particles. Hence, a spherical polyelectrolyte brush (SPB) results, having overall dimensions in the colloidal domain (Figure 1).

The chains are affixed to the particles by a chemical bond and exhibit an excellent stability against coagulation in solution.<sup>9,10</sup> Previous studies demonstrated that

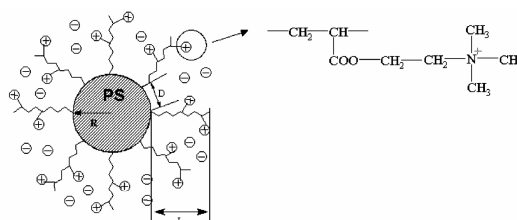


**Figure 1.** Scheme of the cationic spherical polyelectrolyte brush LA2 synthesized and used in this study. Long polyelectrolyte chains are densely attached to solid poly(styrene) particles so that a dense shell of charged chains results on the surface of the cores. The anionic latex LQ3 used herein has the same structure but with the cationic chains being replaced by the anionic poly(styrenesulfonic acid) chains.

the dimensions of the shell can be tuned by the salt concentration in the solution.<sup>9,10</sup> Moreover, direct measurements of the osmotic pressure of aqueous solutions of the SPB<sup>11</sup> demonstrated that ca. 95% of the counterions are confined within the brush as predicted by theory.<sup>12,13</sup> Rheological measurements clearly pointed to the strong mutual repulsion of the particles when dispersed in water.<sup>14</sup>

Evidently, these SPB provide a good model system for a systematic study of the interaction of sterically stabilized particles with solid substrates. Here we present the first results of a study of SPB contacting a negatively charged mica substrate. Atomic force microscopy (AFM) in the intermittent contact mode<sup>15</sup> has been used as tool to investigate the topography and the phase contrast<sup>16</sup> of the samples. Phase contrast results from a combination of different tip-sample interactions such as local adhesion and capillary forces as well as viscoelastic damping. Recent investigations demonstrate that AFM is a powerful method to study the local organization of latex particles on solid substrates.<sup>17–23</sup>

Two different SPB have been studied: (1) An anionic system consisting of chains of poly(styrenesulfonic acid). This system termed LQ3 has been synthesized and characterized in detail recently (see Table 1 in ref 10). (2) The SPB termed LA2 carrying positive charges. These particles have been synthesized and characterized for the present purpose. Figure 1 shows schematically the structure of the cationic SPB LA2. As cationic polyelectrolyte we used poly((2-acryloyl)ethyl)trimethylammonium chloride (poly(flocryl)), which carries quarternized ammonia groups. Poly(flocryl) chains hence represent a quenched polyelectrolyte in which the charges are independent of the pH in the system. The choice of this particular polyelectrolyte derives from its excellent solubility in water and use as technical flocculation agent.<sup>6</sup> The polyelectrolyte chains are attached to a poly(styrene) core of 136 nm (LQ3) and 90 nm (LA2) diameter with low polydispersity. Since the chains can be cleaved off after synthesis, their molecular weight and molecular weight distribution can be determined.<sup>8</sup> Moreover, the total charge of the SPB brush is determined by titration. Hence, all pertinent parameters of the particles are known.<sup>8–10</sup> The only parameter that was varied in our experiments was the charge of the SPB. Differences in the adsorption behavior can hence be explained by different interaction forces of the

<sup>†</sup> Forschungszentrum Karlsruhe GmbH.

<sup>‡</sup> Universität Karlsruhe.

\* Corresponding authors. E-mail: Thomas.Schimmel@physik.uni-karlsruhe.de; Matthias.Ballauff@chemie.uni-karlsruhe.de.

**Table 1. Characterization of the SPB LA2 and LQ3<sup>a</sup>**

sample	$R$ [nm]	$M_n$ [g/mol]	$L_c$ [nm]	$\sigma$ [nm <sup>-2</sup> ]	$L_c/R$	$D$ [nm]
LA2	45	89 700	116	0.049	2.57	5.1
LQ3	68	88 000	108	0.039	1.59	5.7

<sup>a</sup> LQ3 = anionic core-shell latices with 20 mol % poly(NaSS); LA2 = cationic core-shell latices with 56 mol % poly(flocryl);  $R$  = core radius;  $M_n$  = molecular weight of grafted chains as determined by viscosimetry (see ref 8);  $L_c$  = contour length of grafted chains determined from  $M_n$ ;  $\sigma$  = graft density on surface of core particles;  $D$  = the average distance between two neighboring graft points.

negatively charged mica surface with the positively charged LA2 particles or with the negatively charged LQ3 particles. Using these two types of particles, it will be shown that firmly attached polyelectrolyte chains are well-suited to control the interaction of latex particles with solid substrates.

**Experimental Section.** The synthesis of the cationic SPB proceeds along the lines given recently.<sup>8</sup> The photoemulsion polymerization described there proceeds in three steps: In a first step the poly(styrene) core particles are synthesized by a conventional emulsion polymerization. Then a thin shell of the photoinitiator 2-[*p*-(hydroxy-2-methylpropiphenone)]ethylene glycol-methacrylate (HMEM; see ref 8) is polymerized onto these core particles according to the method devised previously.<sup>8</sup> HMEM is a vinyl monomer, and the formation of the shell proceeds under starved conditions so that no new particles are formed in this second step.

In the third step UV/vis radiation is used to generate radicals on the surface of the particles.<sup>8,9</sup> The monomer 2-(acryloyloxy)ethyltrimethylammonium chloride (flocryl, BASF-AG) forming the brush layer of the particles was added to the water phase, and a radical polymerization on the surface was started. In this way a dense layer of poly(((2-acryloyl)ethyl)trimethylammonium chloride) (poly(flocryl)) chains is generated on the surface of the particles by a grafting-from technique.

To avoid possible interaction of the negatively charged surfactant used in the previous synthesis, cetyltrimethylammonium bromide (CTAB; Fluka) has been used to stabilize the core latex particles. For similar reasons the cationic initiator 2,2'-azobis(2-amino-propane) dihydrochloride (V50; WAKO Chemicals) has been used to start the emulsion polymerization of the core particles. The particles are analyzed as described previously<sup>3</sup> by cleaving off the polycation chains by a strong base. The molecular weight of the chains cleaved from the surface of the particles has been determined by viscosimetry as shown recently.<sup>8</sup> Details of the respective steps in the synthesis of the particles and their characterization will be given elsewhere. Table 1 summarizes the characteristic data of both SPB.

All AFM images were taken with a commercial AFM operated in tapping mode. For phase contrast imaging, a home-built phase imaging electronics was used. The principle of phase imaging by AFM is explained elsewhere.<sup>16</sup> Imaging was performed at ambient conditions using bar-shaped silicon cantilevers with a force constant of 40 N/m and a resonance frequency of 170 kHz. The images show unfiltered original data, represented in a linear gray scale.

For sample preparation, a droplet of 20  $\mu$ L of a solution containing the respective polymer particles dispersed in pure water was put onto a freshly cleaved mica surface (muscovite white mica) and dried in air. The concentration of the particles was chosen small enough to avoid multilayer formation. The adsorption

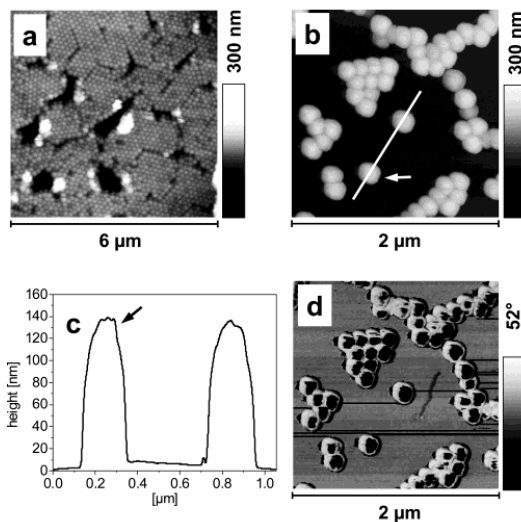


**Figure 2.** Intermittent contact mode AFM images of topography (a, b) and phase contrast (d) of SPB LQ3 on mica. (c) shows the cross section of two single particles along the white line in (b); the arrow in (b, c) assigns the particle in (b) to the corresponding cross section. It is seen that the particles exhibit sharp regular boundaries and smooth surfaces. They show well-defined phase contrast between the particle and the substrate (d) and form a layer that exhibits two- and three-dimensional long-range order on the surface (a).

experiments and AFM experiments were reproduced several times and with different particle series independently yielding comparable results. After drying, studies of the long-time behavior were performed to check whether the particle structures change with time. No such changes as a function of time were observed in our experiments. All AFM data shown in this article show typical structures which are representative for the corresponding sample.

**Results and Discussion. a. Anionic Particles LQ3.** We first discuss the results obtained by AFM for the anionic system LQ3. Figure 2a displays the topography of a larger area, and Figure 2b,d shows images of the spatial structures and the phase imaging data obtained by AFM in intermittent contact mode for LQ3 at larger magnification.

Figure 2b shows the topography of single polymer particles and small particle aggregates. In Figure 2c the cross section of two single particles marked as a white line in Figure 2b shows the regular border of the particles with an average diameter of 200 nm. Taking a closer look at the structure of the particles in Figure 2b, one can see that each particle exhibits a bright center region, which also is obvious as a dark, well-defined area with an average diameter of about 150 nm in the corresponding phase image in Figure 2d. When operating an AFM in intermittent contact mode to image phase contrast, the phase shift is recorded that results between the cantilever excitation piezo driven by a frequency generator and the vibration detected optically by the four-segment photodiode of the AFM. The phase shift depends on the dissipative tip-sample forces such as local adhesion, capillary forces, and viscoelastic damping. The difference in phase shift detected at the edges of the latex spheres seen as a bright rim in Figure 2d compared to the phase shift at

the center part of the latexes seen as black areas can be explained as a result of the different tip-sample contact areas (and thus different dissipative tip-sample forces) when the AFM tip scans across the particle. The tip contacts the rim of the polymer particle with the tip flank whereas the tip apex gets in contact with the center part of the SPB.

The spherical shape of the particles that is expected from synthesis is visible even within the aggregates. The comparison of the particle dimensions reveals that the diameters of the particle images in Figure 2b are comparable with the corresponding diameters in Figure 2d but are significantly smaller (50–60%) than the diameter of the LQ3 cores plus twice the contour lengths of the attached polymer chains (cf. Table 1). Obviously, the poly(styrenesulfonic acid) chains have contracted during the drying process on the substrate. As intermittent contact mode images from pure PS core latexes show a very similar phase contrast as LQ3 particles (not shown here), we can assume that the LQ3 particles exhibit a dense solid shell as expected.

Figure 2a shows a two-dimensional long-range order within the layer of the LQ3 particles. The layer shows small highly ordered arrays of particles divided by cracks or voids. These features have been seen in other studies of negatively charged latexes as well.<sup>17,18</sup> The formation of the arrays takes place in a multistep process: After the deposition of a drop of latex dispersion on the mica surface, the water begins to evaporate and the concentration of the particles increases. Gravitational forces on the small LQ3 particles can be neglected,<sup>25</sup> and the electrosteric stabilization of the particles must lead to a strong mutual repulsion as long as water is present.<sup>9,10,14</sup> This can be argued from the finding that even high concentrations of monovalent added salt (up to 3 M) have no influence on the colloidal stability of these systems.<sup>10</sup> However, when the thickness of the liquid layer of the drying droplet becomes smaller and smaller, the strong lateral capillary force leads to an attractive interaction between the particles. Thus, the film formation and deposition of the particles are expected to take place at the withdrawing rim of the drying drop.

The growth of the two-dimensional array is facilitated by a convective liquid flow at the rim of the drop which is responsible for the transport of the particles to the boundary of the drop. As LQ3 latices consist of a PS core and a negatively charged polymer brush, only a repulsive interaction between the particles and the mica surface is expected. Therefore, particles should move to the boundary of the drop by convective flow without sticking to the surface. Hence, if the evaporation of the water is slow enough, the particles have the possibility to rearrange within the wet latex film. Therefore, this rearrangement leads to the densely packed arrangement of the particles as seen in Figure 2a. This also corresponds to the case of bare poly(styrene) particles studied by many groups so far.<sup>17–22</sup>

**b. Cationic Particles LA2.** A totally different ordering behavior is seen when using suspensions of the cationic SPB LA2 on mica. Figure 3a shows the large-scale arrangement of the particles resulting from drying a dilute suspension at the mica surface. The particles are arranged in long chains that form a two-dimensional network on the substrate. Moreover, Figure 3a shows that the drying process of the droplet has generated a gradient in particle concentration that increases from

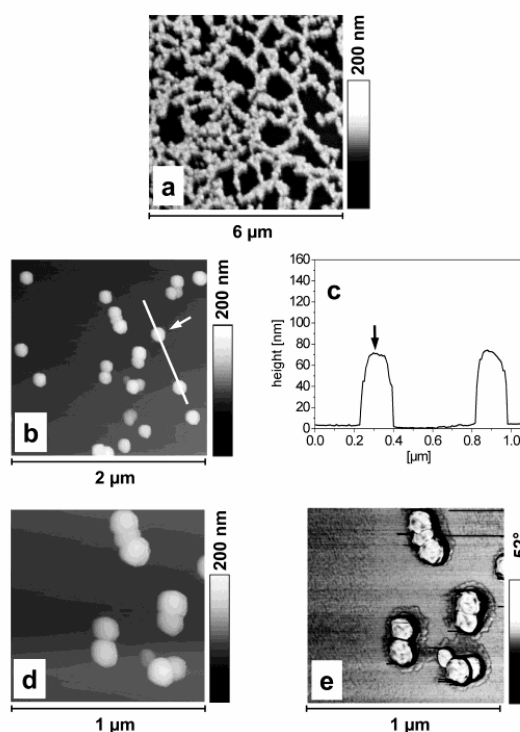


**Figure 3.** Intermittent contact AFM images of the topography (a, b, d) and phase contrast (e) of the cationic SPB LA2 having poly(flocryl) chains attached to their cores. The solid substrate is mica. (c) shows the cross section of two single particles along the white line in (b), and the arrow in (b, c) assigns the particle in (b) of which the cross section has been taken. In (e) the particles show an irregular phase distribution on their surfaces. They are surrounded by a corona of the polyelectrolyte chains that are attached to the solid surface. As shown in (a), the particles tend to form network-like aggregates on the surface without long-range 2D order.

the upper right to the lower left of the picture. In-situ AFM investigations of freshly cleaved mica immersed in a LA2 latex suspension showed that the polymer particles seem to stick to the surface as soon as they get into contact with it.

It is therefore obvious that the attractive interaction between the cationic LA2 particles and the mica surface is much stronger than between LQ3 spheres and mica. As a consequence of this, capillary forces that lead to a dense packing of the anionic spheres is now partially balanced by the adsorption of the cationic LA2 spheres onto the mica surface. Moreover, the adsorbed particles obviously act as nucleation centers for other polymer spheres. This becomes more evident when zooming into Figure 3a. Figure 3b shows that only small disordered aggregates of particles are formed. Therefore, the aggregates seen in Figure 3a consist of few particles only that form a networklike structure.

Zooming into Figure 3b, Figure 3d,e corroborates this explanation for the totally different behavior of the cationic particles LA2 as compared to the anionic particles LQ3: First of all, Figure 3d,e demonstrates that the adsorbed SPB LA2 shows different shapes in the topography image as compared to the corresponding phase image. This is in contrast to the behavior ob-

served for the anionic system LQ3 (see Figure 2b,d). The topography cross section of Figure 3c shows a regular shape of the particles as in the case of LQ3. The phase contrast image of the particles in Figure 3e, however, is not as smooth and well-defined as in the case of LQ3 (Figure 2d). Most importantly, in Figure 3e a corona is observed which is surrounding the particles. This corona is clearly visible in the phase image of Figure 3e but can hardly be detected in the topography image in Figure 3d. It exhibits an average diameter of 220 nm. The size of the particle itself is roughly the same in topography and phase images. The particle diameter thus determined is considerably lower than the diameter of the particles corresponding to fully extended chains (ca. 320 nm; diameter of core plus twice the contour lengths of the attached chains, cf. Table 1). From these finding it must be concluded that the LA2 particles strongly interact with mica.

The corona visible in Figure 3e is due to the positively charged polymer chains on the surface of the LA2 particles that are strongly attached to the negatively charged mica surface. The phase-sensitive detection in the AFM analysis is able to visualize these attached chains directly. Moreover, Figure 3e demonstrates that the chains have not retracted during the drying process. This indicates that the interaction between the polyelectrolyte chains and the surface already exists when water is still present. For geometrical reasons the diameter determined from Figure 3e must still be smaller than the maximal diameter of the particles (cf. Table 1). This is found indeed when comparing the overall diameter including the corona as detected by AFM (ca. 220 nm) to the maximum size derived from the core diameter and the contour length of the chains (ca. 320 nm; see above).

A schematic rendition of the process of drying is given on the right-hand side of Figure 4: The substrate becomes the counterion for the positively charged polyelectrolyte chains and balances a part of the charge of the shell of LA2. The sodium counterions as well as the cations balancing the charge of the mica surface are released in this way. Thus, the entropy of the entire system is increased. This "counterion release force" has recently been the subject of a thorough theoretical study.<sup>23</sup> It is seen experimentally in investigations of the interaction of DNA with appropriate solid substrates.<sup>26,27</sup> The strong interaction of the positive polyelectrolyte chains and the negative surface thus effected must lead to a partial spreading of the chains which is obvious from Figure 3e. Moreover, this attachment counterbalances partially the strong capillary forces that tend to aggregate the particles during the drying process. As a consequence of the sticking of the particles to the surface, a loose network of particles is formed upon drying (see Figure 3a), but no close packing is observed as in the case of the LQ3 particles (see Figure 2a).

It is now obvious that the anionic particles LQ3 (see Figure 2) must interact in a totally different fashion as shown schematically on the left-hand side of Figure 4: The particles are at first repelled from the negatively charged surface. The counterions are kept within the shell upon drying, and a smooth surface results. After evaporation of water the particles are attracted to the surface only by conventional van der Waals attraction if their distance to the surface is small enough.<sup>7</sup> The chains on the surface keep the cores sufficiently above

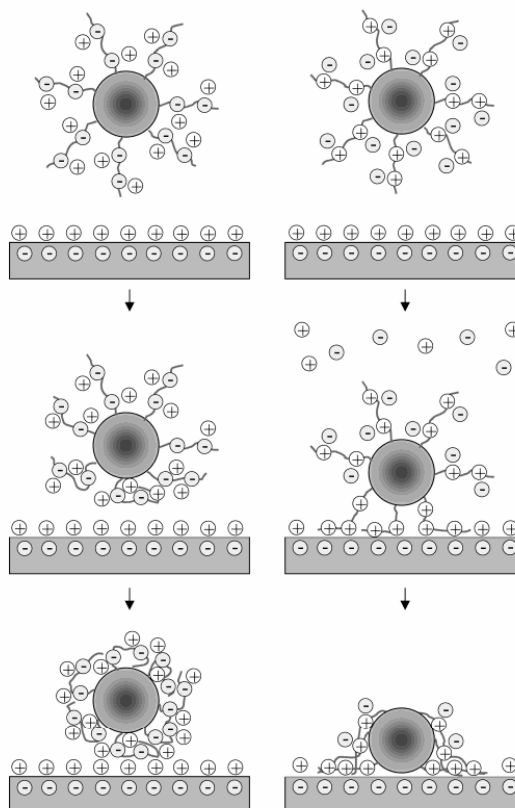


**Figure 4.** Scheme of the interaction of the anionic and the cationic SPB with negatively charged surfaces. The left-hand side displays schematically the interaction of the negatively charged particles LQ3 (see Table 1) with the solid mica substrate whereas the right-hand side displays the interaction of the positively charged spherical polyelectrolyte brushes LA2. The solid substrate which bears a negative charge becomes the counterion of the positive chains attached to the particles. The respective number of counterions both of the particles and of the substrate is therefore released. This leads to a strong attractive force between the particles and the substrate ("counterion release force"; see refs 23, 26, and 27 for further details). The negatively charged particles LQ3 (left-hand side), on the other hand, do not exhibit this interaction with the mica surface. Their spatial structure obtained upon drying resembles the result found for uncoated poly(styrene) particles in previous investigations.<sup>17,18</sup>

the surface, however, unless all water has evaporated. Hence, the van der Waals interaction of the particles with the surface remains small, and their surface diffusion remains unhampered up to the point where virtually all water has been evaporated. This results in a long-range two-dimensional order of the particles on the surface as seen in Figure 2a.

**Conclusions.** An investigation of the interaction of spherical polyelectrolyte brushes with negatively charged surfaces by AFM operated in intermittent contact mode was presented. It was demonstrated that the negative SPB LQ3 forms two-dimensional aggregates of densely packed polymer particles. This can be explained by a particle-particle interaction dominating the repulsive interaction of the particles with the substrate. The

positively charged SPB LA2 exhibits a completely different particle–surface interaction behavior as expected. Here networklike structure films of dried particles without long-range 2D order are formed. This is due to the strong attractive particle–surface interaction of positively charged polyelectrolyte chains in the shell of the LA2 particles. These chains spread over the negative surface and anchor the particles. Hence, a shell of polyelectrolyte chains is a highly efficient means of adjusting the interaction of colloidal particles with solid substrates.

**Acknowledgment.** Financial support by the Center of Functional Nanostructures (CFN) of the Deutsche Forschungsgemeinschaft and of the Fonds der Chemische Industrie is gratefully acknowledged. Y. Mei and M. Ballauff thank the BASF AG for financial support. We thank Oliver Krömer, IPE, Forschungszentrum Karlsruhe GmbH, for his contribution to the development of the home-built phase imaging electronics. Th. Schimmel acknowledges support by the Research Award of the Land Baden-Württemberg.

#### References and Notes

- (1) Israelachvili, J. N. *Intermolecular and Surface Forces*, 2nd ed.; Academic Press: London, 1992.
- (2) Napper, D. H. *Polymeric Stabilization of Colloidal Dispersions*; Academic Press: London, 1983.
- (3) Fleer, G. J.; Cohen Stuart, M. A.; Scheutjens, J. M. H. M.; Cosgrove, T.; Vincent, B. *Polymers at Interfaces*; Chapman and Hall: London, 1993.
- (4) Jusufi, A.; Likos, C. N.; Löwen, H. *Phys. Rev. Lett.* **2002**, *88*, 018301.
- (5) Jusufi, A.; Likos, C. N.; Löwen, H. *J. Chem. Phys.* **2002**, *116*, 11011.
- (6) Distler, D., Ed. *Wässrige Polymerdispersionen*; Wiley-VCH: New York, 1999.
- (7) Russel, W. B.; Saville, D. A.; Schowalter, W. R. *Colloidal Dispersions*; Cambridge University Press: Cambridge, 1989.
- (8) Guo, X.; Weiss, A.; Ballauff, M. *Macromolecules* **1999**, *32*, 6043.
- (9) Guo, X.; Ballauff, M. *Langmuir* **2000**, *16*, 8719.
- (10) Guo, X.; Ballauff, M. *Phys. Rev. E* **2001**, *64*, 051406.
- (11) Das, B.; Guo, X.; Ballauff, M. *Prog. Colloid Polym. Sci.* **2002**, *121*, 34.
- (12) Pincus, P. *Macromolecules* **1991**, *24*, 2912.
- (13) Borisov, O. V.; Birshtein, T. M.; Zhulina, E. B. *J. Phys. II* **1991**, *1*, 521.
- (14) Marra, A.; Pleuvrel-Disdier, E.; Wittmann, A.; Guo, X.; Ballauff, M. *Colloid Polym. Sci.*, in press.
- (15) Zhong, Q.; Inniss, D.; Kjoller, K.; Elings, V. B. *Surf. Sci. Lett.* **1993**, *290*, L688.
- (16) Pang, G. K. H.; Baba-Kishi, K. Z.; Patel, A. *Ultramicroscopy* **2000**, *81*, 35.
- (17) Evers, M.; Palberg, T.; Dingenouts, N.; Ballauff, M.; Richter, H.; Schimmel, Th. *Prog. Colloid Polym. Sci.* **2000**, *115*, 307.
- (18) Evers, M.; Schöpe, H. J.; Palberg, Th.; Dingenouts, N.; Ballauff, M. *J. Non-Cryst. Solids* **2002**, *307–310*, 579.
- (19) Wen, L.; Wu, R. C.; Eschenazi, E.; Papadopoulos, K. *Colloids Surf. A* **2002**, *197*, 157.
- (20) Rakers, S.; Chi, L. F.; Fuchs, H. *Langmuir* **1997**, *13*, 7121.
- (21) Wen, L.; Wu, R. C.; Eschenazi, E.; Papadopoulos, K. *Colloids Surf. A* **2001**, *197*, 157.
- (22) Semmler, M.; Mann, E. K.; Rieck, J.; Borkovec, M. *Langmuir* **1998**, *14*, 5127.
- (23) Fleck, C.; von Grünberg, H. H. *Phys. Rev. E* **2001**, *63*, 061804.
- (24) Johnson, C. A.; Lenhoff, A. M. *J. Colloid Interface Sci.* **1996**, *179*, 587.
- (25) Kralchewsky, P. A.; Nagayama, K. *Adv. Colloid Interface Sci.* **2000**, *85*, 145.
- (26) Wagner, K.; Harries, D.; May, S.; Kahl, V.; Rädler, J. O.; Ben-Shaul, A. *Langmuir* **2000**, *16*, 303.
- (27) Maier, B.; Rädler, J. O. *Macromolecules* **2000**, *33*, 7185 and references given therein.

MA0258399

## 3.2 Effect of Counterions on the Swelling of Spherical Polyelectrolyte Brushes

Eur. Phys. J. E (2005)  
DOI 10.1140/epje/i2004-10089-9

THE EUROPEAN  
PHYSICAL JOURNAL E

### Effect of counterions on the swelling of spherical polyelectrolyte brushes

Y. Mei and M. Ballauff<sup>a</sup>

Physikalische Chemie I, University of Bayreuth, 95440 Bayreuth, Germany

Received 20 August 2004 and Received in final form 4 December 2004 /  
Published online: 1 February 2005 – © EDP Sciences / Società Italiana di Fisica / Springer-Verlag 2005

**Abstract.** We investigate the swelling of colloidal spherical polyelectrolyte brushes in the presence of different counterions. The colloidal particles consist of a solid poly(styrene) core of ca. 100 nm diameter onto which linear polyelectrolyte chains are chemically grafted. Two types of polyelectrolyte chains have been used here: The cationic polyelectrolyte poly(2-(acryloyl)ethyltrimethylammonium chloride)) (PATAc) and the anionic poly(styrenesulfonate) (PSS). Both systems are dispersed in water and the degree of swelling of the surface layer is studied by dynamic light scattering. Adding more and more salt leads to a strong shrinking of the surface layer as expected for polyelectrolyte brushes. It is shown that data obtained at low ionic strength can be collapsed on suitable master curves for monovalent and divalent counterions, respectively. For some ions, however, high salt concentrations may lead to a re-swelling of the brush layer in case of the cationic systems. This points to specific interactions of the counterions with the PATAc chains. This strong specific interaction between the counterions and the attached polyelectrolyte may even lead to flocculation of the particles at intermediate salt concentration. Surprisingly, for iodide and magnesium counterions the solubility increases again if the salt concentration is raised to 1 mol/l. Hence, specific interaction leads to salting-out effects as well as to salting-in effects for these colloidal particles. All specific effects seen at high concentrations of added salt can be explained by the increase of the reduced excluded-volume parameter which is due to the adsorption of salt ions.

**PACS.** 82.35.Lr Physical properties of polymers – 82.35.Rs Polyelectrolytes – 82.70.Dd Colloids

#### 1 Introduction

Polyelectrolyte brushes are systems in which polyelectrolyte chains are attached through an anchor group to a planar or curved surface. The term brush denotes a system in which the grafting density  $\sigma$ , as expressed by the number of grafted chains per unit area, is high enough so that neighboring chains strongly interact and stretch away from the surface [1–5]. Since the first seminal papers of Pincus [2] and of Borisov, Birshtein and Zhulina [3] in 1991, these systems have been the subject of numerous theoretical studies. A survey of these studies may be found in recent reviews [4, 5]. Evidently, the high number of charges present in such a polyelectrolyte brush will lead to a strong repulsive interaction between the attached chains if the ionic strength in the system is low. Hence, the concentration  $c_a$  of salt added to the solution in which the brush is immersed enters as a new decisive variable of the system.

By now, it is generally agreed that there are two limiting cases: i) the osmotic brush which results for low values of  $c_a$  (cf. [5, 6]). Here it can be shown that the counterions

are mostly confined within the brush layer [2]. The high concentration of the confined counterions create an enormous osmotic pressure within the layer which leads to a marked stretching of the polyelectrolyte chains. ii) At the opposite limit, the salted brush, the concentration  $c_a$  of added salt is approaching the ion concentration  $c_s$  within the brush layer. In this regime the screening of the electrostatic interaction will lead to a shrinking of the brush layer. At sufficiently high  $c_a$  the polyelectrolyte brush will resemble uncharged systems. In addition to this, polyelectrolyte brushes may be built up from strong or from weak polyelectrolyte chains. In the latter case, termed *annealed brush*, the state of charging depends on the pH in the system and also on  $c_a$ . For a *quenched brush*, consisting of quenched polyelectrolytes, the charges are fully dissociated and do not depend on the pH.

The predictions for the dependence of the height  $L$  of a planar layer as a function of  $c_a$  [2] compare well with experimental data obtained by various methods on planar systems [7–16]. Work done on annealed polyelectrolyte brushes which consist of weak polyelectrolyte chains has elucidated how the state of charging depends on the pH in the system [9, 14, 16]. Most of the features observed so

<sup>a</sup> e-mail: matthias.ballauff@uni-bayreuth.de

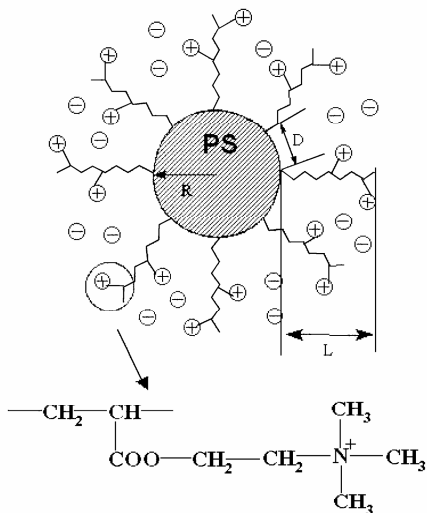


**Fig. 1.** Schematic representation of the spherical polyelectrolyte brush investigated in this study [28]. Cationic polyelectrolyte chains are grafted to colloidal particles made from solid poly(styrene). The particles are immersed in aqueous salt solutions with defined ionic strength. The thickness  $L$  of the brush layer is measured for different ionic strengths in the presence of different counterions.

far are in good agreement with theory and planar polyelectrolyte brushes seem to be rather well understood by now.

Spherical polyelectrolyte brushes (SPB) result if linear polyelectrolyte chains are densely grafted to colloidal spheres [5,17]. Here the radius  $R$  of the core particles enters as an additional decisive length scale. Such SPB may be realized by adsorption of suitable blockcopolymers onto latex particles [18–20] or by micellization of suitable blockcopolymers in water [21–23,4,24]. Polyelectrolyte chains may also be affixed to latex particles by photo-emulsion polymerization [25–28]. Figure 1 schematically displays the structure of such a cationic SPB. If the polydispersity of the core particles is small, the thickness  $L$  of the surface layer can be derived from the core radius  $R$  through  $L = R_H - R$ . Recently, it has been shown [26,27] that a simple model developed by Hariharan *et al.* [29] can be used to model the dependence of  $L$  on salt concentration  $c_a$ .

An explicit assumption underlying virtually all previous theoretical treatment is that the interaction between the polyelectrolyte chains and their counterions is purely electrostatic, no specific effects between the chains and the ions are taken into account. However, ions differ widely with regard to their hydration and ion pairing may come into play at higher concentrations [30]. Indeed, Biesalski *et al.* could recently show that planar brushes of the cationic polyelectrolyte poly(4-vinyl(N-methyl-pyridinium)) (MePVP) collapse first upon addition of potassium iodide but are swollen again at very

high concentrations of this salt [14]. The effect was much less pronounced if other counterions were used. This calls attention on the often neglected role of specific, non-electrostatic interactions in the field of polyelectrolytes [31–33]. It has been shown that linear polyelectrolytes may even demix from aqueous solution if high amounts of salt are added (“salting-out”, see Ref. [34] and further references given there). At highest concentration of salt the solubility may be raised again and the polyelectrolyte becomes soluble again despite the fact that no electrostatic interaction is present anymore at this high ionic strength (“salting-in” [34]).

Here we present a comprehensive study of the thickness  $L$  measured for the cationic spherical polyelectrolyte brushes in solutions of various salts. These systems, the structure of which is displayed in Figure 1, present quenched polyelectrolyte systems. Linear chains of the strong cationic polyelectrolyte poly(2-(acryloyl)ethyltrimethylammonium chloride) (PATAC) have been attached to the core particles. Hence, charge annealing is not to be expected in these SPB. The results obtained here can then be compared to data obtained from the quenched anionic brushes investigated recently [27]. In addition to this, the colloidal stability in the presence of different mono- and divalent salts is investigated. The general goal of this work is to delineate the delicate interplay of electrostatic and ion-specific effects that determines the swelling of the brush layer and the colloidal stability of the particles.

## 2 Theory

### 2.1 Neutral spherical polyelectrolyte brushes

Dynamic light scattering (DLS) used here yields the hydrodynamic radius  $R_H$  measured in the highly dilute regime. As in our previous investigations,  $R_H$  can be used to derive the thickness  $L$  of the brush layer affixed to the core particles having the radius  $R$  by  $L = R_H - R$  [26,27]. Hence, the present investigation of the SPB by DLS leads to the overall thickness of the brush layer as a function of the ionic strength. In this way, the data obtained here can directly be compared to studies of planar systems. A possible electroviscous effect [35,36] can safely be dismissed because most of the counterions are confined within the brush layer (cf. Refs. [37–39] and further citations given there). The measured  $R_H$  derived from the diffusion coefficient is therefore directly the outer radius of the particles, in agreement with recent rheological studies of these and comparable systems [40,41].

As shown in previous studies [26,27] the dependence of  $L$  measured from SPB can be modeled by the modified Daoud-Cotton [42] model developed for uncharged systems and adapted to polyelectrolyte brushes by Russel and coworkers [18,19,29]. In this model the spherical polyelectrolyte brushes are described by a sphere of radius  $R$  onto which  $p$  linear chains are grafted with a grafting density  $\sigma$ . In the brush limit the average distance between the chains is much smaller than the contour length of the chains. The

modeling of the chains is done in terms of blobs of diameter  $\xi(r)$ , where  $\xi(r)$  varies linearly with the radial distance  $r$  from the surface such that  $(1/4)\pi p \xi^2(r) = 4\pi r^2$ . From this it follows in good approximation that:

$$\xi \approx \frac{r}{R\sqrt{\sigma}}. \quad (1)$$

In a good solvent  $\xi$  and the number of Kuhn segments per blob  $N_\xi$  depend on the excluded-volume parameter  $v$  and on the Kuhn length  $l_K$  of the chains through [43]

$$\frac{\xi}{l_K} \approx N_\xi^{3/5} \left( \frac{v}{l_K^3} \right)^{1/5}. \quad (2)$$

The segment density inside a blob is  $\rho = 6N_\xi/\pi\xi^3$ , and the total number of segments within the layer of thickness  $L$  is given by [18]:

$$pN = 4\pi \int_R^{R+L} r^2 \rho(r) dr, \quad (3)$$

where  $N$  is the total number of statistical segments per attached chain. Insertion of equations (1) and (2) into equation (3) and subsequent integration lead to

$$\left( \frac{L}{R} + 1 \right)^{5/3} = 1 + K \frac{L_c}{R} \left( \frac{\sigma v}{l_K} \right)^{1/3}. \quad (4)$$

Here  $L_c$  is the contour length of the chains and  $K$  is a constant of the order unity. Equation (4) hence provides the relation between the brush thickness  $L$  and the ratio  $v/l_K$ .

A detailed discussion of equation (4) and its possible limitations was given by Hariharan, Biver, and Russel [19]. It provides a good description for experimental data in case of neutral brushes [18, 19]. Moreover, it can be used for spherical polyelectrolyte brushes in the presence of high concentrations of added salt, that is, if the electrostatic interaction between the segments is strongly screened [19, 29, 26, 27].

Following the suggestion of Hariharan *et al.*, equation (4) may be rearranged by elementary steps to yield [29]

$$\left( \frac{v}{l_K l^2} \right)^{1/3} \approx \frac{R}{L_c (l^2 \sigma)^{1/3}} \left[ \left( \frac{L}{R} + 1 \right)^{5/3} - 1 \right] \quad (5)$$

if the constant  $K$  is equated to unity. Here  $l$  is the bare Kuhn length of the respective polyelectrolyte chains. For a high ionic strength,  $l_K = l$  and the reduced excluded-volume parameter  $v/l^3$  can be obtained by use of this equation directly from experimental data. For low ionic strength,  $v$  and  $l_K$  depend on  $c_a$  and the evaluation of the data must include this effect as shown in the following.

## 2.2 Charged spherical polyelectrolyte brushes

If the amount of added salt is lowered, *i.e.*, for lower ionic strength, however, the Kuhn length  $l_K$  and the excluded-volume parameter  $v$  become explicit functions of the ionic

strength. The resulting treatment has been developed by Hariharan *et al.* [29] and discussed in detail recently [26, 27]. It proceeds in two steps:

i) The counterions are assumed to remain in the brush. This approximation is well supported by a recent experimental study in which the osmotic pressure of a solution of SPB has been measured [37]. Here, it was found that 95 to 98% of the counterions are osmotically inactive, only 2 to 5% of the counterions may hence leave the brush layer. This is in agreement with recent theoretical deductions [38]. For the present treatment it may therefore safely be assumed that the charges of the polyelectrolyte chains within the brush are exactly balanced by the counterions. Thus, the average concentration of salt  $c_s$  present in the brush layer may be calculated as a Donnan equilibrium between two macroscopic osmotic cells [29].

ii) The polyelectrolyte chains constituting the brush layer are highly charged, that is, the distance  $l_c$  between two charges along the chain is smaller than the Bjerrum length  $l_B$  ( $= 0.714$  nm in  $\text{H}_2\text{O}$  at  $25^\circ\text{C}$ ). Counterion condensation [44, 45] will take place until  $l_c = l_B$ . Therefore it will be assumed that only charges separated by a distance  $l_B$  will be effective, all other charges are assumed to be condensed and will not contribute to the ionic strength in the brush layer [29]. The local ionic strength  $c_s$  (in molar units) within the brush thus follows from the salt concentration  $c_a$  in the system by [29]:

$$c_s = \frac{1}{2} \sum_i \frac{n_i z_i^2}{N_L} = c_a \left[ 1 + \left( \frac{z \bar{\rho}_f}{2e N_L c_a} \right)^2 \right]^{1/2}, \quad (6)$$

where  $n_i$  is the number density of ions of species  $i$ ,  $z_i$  is the valency of the respective ions,  $N_L$  is Avogadro's number,  $e$  the unit charge, and  $z = z_+ = -z_-$ , because we assume a symmetric electrolyte.  $\bar{\rho}_f$  is the average charge density within the brush

$$\bar{\rho}_f = - \sum_i e z_i n_i = \frac{3e R^2 \sigma L_c}{l_B [(R+L)^3 - R^3]}. \quad (7)$$

With these two assumptions the parameters  $v$  and  $l_K$  may now be related to the local ionic strength  $c_s$  that follows from equation (6). Therefore, the ratio  $v/l_K l^2$ , as determined by equation (5), should be a universal function of the Debye length  $\kappa^{-1}$  for the range where the electrostatic repulsion between the chains dominates the measured brush thickness  $L$ .

## 3 Experimental

The cationic spherical polyelectrolyte brushes termed LA1, LA2 and LA3 were synthesized and characterized as described recently [28]. Figure 1 displays the chemical structure of the poly(2-(acryloyl)ethyltrimethylammonium chloride) (PATAC). All pertinent parameters, namely, the core radius  $R$ , the contour length  $L_c$  of the attached chains as well as the grafting density  $\sigma$  (number of chains per unit area) are known from this analysis.

**Table 1.** Properties of the quenched spherical polyelectrolyte brushes used in this study.  $R$ : radius of the core particles;  $L_c$ : contour length of the grafted chains;  $\sigma$ : grafting density of the chains. The data of the systems LQ6 and LQ7 have been taken from reference [27].

Charge	Label	$R$ (nm)	$L_c$ (nm)	$\sigma$ (nm $^{-2}$ )	$L_c/R$
Positive	LA1	45	84	0.050	1.87
Positive	LA2	45	116	0.049	2.57
Positive	LA3	49	149	0.052	3.04
Negative	LQ6	68	165	0.027	2.43
Negative	LQ7	54	141	0.031	2.61

Table 1 gathers these data for the SPB LA2 and LA3. Moreover, these systems have been scrutinized by AFM recently [28]. For a comparison with anionic systems of a quenched SPB we use the data obtained previously [27]. We choose two systems termed LQ6 and LQ7 (see Tab. 1 of Ref. [27]) which are comparable to the cationic systems under scrutiny here. Table 1 displays the characteristic data of these SPB for a comparison.

DLS measurements at different pH and salt concentrations were done as described in references [26,27] using a Peters ALV 4000 light scattering goniometer. In all cases the correlation function has been checked carefully in order to avoid possible disturbances by the onset of aggregation.

From these data the hydrodynamic radius  $R_H$  was calculated using the Stokes-Einstein relation. Here, the viscosity of the respective salt solutions has been used. In particular, concentrated aqueous solutions of  $MgSO_4$  exhibit a much higher viscosity than pure water [46]. Hence, adding 1 mol/l  $MgSO_4$  to water increases the viscosity by a factor of 1.706. This increased background viscosity must be taken into account when deriving the hydrodynamic radius  $R_H$  from the diffusion coefficient as obtained by DLS.

A suspension of the SPB is diluted by the respective salt solution to obtain particle concentrations of the order of 10 ppm. In this way the change of the salt concentration of the system by adding the latex can safely be neglected. Water was purified by reverse osmosis (Millipore Milli-RO) and subsequent ion exchange (Millipore Milli-Q).

## 4 Results and discussion

### 4.1 Dependence of $L$ on ionic strength

The first goal of this study is the comparison of the swelling of SPB bearing positive or negative charge. Hence, the thickness  $L$  (see Fig. 1) is deduced by dynamic light scattering for highly diluted solutions of the SPB. The parameter is the concentration of salt  $c_a$  added to these solutions, that is, the ionic strength in the system. From pure electrostatics there should be no difference between cationic and anionic brushes, of course. The

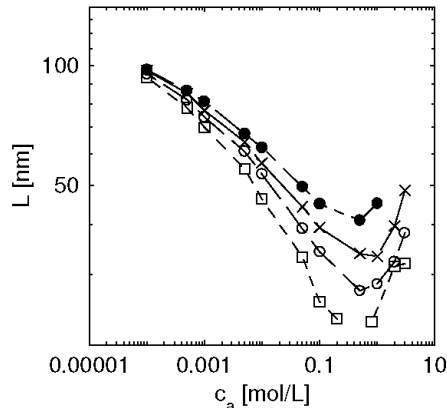


**Fig. 2.** Thickness  $L$  of the brush layer (cf. Fig. 1) as a function of the concentration  $c_a$  of monovalent counterions in solution. Filled circles: LA2 in NaF solution; crosses: LA2 in NaCl solution; open circles: LA2 in NaBr solution, open quadrangles: LA2 in NaI solution. For the characterization of the system LA2, see Table 1. The dashed lines are only guidelines. In case of iodide counterions, the particles precipitate from solution for salt concentrations above 0.1 mol/l. However, still higher iodide concentrations lead to stable solutions again.

theoretical treatment summarized in the preceding sections should hold true for both cases. Moreover, this theory makes no explicit difference between mono- or multivalent counterions but includes this only in the calculation of the ionic strength and of the Debye length  $\kappa^{-1}$  within the brush layer. This is immediately obvious from equation (6). Equation (5) then predicts that the reduced excluded-volume parameter  $v/(l_K l^2)$  should become a universal function of  $\kappa^{-1}$ , as discussed previously for the case of the anionic systems [27]. This comparison tests therefore the validity of equations (6) and (5) at the same time. The underlying assumptions are rather stringent and a number of simplifications had to be introduced. However, the data obtained on the anionic systems in reference [27] validated the model in a semi-quantitative manner.

Figure 2 displays the data obtained for the systems LA2 under consideration here. Similar data have been obtained for the other cationic systems. While Figure 2 shows the data obtained in the presence of different monovalent counterions, Figure 3 displays the same comparison for solutions in which the ionic strength had been adjusted by the divalent sulfate counterions. In all cases to be discussed here symmetric salts have been used to avoid further complications. Hence, we used  $Mg^{2+}$  co-ions. Additional studies revealed that the co-ions have a minor influence on the observed brush thickness  $L$  observed by dynamic light scattering. In all cases the correlation function has been checked in order to validate the data obtained by dynamic light scattering. Data have only been included if the correlation function can be described by a single exponential.

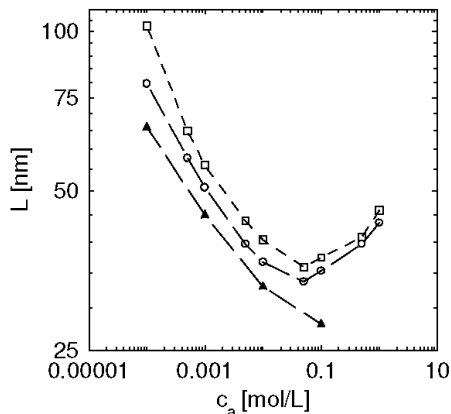


**Fig. 3.** Thickness  $L$  of the brush layer (cf. Fig. 1) as a function of the concentration  $c_a$  of  $\text{MgSO}_4$  in solution. Circles: LA2; quadrangles: LA3; filled triangles: the anionic system LQ7.

Both Figures 2 and 3 reveal that there are marked differences between cationic systems under scrutiny here and the anionic systems studied previously [26,27]. At low ionic strength, all systems exhibit the same strong decrease of  $L$  with increasing salt concentration  $c_a$  as expected.

A new surprising feature can be seen for all cationic systems at high ionic strength: Here the thickness  $L$  increases again for the systems LA2 and LA3 while the decrease with raising  $c_a$  is purely monotonous in case of the anionic systems LQ6 and LQ7 [27]. Different counterions have a different influence: The upturn in case of  $\text{Cl}^-$  ions seems to be more pronounced than in the case of  $\text{Br}^-$  or of  $\text{I}^-$ . The available range of concentrations was limited in case of  $\text{F}^-$  due to the limit of solubility of NaF. Moreover, in case of iodine counterions the shrinking of the brush layer is most pronounced around 0.1 mol/l. Raising the concentration beyond this point leads to flocculation and the particles are salted out. Here, even dilute solutions become turbid and no measurements can be done in this case. However, raising the concentrations of iodide counterions for the cationic system LA2 to still higher values leads to a salting-in and the particles become soluble again. Hence,  $L$  could be determined again at salt concentrations beyond 1 mol/l.

This strong decrease with increasing salt concentration and the raise at highest  $c_a$  is also seen in case of the divalent sulfate counterions where it shows up at smaller salt concentrations. The data are displayed in Figure 3. No precipitation is seen, however, as was observed in case of the  $\text{I}^-$  counterions. The cationic SPB LA2 and LA3 re-swell again at the highest salt concentrations. For the anionic systems LQ6 and LQ7, on the other hand, higher concentrations of magnesium sulfate lead to precipitation, as already observed in reference [27]. No salting-in can be observed for these systems and no data could therefore be obtained for the systems LQ6 and LQ7 beyond 0.1 mol/l

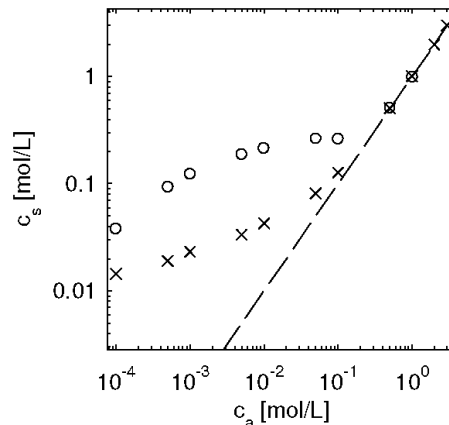


**Fig. 4.** Difference of the concentrations  $c_a$  and  $c_s$  according to equation (6). The circles mark the result obtained for the system LA3 in the presence of a divalent salt. Hence, these data refer to systems in the presence of  $\text{MgSO}_4$ . The crosses display the corresponding values of  $c_s$  if monovalent salt is added. The dashed line marks the points where  $c_s = c_a$ .

(see Fig. 3). Hence, both the anionic as well as the cationic systems exhibit specific effects solely related to the counterions. Evidently, these effects as the re-swelling at high salt concentrations cannot be related to ionic interactions that play no role at such a high ionic strength.

Obviously, there are two regimes of salt concentration for all counterions used here: The first regime is seen at low concentration of added salt where electrostatic interaction still dominates ( $c_a < 0.01$  mol/l). The second regime is seen when the salt concentration is above 0.1 mol/l. Here the electrostatic interaction is fully screened and specific interactions of the polyelectrolyte chains and the respective counterions prevail. Both regimes will be discussed in the following.

#### 4.2 Low ionic strength: Electrostatic interaction in brush layer

The evaluation of the data according to equation (5) requires the calculation of the average salt concentration  $c_s$  within the brush layer according to equation (6) [29,26,27]. Figure 4 displays the results of the calculation done for mono- and divalent counterions. Note that the experimental value of  $L$  is used in each case for this calculation which leads to a concomitant error of the data. The difference between the salt concentration  $c_a$  outside the brush layer and the concentration  $c_s$  inside the layer is negligible for high  $c_a$  as expected. Deviations become visible only if  $c_a < 0.1$  mol/l. Thus, the influence of electrostatic interaction can safely be dismissed for concentrations above this point as already discussed in the preceding section. Hence, in the following the reduced excluded-volume parameter  $v/(l_K l^2)$  will only be evaluated for  $c_a < 0.01$  mol/l.

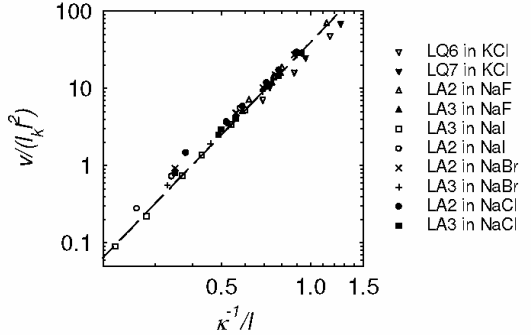


**Fig. 5.** Analysis of the thickness  $L$  of the brush at low ionic strength in the presence of monovalent ions: The ratio  $v/l_K l^2$  obtained from equation (5) is plotted as a function of the Debye length  $\kappa^{-1}$ . The legend gives the systems for which these data have been obtained. Note that this comparison comprises cationic systems (LA2, LA3) as well as anionic systems (LQ6, LQ7) (see Tab. 1). The dashed line marks a slope of 4. All data refer to small concentrations  $c_a$  of added salt ( $c_a \leq 0.01$ ).

Since all structural parameters of the system are known, the evaluation of the reduced excluded-volume parameter  $v/(l_K l^2)$  can be done for all  $L$  measured here and for the data obtained in reference [27]. Figure 5 displays the data obtained in the presence of monovalent salts. Here we restrict the data to  $c_a \leq 0.01$  in order to avoid any non-electrostatic contribution to  $v$ . Figure 6 shows the same parameter obtained in the presence of magnesium sulfate ions.

An important parameter entering this comparison is the bare Kuhn length  $l$  characterizing the backbone of the polyelectrolyte chains. No data are available for the PATAC chains constituting the brush layer of the cationic systems. For all systems under consideration here we used a single value, namely  $l = 2.8$  nm obtained for poly(acrylic acid) [47]. Here the bare Kuhn length  $l$  is just taken as a constant parameter since we aim at the dependence of  $v/(l_K l^2)$  on  $\kappa^{-1}$ . Using this value we include the data obtained previously for the anionic systems in the presence of  $\text{MgSO}_4$  [27].

Within the limits of error, all data for  $v/(l_K l^2)$  can be collapsed on a master curve if the ionic strength is low. This is obvious for monovalent ions (see Fig. 5) and for the divalent magnesium sulfate ions (see Fig. 6). This result corroborates nicely the previous findings obtained solely for different anionic systems [27]. It demonstrates that the strong de-swelling of the SPB in the regime of small concentrations  $c_a$  of added salt is solely due to the screening of the electrostatic interactions. Moreover, the data displayed in Figures 5 and 6 show that this screening is well captured in term of a single parameter, namely  $v/(l_K l^2)$ .

The dashed lines in Figures 5 and 6 mark a slope of 4 which is slightly higher than that found in the previous analysis of the data obtained from anionic systems [27]. This may be due to the fact that only data at low ionic strength have been taken into account for the present anal-

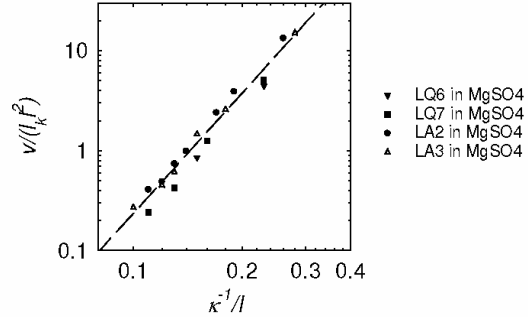


**Fig. 6.** Analysis of the thickness  $L$  of the brush at low ionic strength in the presence of divalent ions: The ratio  $v/l_K l^2$  obtained from equation (5) is plotted as a function of the Debye length  $\kappa^{-1}$ . This figure summarizes all data obtained for divalent counterions. The legend gives the systems for which these data have been obtained. Note that this comparison comprises cationic systems (LA2, LA3) as well as anionic systems (LQ6, LQ7) (see Tab. 1). The dashed line marks a slope of 4. All data refer to small concentrations  $c_a$  of added salt ( $c_a \leq 0.001$ ).

ysis (cf. Fig. 10 of Ref. [27]). A more detailed analysis of  $v/(l_K l^2)$  obtained on a similar system was recently given by Hariharan *et al.* [29]. These authors calculated the excluded-volume parameter  $v$  as well as the persistence length  $l_K$  from a detailed model explicitly taking into account the role of electrostatic repulsion (see the discussion of Fig. 5 in Ref. [29]). In view of the various assumptions that need to be made to arrive at equation (5) it seems to suffice to state that a master curve is obtained: The thickness  $L$  as a function of  $c_a$  can be understood in terms of purely electrostatic interaction.

The above analysis reveals a difference between mono- and divalent counterions: For a given value of  $\kappa^{-1}/l$  the value of  $v/(l_K l^2)$  is larger in the presence of divalent salts (see Fig. 6) than in case of monovalent salts (see Fig. 5). This difference is not predicted by the electrostatic model discussed in the section “Theory”, of course. The overall dependence of  $v/(l_K l^2)$  on  $\kappa^{-1}/l$  is preserved as suggested by Figure 6, however, and the swelling of the brush layer is determined solely by the electrostatic contribution to  $v/(l_K l^2)$ .

### 4.3 Specific interactions at high ionic strength

Figure 2 clearly reveals that different monovalent counterions lead to marked qualitative differences at high ionic strength. For all ions tested here, a strong decrease of  $L$  with  $c_a$  is seen, which is more pronounced when going from  $\text{F}^-$  to  $\text{I}^-$  ions. For  $\text{I}^-$  ions the strong decrease of the layer thickness is even followed by a precipitation of the particles. This fact points to a collapse transition within the brush layer: In case of  $\text{I}^-$  ions this collapse leads to the most dramatic shrinking of the brush so that the particles lose their colloidal stability and flocculate. However, for all ions a re-swelling takes place when  $c_a$  is still raised.

In case of  $I^-$  a salting-in is even observed. All ions therefore lead to the same overall behavior: With increasing salt concentration there is a screening of the electrostatic interaction and a worsening of the solvent power of the polyelectrolyte chains. At high salt concentrations the solvent power must increase again because the brush layer is re-swollen.

The salting-out and subsequent salting-in of cationic polyelectrolyte chains is in full accord with similar studies done on planar brushes by Biesalski, Johannsmann, and Rhe [15]. A comprehensive review has been given recently by Rhe and coworkers [6]. These authors studied the swelling of dense planar brushes composed of linear poly(4-vinyl[N-methyl-pyridinium]) chains. The height of the brush layer was measured by an optical technique in the presence of chloride, bromide, and iodide ions. While  $Cl^-$  lead to exactly the behavior expected for planar polyelectrolyte brushes [7,5],  $I^-$  lead to first a collapse and then a re-swelling of the brush layer. Evidently, the collapse transition as well as the re-swelling cannot be explained by electrostatic interaction. It is in full accord, however, with the behavior of the free polymer in solution [31].

The specific interactions of poly(4-vinyl[N-methyl-pyridinium]) with  $I^-$  chains was recently the subject of a comprehensive review by Volk *et al.* [34], who discussed the various factors influencing the salting-out and salting-in of poly(4-vinyl[N-methyl-pyridinium]). A possible explanation of the unexpected interaction of  $I^-$  with this particular polyelectrolyte might be sought in the formation of charge-transfer complexes. This would render the chains more hydrophobic and hence less water soluble. As for an explanation of the salting-in effect, Volk *et al.* discuss a charge reversal of the chains by the strong adsorptions of  $I^-$ .

In order to analyze our results obtained at high salt concentrations  $c_a$  in a semi-quantitative fashion, we evaluated the thickness  $L$  of the cationic systems LA1 to LA3 by use of equation (4) in order to obtain the reduced excluded-volume parameter  $v/l_K l^2$ . In this analysis the constant  $K$  has been equated to unity. Note that because of the high ionic strength  $l_K \approx l$ . Figure 7 displays the data thus obtained for a concentration of 0.5 M. The systems are not stable in iodide solutions of this concentration. Hence, the data shown in his figure refer only to  $F^-$ ,  $Cl^-$ , and  $Br^-$ . The same analysis is done for all other salt concentrations in which the particles proved to be stable. Good linearity is obtained within given limits of error. Hence, an estimate of the reduced excluded-volume parameter  $v/l_K l^2$  can be obtained from these plots. The slope of these straight lines is increasing when going from bromide to fluoride ions. This is in general agreement with the general trends of these ions in the Hofmeister series (see Ref. [33] and further citations given there). The efficiency of salting-out increases in the series  $F^- < Cl^- < Br^- < I^-$  (see also the discussion of Fig. 5 in Ref. [34]).

Figure 8 displays the reduced excluded-volume parameter  $v/l_K l^2$  obtained at high ionic strength from the

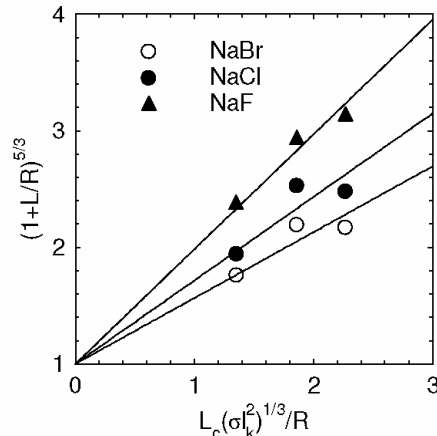


Fig. 7. Plots of the thickness  $L$  of the brush layer attached to the core particles according to equation (4). The concentration of the added salt was 0.5 M in all cases. The salt ions used in each case are indicated in the graph. Data referring to solutions with 0.5 M  $I^-$  could not be obtained because the particles are not stable under these conditions and flocculate (see the discussion of Fig. 2).

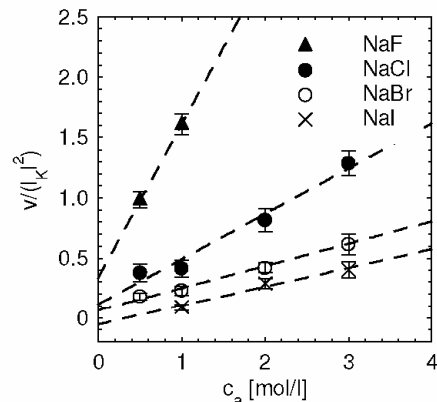


Fig. 8. The reduced excluded-volume parameter  $v/l_K l^2$  obtained at high ionic strength from the analysis of  $L/R$  as shown in Figure 7 as a function of the concentration  $c_a$  of added salt. The salt ions used in each case are indicated in the graph.

analysis of  $L/R$  as shown in Figure 7 as a function of the concentration  $c_a$  of added salt. Within the given limits of error,  $v/l_K l^2$  increases linearly with  $c_a$ . This finding points directly to the adsorption of the salt ions directly on the polyelectrolyte chains: Assuming an adsorption/desorption equilibrium between the free ions in solution and the ions bound to the chains, the amount of adsorbed ions should increase with the number of free ions. This requires that the number of adsorbed ions is not too high, *i.e.*, far below saturation. The data plotted in

Figure 8 supports this idea: The parameter  $v/l_K l^2$  reflects possible changes of  $v$  as well as of  $l_K$  with the adsorption of ions. If  $v$  could be measured alone, adsorption of ions would lead to a quadratic dependence of  $v$  on salt concentration as discussed by Currie *et al.* [48]. However, the reduced excluded-volume parameter  $v/l_K l^2$  depends also on  $l_K$  which may increase upon adsorption of ions, too. If one disregards the latter effect in a more qualitative discussion,  $v/l_K l^2$  gives mainly the balance between the repulsive and attractive interactions of the segments which is now changed by adsorption of ions. In case of smaller ions, *e.g.*,  $F^-$ , raising the concentration first leads to a stronger and stronger screening and to the concomitant decrease of  $L$ . Raising  $c_a$  further then leads to an increase of  $v/l_K l^2$  because of the adsorption of ions. This is followed by a re-swelling of the brush layer because of the increase of the size of the segments, *i.e.* of  $v$ . Hence, the variation of  $v$  through adsorption of ions would reasonably explain the results displayed in Figures 1 and 2.

In case of  $I^-$  a non-negligible attractive force between the segments must be invoked to explain the collapse of the surface layer and the subsequent flocculation. This is also reflected in the fact that  $v/l_K l^2$  vanishes for  $I^-$  around 0.5 M (see Fig. 8). Possible van der Waals interaction between the large  $I^-$  ions or dipole/dipole interactions may be held responsible for this attractive force which, together with the strong screening of the electrostatic repulsion, leads to a vanishing of  $v/l_K l^2$ . Evidently, the repulsive interaction prevails again at high salt concentrations and a salting-in takes place.

The data summarized in Figure 3 demonstrate that the divalent sulfate counterions lead to the same effect in the case of the cationic systems: First, there is a strong shrinking, already discussed in the preceding section, but high salt concentrations lead to a re-swelling of the layer. Here again the increase in  $v/l_K l^2$  through adsorption of ions may be invoked to explain this finding.

## 5 Conclusion

We have presented a comprehensive investigation of the swelling of cationic and anionic spherical polyelectrolyte brushes as a function of the ionic strength in the system. The ionic strength has been changed through the addition of mono- and divalent counterions. The interaction of the counterions with the cationic and the anionic brush layers may be classified as follows: At lowest ionic strength electrostatic interaction prevails and the brush layer is swollen in all cases by the osmotic pressure of the counterions. Intermediate salt concentrations lead to a partial screening of the electrostatic interaction and to a shrinking of the brush layer. This effect can be well captured by the theory of Hariharan *et al.* [29]. In case of cationic brushes, however, the shrinking becomes very pronounced around salt concentrations of 0.1 mol/l. In some cases there is even a collapse of the surface layer due to specific interactions between the polyion and the counterions. Cationic systems re-swell if immersed in concentrated salt solutions ("salting-in"). This is observed for monovalent as well

as for divalent counterions. The analysis of the reduced excluded-volume parameter  $v/(l_K l^2)$  suggests that there is an adsorption of the counterions at high salt concentrations. The increase of  $v/(l_K l^2)$  thus effected leads to the re-swelling of the brush layer. The salting-in behavior thus finds an explanation in the increase of  $v$  due to the adsorption of salt ions. All data demonstrate that specific effects of different counterions lead to a behavior of the brush layer not expected from a purely electrostatic model.

Financial support by the Deutsche Forschungsgemeinschaft, Sonderforschungsbereich 481 Bayreuth, by the Fonds der Chemischen Industrie, and by the BASF AG is gratefully acknowledged.

## References

1. G.J. Fleer, M.A. Cohen Stuart, J.M.H.M. Scheutjens, T. Cosgrove, B. Vincent, *Polymers at Interfaces* (Chapman and Hall, London, 1993).
2. P. Pincus, *Macromolecules* **24**, 2912 (1991).
3. O.V. Borisov, T.M. Birshtein, E.B. Zhulina, *J. Phys. II* **1**, 521 (1991).
4. F. Dubreuil, P. Guenon, *Eur. Phys. J. E* **5**, 59 (2001).
5. J. R uhe *et al.*, *Adv. Polym. Sci.* **165**, 79 (2004).
6. R. Konradi, H. Zhang, M. Biesalski, J. R uhe, in *Polymer Brushes*, edited by K. Caster (Wiley-VCH, Weinheim, 2004).
7. H. Ahrens, S. F orster, C.A. Helm, *Phys. Rev. Lett.* **81**, 4172 (1998).
8. M. Biesalski, J. R uhe, D. Johannsmann, *J. Chem. Phys.* **111**, 7029 (1999).
9. E.P. K. Currie, A.B. Sieval, M. Avena, H. Zuilhof, E.J.R. Sudh olter, M.A. Cohen Stuart, *Langmuir* **15**, 7116 (1999).
10. S.W. An, P.N. Thirtle, R.K. Thomas, F.L. Baines, N.C. Billingham, S.P. Armes, J. Penfold, *Macromolecules* **32**, 2731 (1999).
11. Y. Tran, P. Auroy, L.-T. Lee, *Macromolecules* **32**, 8951 (1999).
12. E.P. K. Currie, A.B. Sieval, G.J. Fleer, M.A. Cohen Stuart, *Langmuir* **15**, 7116 (1999).
13. Y. Tran, P. Auroy, *Eur. Phys. J. E* **5**, 65 (2001).
14. M. Biesalski, D. Johannsmann, J. R uhe, *J. Chem. Phys.* **117**, 4988 (2002).
15. M. Biesalski, D. Johannsmann, J. R uhe, *J. Chem. Phys.* **120**, 8807 (2004).
16. D. Bendejacq, V. Ponsinet, M. Joanicot, *Eur. Phys. J. E* **13**, 3 (2004).
17. M. Ballauff, in *Polymer Brushes*, edited by K. Caster (Wiley-VCH, Weinheim, 2004).
18. C. Biver, R. Hariharan, J. Mays, W.B. Russel, *Macromolecules* **30**, 1787 (1997).
19. R. Hariharan, C. Biver, J. Mays, W.B. Russel, *Macromolecules* **31**, 7506 (1998).
20. R.D. Wesley, T. Cosgrove, L. Thomson, S.P. Armes, N.C. Billingham, F.L. Baines, *Langmuir* **16**, 4467 (2000).
21. M. Moffit, K. Khougaz, A. Eisenberg, *Acc. Chem. Res.* **29**, 95 (1996).
22. N.S. Cameron, M.K. Corbierre, A. Eisenberg, *Can. J. Chem.* **77**, 1311 (1999).

23. F. Muller, M. Delsanti, L. Auvray, J. Yang, Y.J. Chen, J.W. Mays, B. Deme, M. Tirell, F. Guenon, *Eur. Phys. J. E* **3**, 45 (2000).
24. S. Förster, N. Hermsdorf, Ch. Böttcher, P. Lindner, *Macromolecules* **35**, 4096 (2002).
25. X. Guo, A. Weiss, M. Ballauff, *Macromolecules* **32**, 6043 (1999).
26. X. Guo, M. Ballauff, *Langmuir* **16**, 8719 (2000).
27. X. Guo, M. Ballauff, *Phys. Rev. E* **64**, 051406 (2001).
28. Y. Mei, A. Wittmann, G. Sharma, M. Ballauff, Th. Koch, H. Gliemann, J. Horbach, Th. Schimmel, *Macromolecules* **36**, 3452 (2003).
29. R. Hariharan, C. Biver, W.B. Russel, *Macromolecules* **31**, 7514 (1998).
30. J.M. G. Barthel, H. Krienke, W. Kunz, *Physical Chemistry of Electrolyte Solutions, Modern Aspects* (Springer, Heidelberg, 1998).
31. M. Beer, M. Schmidt, M. Muthukumar, *Macromolecules* **30**, 8375 (1997).
32. I. Sabbagh, M. Delsanti, *Eur. Phys. J. E* **1**, 75 (2000).
33. See the recent reviews, in W. Kunz, P. Lo Nostro, B.W. Ninham, *Curr. Opin. Colloid Interface Sci.* **9** (2004).
34. N. Volk, D. Vollmer, M. Schmidt, W. Oppermann, K. Huber, *Adv. Polym. Sci.* **166**, 29 (2004).
35. W.B. Russel, D.A. Saville, W.R. Schowalter, *Colloidal Dispersions* (Cambridge University Press, Cambridge, 1989).
36. See the discussion of electroviscous effects, in M. Kollmann, G. Naegelé, *J. Chem. Phys.* **113**, 7672 (2000).
37. B. Das, X. Guo, M. Ballauff, *Prog. Colloid Polym. Sci.* **121**, 34 (2002).
38. A. Jusufi, C.N. Likos, M. Ballauff, *Colloid Polym. Sci.* **282**, 910 (2004).
39. W. Groenewegen, A. Lapp, S.U. Egelhaaf, J.R.C. van der Maarel, *Macromolecules* **33**, 4080 (2000).
40. K.A. Vaynberg, N.J. Wagner, *J. Rheol.* **45**, 451 (2001).
41. A. Marra, E. Peuvrel-Disdier, A. Wittmann, X. Guo, M. Ballauff, *Colloid Polym. Sci.* **281**, 491 (2003).
42. M. Daoud, J.P. Cotton, *J. Phys. (Paris)* **43**, 531 (1982).
43. P.G. de Gennes, *Scaling Concepts in Polymer Physics* (Cornell University Press, Ithaca, New York, 1979).
44. G. Manning, *Annu. Rev. Phys. Chem.* **23**, 117 (1972).
45. See the discussion of this point, in M. Deserno, Ch. Holm, J. Blaul, M. Ballauff, M. Rehahn, *Eur. Phys. J. E* **5**, 97 (2001).
46. M.D. Lechner, *Physikalisch-chemische Daten*, Band 1 (Springer-Verlag, 1992).
47. M. Tricot, *Macromolecules* **17**, 1700 (1984).
48. E.P. K. Currie, G.J. Fleer, M.A. Cohen Stuart, O.V. Borisov, *Eur. Phys. J. E* **1**, 27 (2000).

### **3.3 Interaction of spherical polyelectrolyte brushes with CaCO<sub>3</sub> and cellulose fibers.**

#### **Mechanistic studies and their application in papermaking**

**Y. Mei<sup>1</sup>, C. Abetz<sup>2</sup>, O. Birkert<sup>3</sup>, V. Schädler<sup>4</sup>, R. J. Leyrer<sup>3</sup>, M. Ballauff<sup>1\*</sup>**

*1. Lehrstuhl für Physikalische Chemie I, University of Bayreuth, 95440 Bayreuth, Germany*

*2. Bayreuther Institut für Makromolekülforschung, University of Bayreuth, 95440 Bayreuth, Germany*

*3. Polymerforschung, BASF Aktiengesellschaft, 67056 Ludwigshafen, Germany*

*4. ISIS, 8 allée Gaspard Monge, 67083 Strasbourg, France*

*\* Email of corresponding author: [matthias.ballauff@uni-bayreuth.de](mailto:matthias.ballauff@uni-bayreuth.de)*

#### **Abstract**

Here we present a comprehensive study of the interaction of spherical polyelectrolyte brushes (SPB) with cationically modified polyacrylamide, CaCO<sub>3</sub> particles and cellulose fibers. A link to the use of this system as a model for retention aids in the papermaking process is elaborated: Anionically functionalized spherical polyelectrolyte brushes with a high cation exchange capacity are used together with cationically modified polyacrylamide as model system for fiber flocculation and deposition of CaCO<sub>3</sub> which are integral steps in the papermaking process. The flocculation efficiency is tested by means of a dynamic drainage jar. Field emission scanning electron microscopy (FESEM) and atomic force microscopy (AFM) are used to analyze the system, the structure of the agglomerated flocs and the mechanism of floc formation. The data suggest that the flocculation efficiency can be attributed to a high cation exchange capacity of SPB in combination with a flexibility of grafted polyelectrolyte chains. FESEM images and AFM support the model of anionic SPB's acting as a particle bridge between fibers and CaCO<sub>3</sub>.

## 1. Introduction

Polyelectrolyte brushes are systems in which polyelectrolyte chains are densely attached to a planar or curved surface. Since the first seminal papers of Pincus [1] and of Borisov, Birshtein and Zhulina [2] in 1991 these systems have been the subject of numerous theoretical studies. Up to now, it has been shown that polyelectrolyte brushes can dramatically affect the surface properties of a surface such as adhesion [3], lubrication [4], wettability [5], friction [6] and biocompatibility [7] etc. Furthermore, colloidal particles with attached polyelectrolyte brushes may greatly enhance their stability against flocculation [8]. On the other hand, SPB can be considered as flocculation agent of potentially high efficiency provided that the charged brushes interact with an appropriate counterpart in a multi-component flocculation system. In the present paper we will focus on the use of SPB in such a multi-component system in which charged particles are flocculated in an aqueous environment. The retention of  $\text{CaCO}_3$  and cellulose fibers is the main purpose in the paper making process. Controlling electrostatic interactions and their dynamics in fiber and filler flocculation is one of the key to modern papermaking.

Simply speaking, papermaking can be viewed as a dewatering process of a dilute pulp suspension on a sieve. The average mesh size of a dewatering sieve is of about the same dimension as the cellulose fibers. However, large amount of particles that are much smaller than the average mesh size are present in industrial pulp slurry, such as fiber fragments (fines) and fillers, mostly ground  $\text{CaCO}_3$  (GCC). PCC and kaolin are also very common fillers and PCC is actually taking over from GCC. Typical GCC slurry contains particles of ca. 1-5  $\mu\text{m}$  average diameter. In order to retain fines and fillers during the dewatering process on the coarse sieve, so-called retention-aids are used. These retention-aids induce flocculation of fibers, fillers and fines in a complex slurry in which further components such as dyes, sizing agents or impurities from recycled (deinked) paper etc. may be present [9]. In the search for more efficient flocculants dual-component retention systems have proven to be particularly interesting. All dual systems consist of two strongly interacting polymers or colloidal particles, which are added to the stock subsequently. In many cases dual component flocculation systems exhibit stronger flocculating ability than the corresponding single-component retention systems [10-13]. The mechanism explaining this high efficiency is not fully understood. The primary interaction between the two components in the dual system may either be based upon strong hydrogen-bonding [14] or electrostatic interaction [12, 13, 15]. Another important motivation for the papermaker to use dual rather than single component systems is that they tend to

cause flocculation into much finer and denser flocs, thus creating paper sheets of better optical appearance due to high homogeneity (so-called formation).

Currently, the most popular dual flocculation system is the so-called microparticle system, consisting of a high molecular weight primary retention aid in combination with a colloidal particle that usually carries the opposite charge. Typical primary flocculants are copolymers of acrylamide and cationically charged comonomers, or cationically modified starches. As the second component colloidal silica [19, 20] or montmorillonite (bentonite) types of layered silica are frequently used. Compared with conventional single- and other dual-component retention systems, the microparticle retention system shows many significant advantages [21-23], including increased retention and drainage with no sacrifice in formation and better performance even in the presence of high concentrations of interfering substances. Most of the advantages can be attributed to compact flocs resulting in an open and uniform sheet formation [24].

In order to obtain deeper insight into dual flocculation systems, it is necessary to use model systems that show well-defined surface characteristics. Here we present a comprehensive study of the interaction of spherical polyelectrolyte brushes with  $\text{CaCO}_3$  particles and model cellulose fibers. Anionically functionalized spherical polyelectrolyte brushes and cationically modified polyacrylamide are used as efficient model compounds to achieve fiber flocculation and deposition of  $\text{CaCO}_3$ . Field emission scanning electron microscopy (FESEM) and atomic force microscopy (AFM) are used to analyze the final floc structure.

## 2. Experimental Section

### 2.1. Materials

Ground calcium carbonate (Hydrocarb OG) obtained from OMYA GmbH was used without further treatments: 60 wt% of the particles are less than 2  $\mu\text{m}$  in diameter. This material is wet-ground in the presence of a polyacrylic dispersing agent and then sprays dried [25]. Bentonite for water-based systems (Fluka) was used as received. The cation exchange capacity (CCE) of this material given by the supplier is 0.80 meq/g. As primary flocculation agent cationically modified polyacrylamide (CPAM) was used: Polymin<sup>®</sup> KP 2515 provided by BASF Aktiengesellschaft had a charge density of 1.7 meq/g.

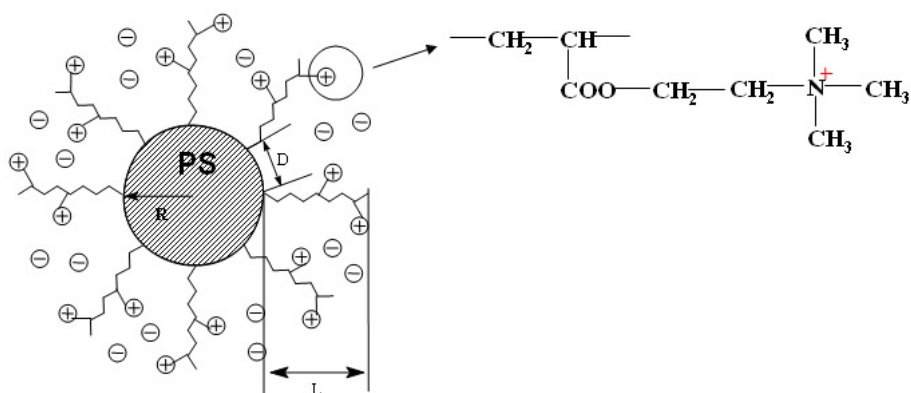


Figure 1. Schematic structure of cationic SPB with PATAc brush

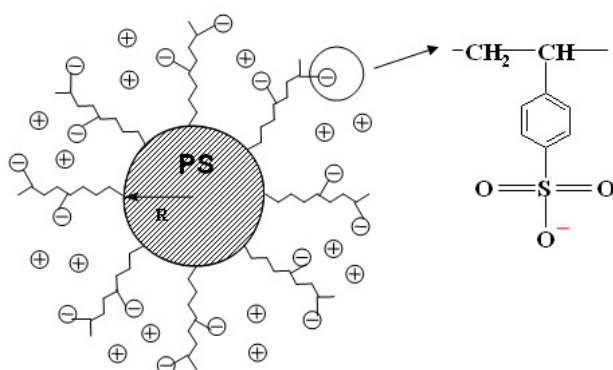


Figure 2. Schematic structure of anionic SPB with PSS brush

Cationic and anionic spherical brushes were synthesized and characterized as described recently [26, 27]. Figure 1 and 2 show the chemical structure of poly(2-(acryloyloxy)ethyltrimethylammonium chloride) (PATAc) and poly(styrene sulfonate) (PSS) brushes, respectively. All pertinent parameters, namely the core radius of polystyrene ( $R$ ), the contour length ( $L_c$ ) of the attached chains as well as the grafting density ( $\sigma$ ; number of chains per unit area) are known from the analysis [26], table 1 gathers these data for the SPB LA2, LB1 and LB2. Detailed studies of the spherical polyelectrolyte brush systems were performed by atomic force microscopy [26], rheology [28], dynamic light scattering [29], and small angle X-ray scattering [30].

The model system of pulp slurry selected for the retention experiments was composed of 30% ground calcium carbonate and 70% bleached chemical fibers, which consisted of 70% birch sulphate (SR 33°) and 30% pine sulphate (SR70°). The final concentration of pulp slurry was adjusted to 0.8 wt%, pH was set to 8.1. The pulp slurry was prepared in BASF AG and used within 24 hours.

**Table 1.** Characterization of the SPB LA2, LB1 and LB2

Label	Charge	Brush	R [nm]	L <sub>c</sub> [nm]	M <sub>η</sub> [g/mol]	σ [nm <sup>-2</sup> ]	D [nm]	L <sub>c</sub> /R	CEC [meq/g]
LA2	positive	PATAC	45	116	89700	0.049	5.1	2.57	-
LB1	negative	PSS	58	103	84300	0.065	4.4	1.78	1.50
LB2	negative	PSS	25	141	115800	0.040	5.6	5.64	2.27

*R*: core radius of polystyrene;

*M<sub>η</sub>*: molecular weight of grafted chains as determined by viscosimetry;

*L<sub>c</sub>*: contour length of grafted chains determined from *M<sub>η</sub>*;

*σ*: graft density on surface of core particles;

*D*: the average distance between two neighbouring graft points;

*CEC*: cation exchange capacity.

## 2.2. Methods

### 2.2.1. Dynamic Drainage Jar

The dynamic drainage jar (DDJ) is a common and reliable tool to evaluate retention and drainage of single or multi-component flocculation systems under conditions which are quite similar to large-scale paper making processes. Importantly, the DDJ can simulate the impact of shear as induced e.g. by screens in paper machines [31]. In the present work a DDJ with a 200-mesh bottom screen; and an impeller speed of 400 or 900 rpm was used.

The retention efficiency of each flocculation system is quantified using the so-called first pass retention (FPR) and the corresponding ash retention (AR) defined as follows [32-34]:

$$FPR = \frac{C_i - C_0}{C_i} \times 100\%$$

$$AR = \frac{A_i - A_0}{A_i} \times 100\%$$

where *C<sub>i</sub>* and *C<sub>0</sub>* are the concentration of colloidal particles in the stock before drainage and in the filtrate, respectively. *C<sub>i</sub>* and *C<sub>0</sub>* are obtained by filtering the respective suspension using a filter paper and weighing the fully dried filtrate. *A<sub>i</sub>* and *A<sub>0</sub>* are the total inorganic (“ash”) content of the stock before drainage and in the

filtrate respectively. The latter is determined by incineration the filtrated material at 500°C for 5 hours.

In a typical flocculation sequence 0.04% CPAM (wt% with respect to solid pulp) was added into the 0.8 wt% paper suspension in order to induce agglomeration of fibers and fillers. Subsequently, shear of 900 rpm was applied for 20 s, inducing partial break-down of the primary flocs. Then, bentonite or SPB was added at a amount between 0 and  $3.2 \times 10^{-2}$  g/l (0 to 0.40 wt% with respect to the solid contents in the primary pulp suspension). During the addition of the SPB (or bentonite) the mixture was stirred at 400 rpm for 15 s, at which again formation of flocs in the pulp suspension occurred. Stirring continued during the drainage.

### **2.2.2. Field Emission Scanning Electron Microscopy (FESEM)**

Field Emission Scanning Electron Microscopy is a powerful tool for topographic analysis. It produces clearer, less electrostatically distorted images with generous depth of field and ultrahigh spatial resolution down to a few nanometers. With special detectors not only topographic information but also compositional information can be obtained. FESEM is suitable for the observation of the surface of fibril aggregates [35].

In order to get clearer images from FESEM, the retention test mentioned above was repeated in a smaller scale, namely 0.2% fibers and 0.1% CaCO<sub>3</sub> fillers. CPAM, SPB and bentonite were kept in the same weight concentrations in relation to solid contents of pulp slurry. Floc samples collected from each stage of retention test were dried in air and coated with a very thin layer (circa 1nm) of platinum to get electric conductivity and captured by FESEM Leo1530. All the measurements were performed in the Bayreuther Institut für Makromolekülforschung of Bayreuth University.

### **2.2.3. Atomic Force Microscopy (AFM)**

AFM measurements were performed using the NanoScope IIIa (Digital Instruments Inc.) to investigate the morphology of the fiber surfaces. The images were scanned in tapping mode in air using commercial Si cantilevers (Digital Instruments Inc.) with a resonance frequency of 320 kHz. Images of at least four different areas were scanned for each sample. The images show unfiltered original data. All the AFM data in this article show typical morphology which is representative for the corresponding sample.

The samples used for AFM were prepared as for the FMSEM except of coating with platinum. A droplet of 40  $\mu\text{L}$  of pulp slurry containing the respective SPB particles,  $\text{CaCO}_3$  Filler and fibers was put onto a freshly cleaved mica surface (muscovite white mica, Plano GmbH) and dried in air. All the measurements were performed in the Lehrstuhl für Physikalische Chemie II of Bayreuth University.

### 3. Results and Discussion

#### 3.1. Cationic and Anionic Spherical Polyelectrolyte Brushes as Dual-Component Retention-Aid

Figure 3 and 4 show FPR and AR with different retention-aids. Without any additive, the FPR and AR are at a very low level. The FESEM image Figure 5a shows the distribution of negatively charged fibers and  $\text{CaCO}_3$  without any additive. The micrograph reflects the fact that in the dilute a pulp slurry fibers and  $\text{CaCO}_3$  are well dispersed without large agglomerates of pigments and fines. The lack of agglomeration as observed on the mica surface is in agreement with the very low retention value as shown in Figure 3 at low additive concentration.

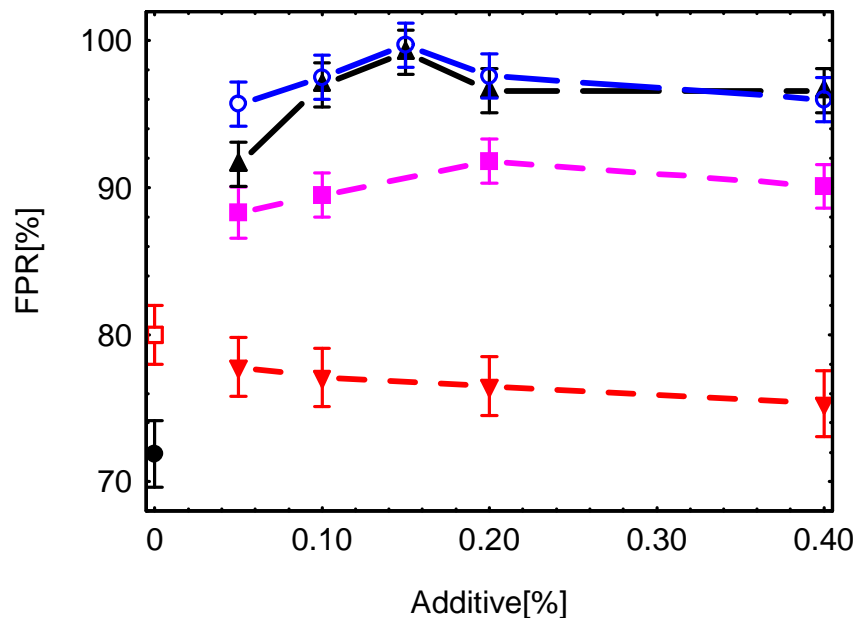


Figure 3. First-pass-retention in presence of different retention-aids. The dashed lines are guides to the eye.

- = blank experiment, without any additive;
- =0.04% CPAM;
- =0.04% CPAM with varying amounts of LB2;

- ▲=0.04% CPAM with varying amounts of LB1;
- =0.04% CPAM with varying amounts of bentonite;
- ▼=0.04% CPAM with varying amounts of LA2.

High molecular weight CPAM is an effective flocculation agent and can be used as single-component retention-aid [36, 37]. The used CPAM Polymin<sup>®</sup> 2515 shows strong flocculating ability in the retention experiments. With only 0.04% dosage, the AR was evidently improved from 19.4% to 43.3% (see Figure 4). The increase in FPR and AR due to addition of CPAM must be due to an agglomeration process in which mainly CaCO<sub>3</sub> is involved: either by forming CaCO<sub>3</sub> agglomerates or by binding onto the fiber surface. In Figure 5b the formation of large CaCO<sub>3</sub> agglomerates can be clearly seen. Note that the size of an entire agglomerate with a three-dimensional network structure is so big that only a minor part is shown in the FESEM image in Figure 5b.

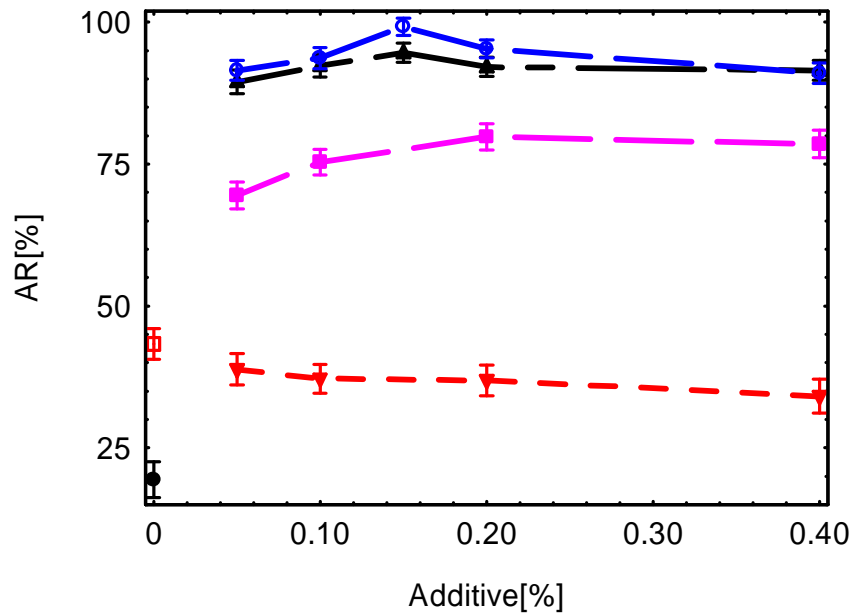


Figure 4. Ash-retention in the presence of different retention-aids. The dashed lines are guides to the eye.

- = blank experiment, without any additive;
- =0.04% CPAM;
- =0.04% CPAM with varying amounts of LB2;
- ▲=0.04% CPAM with varying amounts of LB1;
- =0.04% CPAM with varying amounts of bentonite;
- ▼=0.04% CPAM with varying amounts of LA2.

The effect of shear upon the agglomerate effect can be clearly seen by comparing Figure 5b and 5c: A large number of  $\text{CaCO}_3$  aggregates that have been attached to fibers appear as separate agglomerates on the mica surface in Figure 5c, indicating that they have been detached via shear forces.

The classical microparticle system consisting of bentonite and CPAM shows high performance in both retention and drainage. As shown in Figure 3 and 4, the FPR and AR reach a maximum of 91.8% and 79.8%, respectively. Hence, the obtained retention criteria are much better than that of CPAM used alone. Although a few free  $\text{CaCO}_3$  particles are still seen in the Figure 5d, most of them are now linked to fibers.

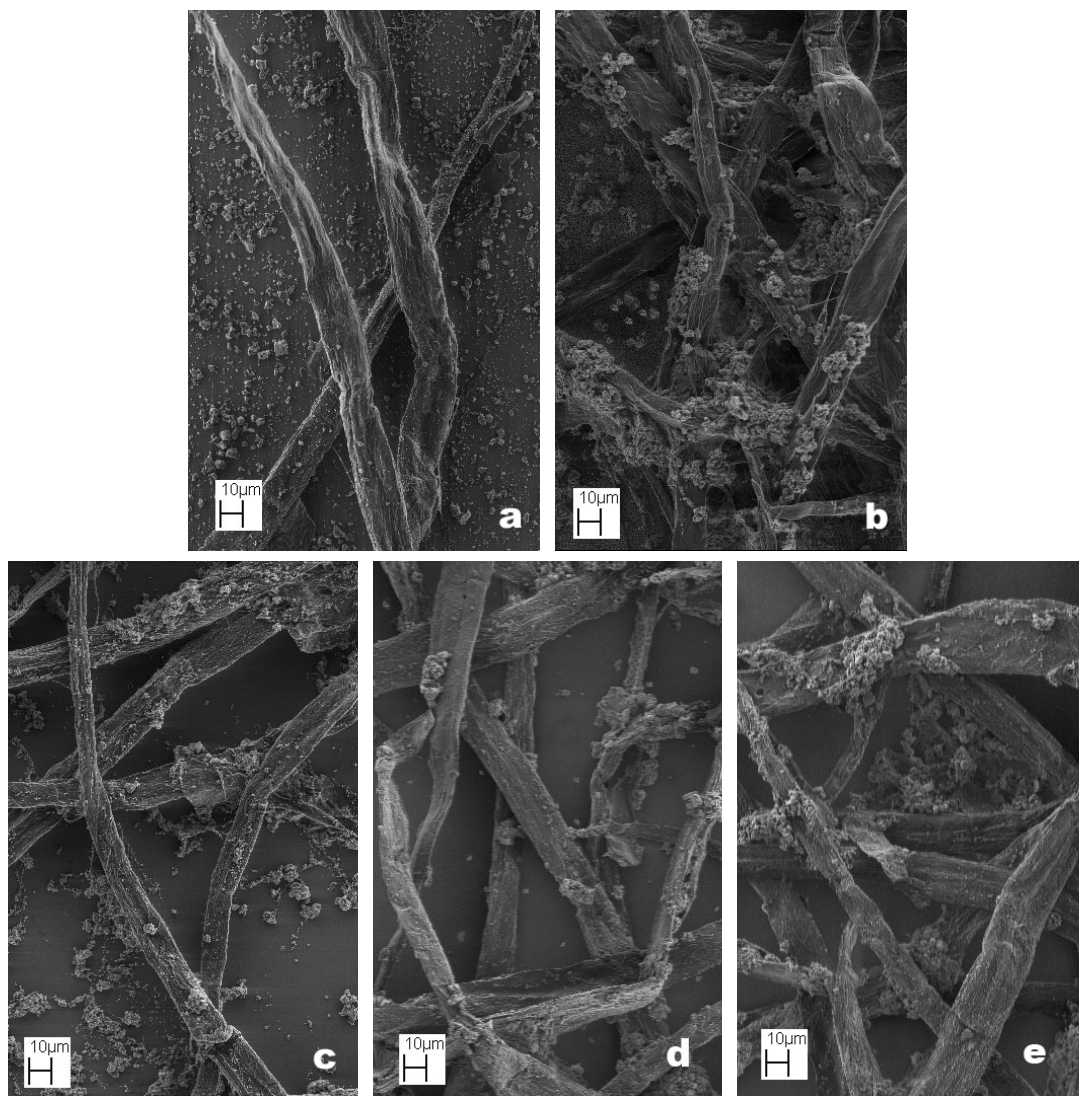


Figure 5. FESEM images of fibers and  $\text{CaCO}_3$  particles at different stages of retention test.

- (a). Fibers and  $\text{CaCO}_3$  without any additive;
- (b). Agglomerate caused by CPAM;
- (c). Influence of shear after (b);

- (d). Agglomerate caused by addition of bentonite after shear (c)
- (e). Agglomerate caused by addition of SPB LB2 after shear (c)

In analogy to the bentonite-based microparticle system CPAM is now combined with anionic SPB (LB1 or LB2) to give excellent drainage and retention, as shown in Figure 3 and 4. Note that similarly as bentonite, LB1 and LB2 exhibit a significant excess of anionic charges at their surface. In the case of SPB LB2 as dual system in combination with CPAM the FPR and AR were increased to 99.7% and 99.2%, respectively, which means nearly all the raw materials remain in paper sheets. Comparison of the FESEM micrographs shown in Figure 5d and 5e indicates that the re-agglomeration process by both layered silica (bentonite) and SPB give rise to a rather uniform attachment of  $\text{CaCO}_3$  particles onto the fibers. Apparently, anionic SPB act as efficient co-flocculants in a similar way as the layered silica. Both SPB and bentonite exhibit a high surface area such that negative surface charges can interact with CPAM moieties. However, it can be assumed that the hydrodynamic corona of SPB's is very distinct from that of bentonite platelets.

The cation exchange capacity (CEC) is a value given on a clay material (or similar material) to indicate its capacity to hold positively charged ions (cations). From the molecular weight of grafted polymer brush and grafting density the theoretical CEC of SPB can be calculated. As shown in Table 1 the CEC of LB1 and LB2 are 1.50 meq/g and 2.27 meq/g, respectively, while that of bentonite is only 0.80 meq/g. Obviously, the high CEC of anionic SPB due to polyelectrolyte chains in the corona favours strong interaction with other colloidal particles such as  $\text{CaCO}_3$  via the CPAM. Similarly, modified spherical polyelectrolyte brushes can also be used as nanoreactor, high performance catalyst or protein adsorbent due to the evidently enlarged specific surface area and charges in polymer brushes, which was proofed by Sharma *et al.* [38] and Wittemann [39] *et al.* recently.

On the other hand, if a cationic spherical polyelectrolyte brush (as LA2) is chosen in combination with cationic polyacrylamide the flocculation efficiency is not improved compared to the single component flocculation as shown by the FPR and AR values in Figure 3 and 4, respectively. This suggests that the cationic LA2 hardly interacts with the sheared macroflocs, indicating that, indeed, the macroflocs show positive surface charge after shearing due to excess cationic flocculant (CPAM). Consequently the sheared flocs cannot be flocculated by a second cationic additive. The repulsion induced by redundant charges even reduces the retention of fibers and  $\text{CaCO}_3$  fillers. Therefore both the FPR and AR decrease slightly with increasing amount of LA2 (see Figure 3 and 4).

### 3.2. Flocculation Mechanism of Anionic SPB as Dual Retention-Aid

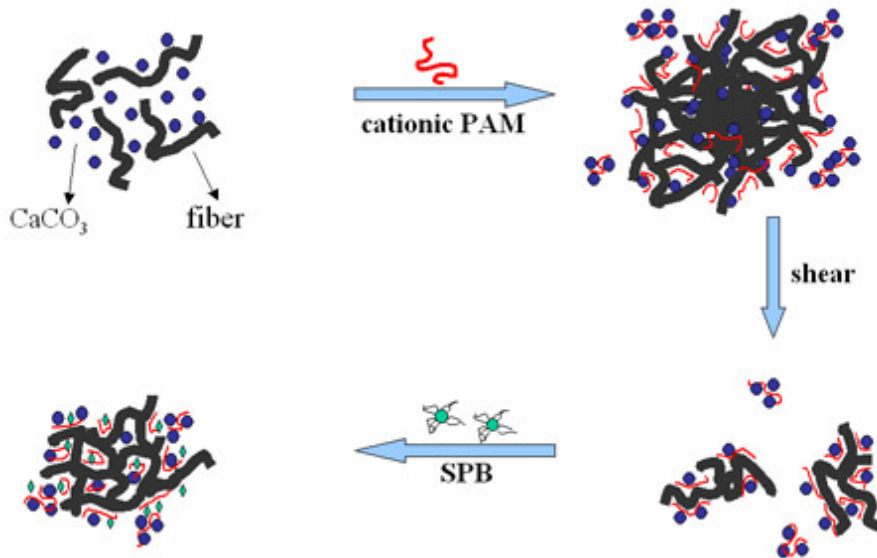


Figure 6. Suggested flocculation mechanism in the case of anionic SPB as dual retention-aid.

The flocculation mechanism in paper making due to retention-aids was studied by many authors [16-19, 23, 40-42, 46]. According to the interactions between retention-aids and paper raw materials they can be summarized in three fundamental mechanisms, namely charge neutralization, bridging, and patch flocculation mechanisms [43, 44]. In practice, modern retention-aid systems as used in papermaking industry consist of several components, and usually combine more than one mechanism. According to the retention tests and the FESEM images the flocculation mechanism of anionic SPB as dual retention-aid can be summarized in four steps, which is similar to that of microparticle retention-aid [45]. As shown in Figure 6: At first, fibers, fines and fillers in pulp slurry are homogeneously dispersed because of vigorous stirring; upon addition of cationic flocculant the negative surface charges of the paper suspension is largely neutralized, and a macrofloc is obtained. During this step, a rather non-uniform distribution of cationic polymeric flocculant between fibers, fines and fillers is obtained (see Figure 8a). During the subsequent shearing macroflocs are partially redispersed into finer flocs. Importantly, these flocs now exhibit mainly a cationic surface charge due to the flocculant. Note that the specific surface area of the given GCC particles is only about  $12 \text{ m}^2/\text{g}$  [42], hence the amount of cationic flocculation which is necessary to give rise to excess cationic surface charge after the shear is very small. During the last step, negatively charged SPB is added to the pulp slurry. They neutralize the excess positive charges on microflocs and build a consistent tight network due to the high specific surface area

and cation exchange capacity. During the latter agglomeration step most  $\text{CaCO}_3$  particles are incorporated into the flocs or patched on larger fibers due to the anionic SPB.

### 3.3. Deposition Mechanism of $\text{CaCO}_3$ on Fibers

According to Alince *et al.* [46] the deposition of  $\text{CaCO}_3$  on fibers can be summarized as followed: (I) In the presence of CPAM,  $\text{CaCO}_3$  fillers deposits with an intermediate bond on the fibers (see Figure 7a); (II) In the presence of CPAM and bentonite at optimum dosages, a much stronger bond is provided by bentonite particles (Figure 7b). Alince *et al.* suggested that bentonite may further delaminate upon dilution, thus causing the  $\text{CaCO}_3$  to partially detach from the fiber and may further coagulate (see Figure 7b) [39]. Some of the released particles can be observed e.g. in Figure 5d.

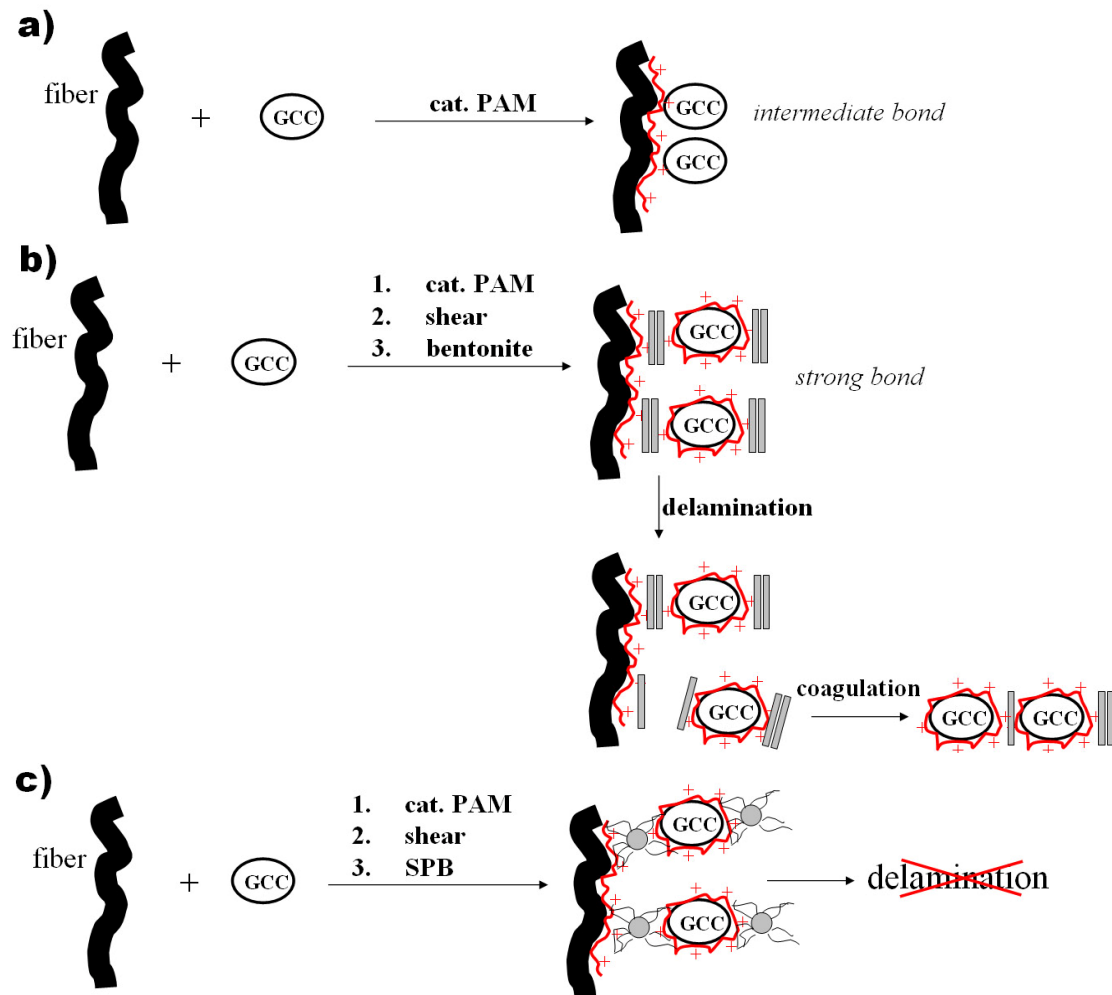


Figure 7. Deposition of  $\text{CaCO}_3$  on fibers in the presence of different retention-aids. (a). Deposition of  $\text{CaCO}_3$  on fibers caused by CPAM [46];

- (b). Deposition of  $\text{CaCO}_3$  on fibers caused by CPAM and bentonite [46];
- (c). Deposition of  $\text{CaCO}_3$  on fibers caused by CPAM and anionic SPB.

It is important to note that the theoretical surface area of the bentonite (montmorillonite) is about  $800 \text{ m}^2/\text{g}$  [47, 48] where as for the polystyrene core of LB1 and LB2, the theoretical specific surface area is only about  $49 \text{ m}^2/\text{g}$ ,  $114 \text{ m}^2/\text{g}$ , respectively. On the other hand, spherical particles do not show delamination (see Figure 7c). The key question is then, why the dual flocculation system using anionic SPB's works so efficiently despite their minor specific surface area compared to bentonite. The data suggest, that bentonite does not delaminate completely in practice, so that it can not reach the theoretical surface area; on the other hand, the high cation exchange capacity (see Table 1) along with the particle character of the SPB's is responsible for their flocculation efficiency in the present model system, rather than their apparent specific surface area (theoretical CEC = 1.50 and 2.27 meq/g for LB1 and LB2, respectively – compared to 0.8 meq/g for bentonite). In addition, one can argue that in the case of the SPB's *flexible* anionic polymer brushes grafted on polystyrene cores, give rise to a whole corona of anionic charges rather than just a surface charge as in the case of a montmorillonite. The flexible polymer brushes may adopt a more appropriate conformation in order to fit the rugged surface of fibers and  $\text{CaCO}_3$  particles compared to a flat layer silica surface.

Figure 8 shows FESEM images of flocs as a result of different flocculation systems. Using only CPAM,  $\text{CaCO}_3$  particles are observed on the fibers, but they are only loosely bound by Polymer composite bridges (Figure 8a). In the case of the microparticle system, in which bentonite is added after shear a quite different micrograph was obtained: In Figure 8b) bentonite platelets can be observed on both the fiber and the  $\text{CaCO}_3$  particle, thus acting as glue between the latter. In Figure 8c SPB's are observed on both the cellulose and the  $\text{CaCO}_3$  particles. These images strongly support the mechanism suggested by Alinec *et al.* [46].

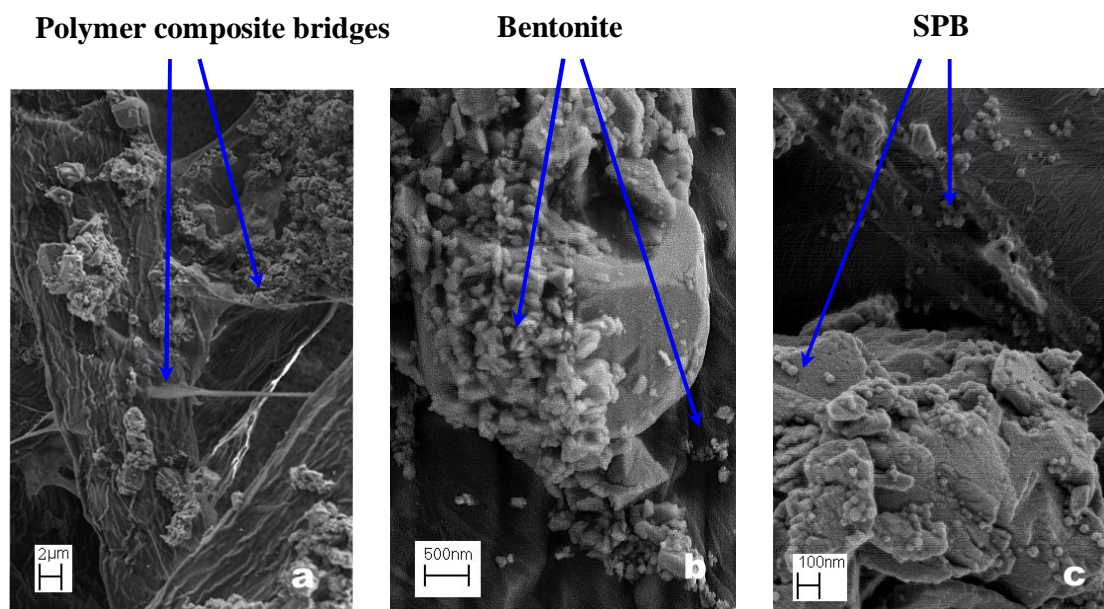


Figure 8. FESEM images of flocs caused by different retention-aids.

- (a). Deposition of  $\text{CaCO}_3$  in presence of CPAM. Polymer composite bridges are observed;
- (b). Deposition of  $\text{CaCO}_3$  in presence of bentonite and CPAM. Bentonite and  $\text{CaCO}_3$  are observed;
- (c). Deposition of  $\text{CaCO}_3$  in presence of LB2 and CPAM. SPB and  $\text{CaCO}_3$  are observed.

The surface roughness of the cellulose could be confirmed by AFM. In Figure 9a and b the morphology of the pure paper fiber on mica is observed showing rugged surface as can be seen in Figures 9c and 9d the rugged surface of fibers was smoothed upon addition of the dual flocculation system CPAM and SPB (LB1). In addition, due to the incorporation of  $\text{CaCO}_3$  micron-scale agglomerates are observed in the Figure 9c and 9d. It can be clearly seen that SPB are preferentially adsorbed on the filler particles rather than on the cellulose.

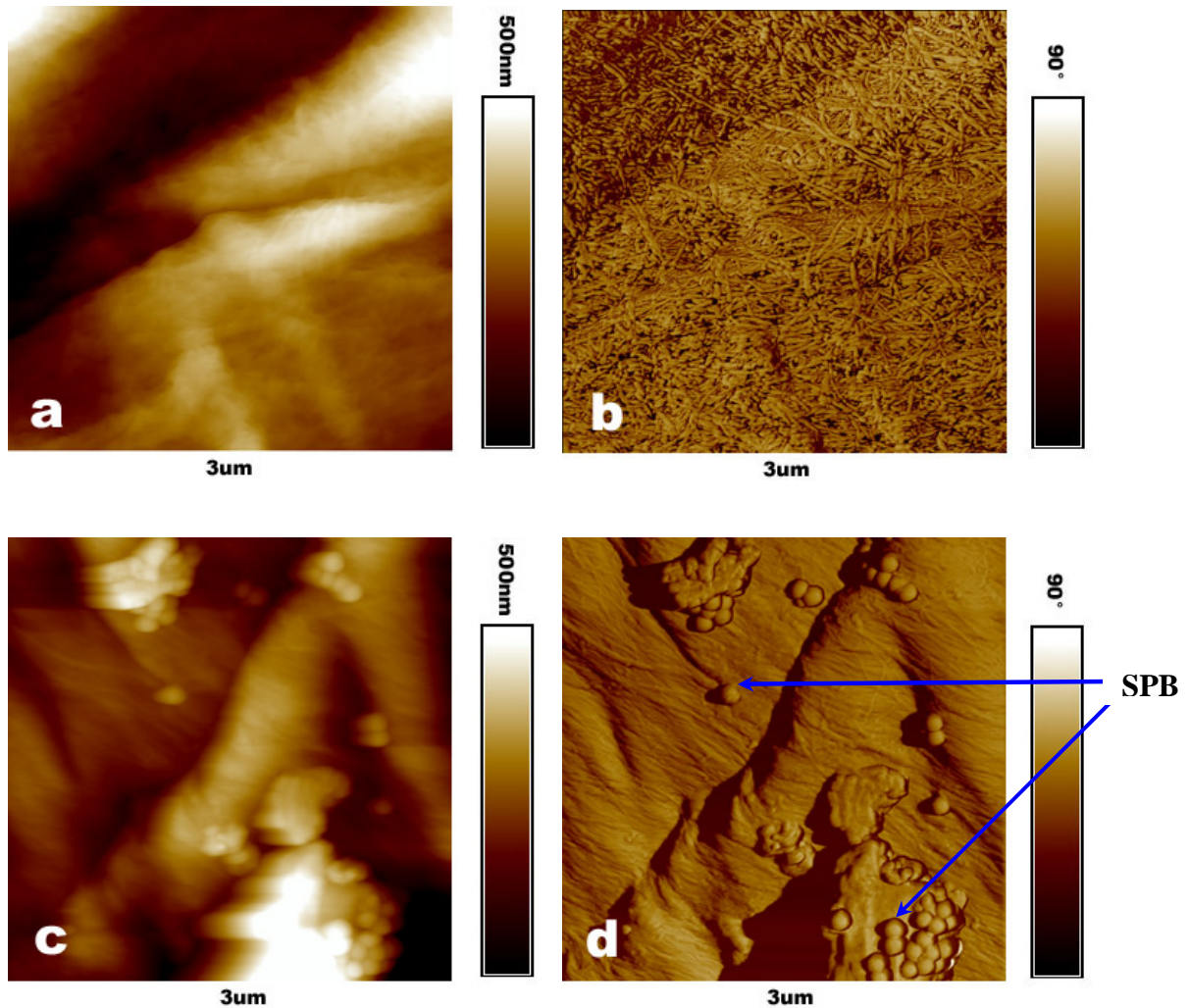


Figure 9. Comparison of morphology of fiber and floc caused by retention-aid system by means of AFM.

(a), (b). Topography and phase images of fiber on mica;

(c), (d). Topography and phase images of floc caused by LB1 and CPAM. The deposited  $\text{CaCO}_3$  and SPB particles are observed.

#### 4. Conclusions

We synthesized anionic and cationic spherical polyelectrolyte brushes (SPB). They were tested as dual flocculation system in combination with cationically modified polyacrylamide (CPAM), and compared with a traditional “microparticle” system in which bentonite acts as secondary flocculant. The anionic CPAM / SPB system shows high flocculation efficiency as tested under sheared conditions using a dynamic drainage jar. The high retention level of the SPB dual system contrasts with the apparent low specific surface area which is about an order of magnitude lower than a conventional bentonite. The data suggest that the flocculation efficiency can be

attributed to a high cation exchange capacity of SPB in combination with a flexibility of grafted polyelectrolyte chains. FESEM images and AFM support the model of anionic SPB's acting as a particle bridge in between fibers and CaCO<sub>3</sub> fillers.

## 5. Acknowledgement

Yu Mei acknowledges financial support of BASF AG gratefully. We thank Dr. Oliver Koch and Reinhard Barthel for the assistance in retention test.

## 6. References

1. Pincus, P. *Macromolecules* 1991, 24, 2912.
2. Borisov, O. V.; Birshtein, T. M.; Zhulina, E. B. *J Phys II (France)* 1991, 1, 521.
3. Norton, L.J.; Smiglova, V.; Pralle, M.U.; Hubenko, A.; Dai, K.H.; Kramer, E.J.; Hahn, S.; Beglund, C.; Dekoven, B. *Macromolecules*, 1995, 28, 1999.
4. Uyama, Y.; Tadokoro, H.; Ikada, Y. *J Appl Polym Sci*, 1990, 39, 489.
5. Luzinov, I.; Minko, S.; Senkovsky, V.; Voronov, A.; Hild, S.; Marti, O.; Wilke, W. *Macromolecules*, 1998, 31, 3945.
6. Leger, L.; Raphael, E.; Herve, H. *Adv Polym Sci*, 1999, 138, 185.
7. Kulik, E.; Ikada, Y. *J. Biomed Mater Res*, 1996, 30, 295.
8. Israelachvili, J. N. *Intermolecular and Surface Forces*, 2nd edition, 1992, Academic Press, London.
9. Rojas, O. J.; Hubbe, M. A. *J Dispersion Sci Technol*, 2004, 25(6), 713-732.
10. Xiao, H.; Pelton, R.; Hamielec, A. *J Colloid Interface Sci* 1995, 175, 166.
11. Pelton, R. H.; Allen L. H.; Nugent, H. M. *Tappi* 1981, 64(11), 89.
12. Lindström, T.; Glad-Nordmark, G.; *J Colloid Interface Sci* 1984, 97(1), 62.
13. Wagberg, L.; Lindström, T. *Colloids Surface* 1987, 27, 29.
14. Wang, F.; Tanaka, H. *J Appl Polym Sci*, 2000, 78, 1805-1810
15. Wagberg, L.; Odberg, L. *Nordic Pulp and Paper Res J*, 1991, 6, 117.
16. Swerin, A.; Odberg, L.; Sjodin, U. *Paper Technology*, 1992, 33(12), 28-29.
17. Swerin, A.; Odberg, L. *Nordic Pulp and Paper Research Journal*, 1996, 11(1), 22-29.
18. Swerin, A.; Odberg, L. *Fundamentals of Papermaking Materials*, Pira International, UK, 1997, 265-350.
19. Yan, Z.; Deng, Y. *Chemical Engineering Journal*, 2000, 80, 31-36.
20. Breese, J.; Nilsson, L. *Papermaker*, 1995, 2, 43-45.

21. Covarrubias, R. M.; Paracki, J.; Mirza, S. *Appita Journal*, 2002, 55(4), 272-275, 280.
22. Liu, J. *Paper Technology*, 1999, 40(3), 41-43.
23. Asselman, T.; Alince, B.; Garnier, G.; van de Ven, T.G.M. *Nordic Pulp and Paper Research Journal*, 2000, Vol.15, 5, 515.
24. Alexander, S. D.; Dobbs, R. J. *Tappi Journal*, 1987, 60(12), 117-220.
25. Schoelkopf, J.; Ridgway, C. J.; Gane, P. A. C.; Matthews, G. P.; Spielmann, D. C. *Journal of Colloid and Interface Science*, 2000, 227, 119–131.
26. Mei, Y.; Wittemann, A.; Sharma, G.; Ballauff, M.; Koch, Th.; Gliemann, H.; Horbach, J.; Schimmel, Th. *Macromolecules*, 2003, 36, 3452.
27. Guo, X.; Weiss, A.; Ballauff, M. *Macromolecules*, 1999, 32, 6043.
28. Marra, A.; Peuvrel-Disdier, E.; Wittmann, A.; Guo, X.; Ballauff, M. *Colloid Polym Sci*, 2003, 281, 491-496.
29. Guo, X.; Ballauff, M. *Langmuir*, 2000, 16, 8719.
30. Robillard, Q. de; Guo, X.; Ballauff, M.; Narayanan, T. *Macromolecules*, 2001, 33, 9109.
31. Mark, R. E.; Habeger, C. C.; Borch, J.; Lyne, M. B. *Handbook of Physical Testing of Paper*, 2001, Vol. 1, 2nd Ed., New York.
32. Physical and Chemical Standards Committee, Consistency of stocks, Technical Section. Canadian Pulp & Paper Association: Montreal, 1993.
33. Reid, I.; Ricard, M. *Enzyme and Microbial Technology*, 2000, 26, 117.
34. Physical and Chemical Standards Committee, Ash of paper and paperboard, Technical Section. Canadian Pulp & Paper Association: Montreal, 1986.
35. Duchesne, I.; Hult, E. L.; Molin, U.; Daniel, G.; Iversen, T.; Lennholm, H. *Cellulose*, 2001, 8, 103–111.
36. Wagberg, L.; Zhao, X.; Fineman, I.; Li, F. *Tappi Journal*, 1990, 73(4), 177-182.
37. Pelzer, R. *IPW*, 2003, 10, 27-33.
38. Sharma, G.; Ballauff, M. *Macromol Rapid Commun*, 2004, 25, 547–552.
39. Wittemann, A.; Haupt, B.; Ballauff, M. *Phys Chem Chem Phys*, 5 (8), 1671, (2003).
40. Petzold, G.; Mende, M.; Lunkwitz, K.; Schwarz, S.; Buchhammer, H. *Colloids and Surfaces A*, 2003, 218, 47-57.
41. Asselman, T.; Garnier, G. *Langmuir*, 2000, 16, 4871-4876.
42. Ono, H.; Deng, Y. *Journal of Colloid and Interface Science*, 1997, 188, 183-192.
43. Beck, U.; Müller, F.; Goossens, J.; Rohloff, E.; Tretter, H. *Wochenbl f Papierf*, 1977, 105, Nr. 11-12, 391-398.
44. Runkana, V.; Somasundaran, P.; Kapur, P. *Journal of Colloid and Interface Science*, 2004, 270, 347.

45. Swerin, A.; Sjödin, U.; Ödberg, L. *Nordic Pulp and Paper Research Journal*, 1993, 8(4), 389.
46. Alinec, B.; Bednar, F.; van de Ven, T.G.M. *Colloids and surfaces A*, 2001, 190, 71-80.
47. van Olphen, H.; *An introduction to clay colloid chemistry*, Second edition, Wiley-Interscience, 1977, New York.
48. Theng, B.K.G. *Formation and Properties of Clay-Polymer Complexes*, 1979, Elsevier, Amsterdam.

## Summary

In this thesis, the preparation of cationic spherical polyelectrolyte brushes by photo-emulsion polymerization has been presented for the first time. The structure and properties of the cationic SPB, have been comprehensively investigated by dynamic light scattering and atomic force microscopy, and compared with anionic SPB. Moreover, both of them were tested as dual retention-aid in conjunction with cationically modified polyacrylamide in papermaking.

The synthesis of cationic spherical polyelectrolyte brushes was achieved in three steps: Firstly, poly(styrene) core latices were prepared by conventional emulsion polymerization using cetyltrimethyl ammonium bromide (CTAB) as the cationic surfactant and 2,2'-azobis(2-amidinopropane)dihydrochloride (V50) as the cationic initiator; In the second step, a very thin layer of photoinitiator was brought on the surface of the PS core between remained styrene and photoinitiator containing a vinyl group under starved condition; At last, the soluble monomer was added to the modified core latex. Polymerization was initiated by the photoinitiators attached to the surface of PS cores under UV/Vis-radiation. Polyelectrolyte brushes grew on the surface of the PS core particles and spherical polyelectrolyte brushes consisting of PATAc or PVBTMAC were obtained.

The process of the photo emulsion polymerization monitored by dynamic light scattering showed that brush thickness can be controlled by adjusting the amount of monomer. The SPB latices were characterized by transmission electron microscopy (TEM) and disk centrifugation (DCP), which proved a well-defined distribution of SPB particles. The core-shell morphology of SPB was confirmed by atomic force microscopy for the first time. The molecular weight of grafted brushes was achieved by cleaving off polyelectrolyte brushes from the surface of PS core by a strong base and subsequent measurement using Ubbloehde capillary viscometer. The radius  $R$  of PS core, grafting density  $\sigma$  and contour length  $L_c$  of polyelectrolyte brushes, the distance between two neighboring grafting points can be determined.

The interaction of SPB with negatively charged surfaces was investigated by AFM operated in Tapping Mode. It was demonstrated that the negative SPB forms two-dimensional aggregates of densely packed polymer particles, which can be explained by a particle-particle interaction dominating the repulsive interaction of the particles with the mica substrate. The positively charged SPB exhibits a completely

different particle-surface interaction behaviour from that of negatively charged SPB. Here network-like structure films of dried particles without long-range 2D order are formed, which is due to the strong attractive particle-surface interaction of positively charged polyelectrolyte chains in the shell of the cationic SPB particles. These chains spread over the negatively charged mica surface and anchor the particles. Hence, a shell of polyelectrolyte chains is a highly efficient means of adjusting the interaction of colloidal particles with charged solid substrates.

The swelling behavior of cationic and anionic SPB as a function of ionic strength in the system were studied by DLS. The ionic strength has been changed by the addition of mono- and divalent counterions. Adding more and more salt leads to a strong shrinkage of the surface layer as expected for polyelectrolyte brushes. For some ions, however, high salt concentrations may lead to a re-swelling of the brush layer in case of the cationic systems. This points to specific interactions of the counterions with the PATAC chains. This strong specific interaction between the counterions and the attached polyelectrolyte may even lead to flocculation of the particles at intermediate salt concentration. Surprisingly, for sodium iodide and magnesium sulfate the solubility increases again if the salt concentration is raised to 1 mol/l. The interaction of the counterions with the cationic and the anionic brush layers may be classified as follows: at lowest ionic strength electrostatic interaction prevails and the brush layer is swollen in all cases by the osmotic pressure of the counterions. Intermediate salt concentrations lead to a partial screening of the electrostatic interaction and to a shrinkage of the brush layer. This effect can be well captured by the theory of Hariharan *et al.* [Hariharan *et al.* 1998]. In case of cationic brushes, however, the shrinkage becomes very pronounced around salt concentrations of 0.1 mol/l. In some cases there is even a collapse of the surface layer due to specific interactions between the polyion and the counterions. Cationic systems re-swell if immersed in concentrated salt solutions (“salting-in”). This is observed for monovalent as well as for divalent counterions. The analysis of the reduced excluded-volume parameter  $v/(l_K l^2)$  suggests that there is an adsorption of the counterions at high salt concentrations. The increase of  $v/(l_K l^2)$  thus leads to the re-swelling of the brush layer. The salting-in behavior thus finds an explanation in the increase of  $v$  due to the adsorption of salt ions. All data demonstrate that specific effects of different counterions lead to a behavior of the brush layer not expected from a purely electrostatic model. All specific effects seen at high concentrations of added salt can be explained by the increase of the reduced excluded-volume parameter which is due to the adsorption of salt ions.

Cationic and anionic SPB were tested as dual-component retention system in combination with cationically modified polyacrylamide (CPAM), and compared with the traditional “microparticle” system in which bentonite acts as secondary flocculant. The anionic SPB-based system shows high flocculation efficiency as tested under sheared conditions using a dynamic drainage jar. The high retention level of the SPB dual-component retention system can be explained by the enlarged specific surface area and cation exchange capacity of SPB, which are caused by grafted flexible polyelectrolyte chains. Furthermore, chemically grafted polyelectrolyte brushes show more advantages than bentonite, which may further delaminate upon dilution and cause  $\text{CaCO}_3$  fillers partially detach from the fiber. Images from field emission scanning electron microscopy (FESEM) of difference stages of retention testes suggest that the flocculation mechanism of anionic SPB and CPAM as dual-component retention system can be summarized in three steps: at first, excessive CPAM were added to bind cellulose fibers and  $\text{CaCO}_3$  fillers and formed loose macroflocs with positive charges; then the agglomerations were broken into microflocs by strong shear strength; at last, anionic SPB with negative charges were added and caused much finer and denser flocs, thus creating paper sheets with better optical appearance due to higher homogeneity. Images from FESEM images and AFM support the model of anionic SPB’s acting as a particle bridge between fibers and  $\text{CaCO}_3$  fillers.

## Zusammenfassung

Im Rahmen der vorliegenden Arbeit wurde die Synthese von kationischen sphärischen Polyelektrolytbürsten auf der Oberfläche von Polystyrol-Partikel durch Photo-Emulsionspolymerisation erstmals vorgestellt. Weiterhin wurden die Struktur und Eigenschaften dieser sphärischen Polyelektrolytbürsten durch Scheibenzentrifugation (DCP), Transmissionselektronenmikroskopie (TEM), Rasterkraftmikroskopie (AFM) und dynamische Lichtstreuung (DLS) untersucht. Die Eigenschaften der anionischen und kationischen SPB wurden miteinander verglichen. Darüber hinaus wurden beide in Kombination mit kationischen Polyacrylamid (CPAM) als Dual-Retentionssystem getestet. Die Flockungsmechanismen wurden durch AFM und Rasterelektronenmikroskopie (FESEM) untersucht.

Die Synthese der kationischen sphärischen Polyelektrolytbürsten wurde in drei Schritten durchgeführt. Zuerst wurde ein Polystyrol Kern-Latex durch eine konventionelle Emulsionspolymerisation mittels kationischen Emulgator Cetyltrimethylammoniumbromid (CTAB) und Initiator 2,2'-azobis(2-amidinopropane) dihydrochlorid (V50) hergestellt. Im zweiten Schritt wurde eine sehr dünne Schicht des Photoinitiators HMEM [Guo *et al.* 1999] auf die Kernoberfläche aufgebracht durch eine Copolymerisation von nicht umgesetztem Styrol mit Photoinitiator, der eine Vinyl-Gruppe aufweist. Im letzten Schritt wurden wasserlösliche kationische Monomere (z.B. ATAC, VBTMAC usw.) im Kern-Latex gelöst und die Polymerisation durch den auf der Kernoberfläche gebundenen Photoinitiator durch UV-Strahlung initiiert. Polyelektrolytbürsten bildeten sich auf der Oberfläche der PS-Kern-Partikel.

Der durch DLS überwachte Prozess der Photo-Emulsionspolymerization zeigte, dass die Schalendicke der Polyelektrolytbürsten durch die eingesetzte Menge des Monomers kontrolliert werden kann. Die SPB-Latices wurden durch TEM und Scheibenzentrifugation charakterisiert, um die enge Verteilung der SPB-Partikel nachzuweisen. Die Kern-Schale-Struktur wurde mittels AFM erstmals bestätigt. Die Bestimmung des Molekulargewichtes der gepfropften Polyelektrolytbürsten erfolgte mit einem Ubbelode-Kapillarviskosimeter nach der Abspaltung der Polymer Ketten in NaOH-Lösung. Der Kernradius ( $R$ ), Belegungsdichte ( $s$ ) und Kontourlänge ( $L_c$ ) können gemessen oder berechnet werden.

Die Wechselwirkung zwischen den SPB und einer negativ geladenen Oberfläche wurde durch AFM im *Tapping Mode* untersucht. Es zeigt sich, dass negative SPB eine 2D-Aggregation dicht gepackter Polymerpartikel bilden, welche durch die die Partikel-Partikel-Wechselwirkung dominierende abstossende Wechselwirkung zwischen SPB-Partikel und der Glimmeroberfläche erklärt werden kann. Positive geladene SPB zeigten eine total unterschiedliche Partikel-Oberfläche-Wechselwirkung im Vergleich zu negativ geladenen SPB. Hier bildet sich eine Netzwerk-Struktur der getrockneten Partikel aus wegen der attraktiven Partikel-Oberfläche Wechselwirkung der positiv geladenen Polyelektrolytketten der kationischen SPB-Partikel. Die Polymerketten verteilen sich auf der negativ geladenen Glimmeroberfläche und verankern die Partikel. Deswegen ist die Polyelektrolytschale eine sehr effektive Methode die Wechselwirkung zwischen kolloidalen Partikel und einer geladenen Oberfläche zu kontrollieren.

Die Quellungsverhalten der kationischen und anionischen SPB als Funktion der Ionenstärke wurde durch DLS untersucht. Die Ionenstärke wurde durch Zusatz mono- und divalenter Gegenionen variiert. Zunehmende Fremdsalzkonzentration führt zu einem starken Schrumpfen der Polymerschicht. Bei bestimmten Gegenionen führt eine höhere Salzkonzentration zu einer Zunahme der Schalendicke im Fall des kationischen Systems. Es weist auf eine spezifische Wechselwirkung zwischen Gegenionen und PATAC Ketten hin. Die starke spezifische Wechselwirkung zwischen Gegenionen und Polyelektrolytketten in einen bestimmten Bereich der Fremdsalzkonzentration führt sogar zum Ausflockung der Partikel. Für Natriumjodid und Magnesiumsulfat nimmt die Löslichkeit der SPB wieder zu, wenn die Fremdsalzkonzentration bis zu 1 mol/l erhöht wird. Die Wechselwirkung der Gegenionen mit kationischen und anionischen Polyelektrolytbürsten kann wie folgt zusammengefasst werden: Bei niedrigen Ionenstärken dominiert die elektrostatische Wechselwirkung und die Polymerschale ist gequollen wegen des osmotischen Druckes der Gegenionen. Mittlere Ionenstärken führen zu einer teilweise Abnahme der elektrostatischen Wechselwirkung und einem Schrumpfen der Polymerschale. Dieser Effekt kann durch ein modifiziertes Daoud-Cotton-Modell [Hariharan *et al.* 1998] erklärt werden. Im Fall kationischer Polymerbürsten ist das Schrumpfen sehr stark bei einer Fremdsalzkonzentration von 0.1 mol/l. In einigen Fällen resultiert sogar ein In-sich-zusammenfallen der Polymerschale wegen der spezifischen Wechselwirkung zwischen den Polyionen und Gegenionen. Das kationische System quillt in konzentrierten Fremdsalzlösungen (*“salting-in”*). Es wurden nicht nur beim Fall mono- sondern auch divalenter Gegenionen aufgetaucht. Die Analyse des reduzierten *excluded-volume-parameters*  $v/(l_k l^2)$  weist auf eine Adsorption der Gegenionen in konzentrierter Fremdsalzlösung hin. Der Effekt der Zunahme von  $v/(l_k l^2)$

führt zu einem Anquellen der Polymerschale. Das *Salting-in* Verhalten erklärt sich durch die Zunahme von  $v$  wegen der Adsorption der Gegenionen. Alle Daten zeigen, dass der spezifische Effekt der unterschiedlichen Gegenionen zu einem vom reinen elektrostatischen Modell nicht erwarteten Verhalten der Polymerschale führt. Die spezifischen Effekte bei hohen Konzentrationen können durch die Zunahme des reduzierten *excluded-volume-parameters* wegen der Adsorption der Gegenionen erklärt werden.

Kationische und anionische SPB wurden in der Kombination mit CPAM als Dual-Retentionssystem getestet, und mit dem traditionellen Mikropartikel-Retentionssystem bestehend aus Bentonit und CPAM verglichen. Das auf anionischen SPB basierende Retentionssystem zeigt eine höhere Flockungseffizienz unter Scherkraft vom *dynamic drainage jar* (DDJ). Die höhere Retentionsfähigkeit kann durch die erhöhte spezifische Oberfläche und Kationenaustauschfähigkeit, die von den auf der Oberfläche des PS-Kerns aufgepfropften flexiblen Polyelektrolytbürsten verursacht wird, erklärt werden. Weiterhin zeigen die chemisch gebundenen Polyelektrolytbürsten mehr Vorteile als Bentonite, die im Wasser delaminieren wird und die teilweise Abtrennung der  $\text{CaCO}_3$ -Partikel von den Fasern verursacht. FESEM-Bilder von den verschiedenen Stufen der Retentionstests deuten darauf hin, dass der Flockungsmechanismen von anionischen SPB und CPAM als Dual-Retentionssystem in drei Schritten zusammengefasst werden kann: Zum ersten wurden übermäßige CPAM in Papierstoff eingesetzt, um Zellulose-Fasern und  $\text{CaCO}_3$  zu binden und lockere Makroflockung mit positiven Ladungen zu bilden; Dann wurden die lockere Flockung durch Scherkraft zu Mikroflokkung zerkleinert; Zum Schluss wurden anionische SPB mit negativen Ladungen eingesetzt, und erzeugt kleinere und dichtere Flockung. Dadurch hat das hergestellte Papier durch höhere Homogenität ein besseres optisches Aussehen. Bilder aus FESEM und AFM bestätigen das Modell, welches anionische SPB als ein Bindeglied zwischen Fasern und  $\text{CaCO}_3$  vorsieht.

## Appendix

### Experiments and Methods

#### 1 Synthesis of SPB Latices

The synthesis of anionic SPB latices, which was first developed by Guo *et al.* [1], was carried out by three steps. In the first step, a PS core latex with a narrow size distribution was synthesized by conventional emulsion polymerization. Afterwards, a thin layer of photoinitiator is brought on the surface of PS cores. In the final stage, the monomer (e.g. AA or NaSS etc.) dissolved in water polymerizes on the surface of PS core under UV/Vis-radiation. Similarly, modified anionic SPB were also synthesized by the same method. Here Saat 6772 (PS core, 23nm core radius, 33.3% solid content) obtained from BASF AF was used as seed to get bigger specific surface area. To compare the influence of different kind of charge on the surface properties of latex particle cationic SPB latices were synthesized in three steps similarly, as shown in figure 1. To avoid possible interaction of the negatively charged surfactant used in the previous synthesis, cetyltrimethylammonium bromide (CTAB, Fluka) has been used to stabilize the core latex particles. For similar reasons the cationic initiator 2,2'-azobis(2-amidinopropane) dihydrochloride (V50, WAKO Chemicals) has been used to start the emulsion polymerization. In the final stage, a cationic monomer (e.g. ATAC or VBTMAC etc.) dissolved in water polymerizes on the surface of PS core under UV/Vis-radiation.

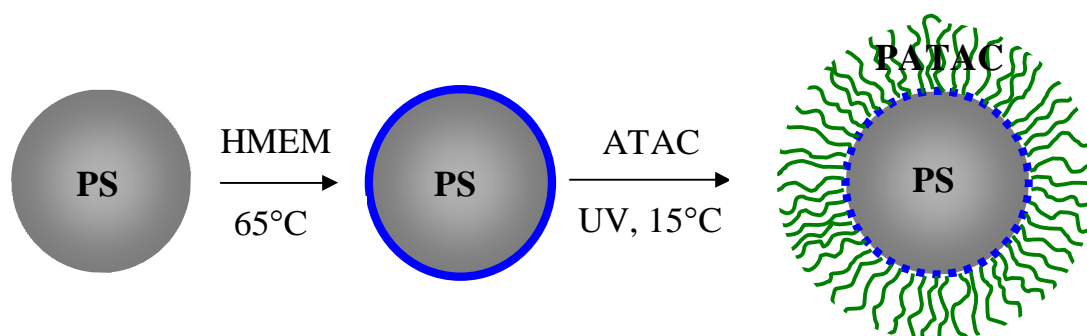


**Figure 1** Schematic diagram of the synthesis of cationic SPB. In the first step, cationic PS core latices were synthesized by emulsion polymerization. Afterwards, a very thin layer of photoinitiator was brought on PS cores. At last, cationic monomer (e.g. ATAC or VBTMAC etc.) dissolved in water polymerized on the surface of PS cores under UV/VIS-radiation.

## 1.1 Chemicals

1-[4-(2-hydroxyethoxy)-phenyl]-2-hydroxy-2-methyl-1-propanone (Irgacure 2595, Ciba), pyridin (Fluka), methacryloyl chloride (MC, Fluka), cetyltrimethylammonium bromide (CTAB, Fluka), potassium persulfate (KPS, Fluka), sodium dodecylsulfate (SDS, Aldrich), and 2,2'-azobis(2-amidinopropane)dihydrochloride (V50, Wako), potassium chloride (Fluka), sodium fluoride (Fluka), sodium chloride (Fluka), sodium bromide (Fluka), sodium iodide (Fluka), sodium hydroxide (Fluka), hydrochloric acid standard solutions (Fluka), (ar-vinylbenzyl)-trimethylammonium chloride (VBTMAC, Fluka), 4-vinylbenzenesulfonic acid sodium salt (NaSS, Fluka), anhydrous calcium chloride (Fluka), bentonite for water-based systems (Fluka) and cationic polyacrylamide (Polymin<sup>®</sup> KP 2515 special, BASF) were used as received without further purification.

To remove the inhibitor 4-*tert*-butylcatechol styrene (BASF) was washed three times with 10% aqueous sodium hydroxide solution, followed by water, dried overnight at 4 °C over anhydrous CaCl<sub>2</sub>, and subsequently distilled under reduced pressure (16 mbar, 33 °C). (2-(acryloyloxy)ethyl)trimethyl ammonium chloride (ATAC, BASF) was extracted with acetone to remove the inhibitor.

All the solvents were of analytical grade and used as received. The deionized water ( $\kappa \leq 0.05 \mu\text{S}/\text{cm}$ ) used was purified by reverse osmosis (Millipore Milli-RO) and subsequent ion exchange (Millipore Milli-Q).

## 1.2 Synthesis of Photo Initiator HMEM

HMEM was synthesized by the Schotten-Baumann reaction (Figure 2) of 94.8 g of Irgacure 2595 and 43.1 g of MC in 600 ml of acetone using 50 ml of pyridine as catalyst. At first, Irgacure 2595 was dissolved in the mixture of acetone and pyridine. Then MC was added drop wise by a dosing motor (Razel) into the solution at 0 °C. After the addition of MC, the mixture was stirred for 12h at room temperature. At last, the solvent was evaporated under vacuum, and the resulting product was exhaustively washed with water. Further purification was achieved through chromatography of silica gel (Silica gel 60, Fluka) using acetone as eluent where the thin-layer chromatography (Merck Aluminum oxide 60 F<sub>254</sub> neutral, Type E) serves as analytical method. The overall yield was about 40%.

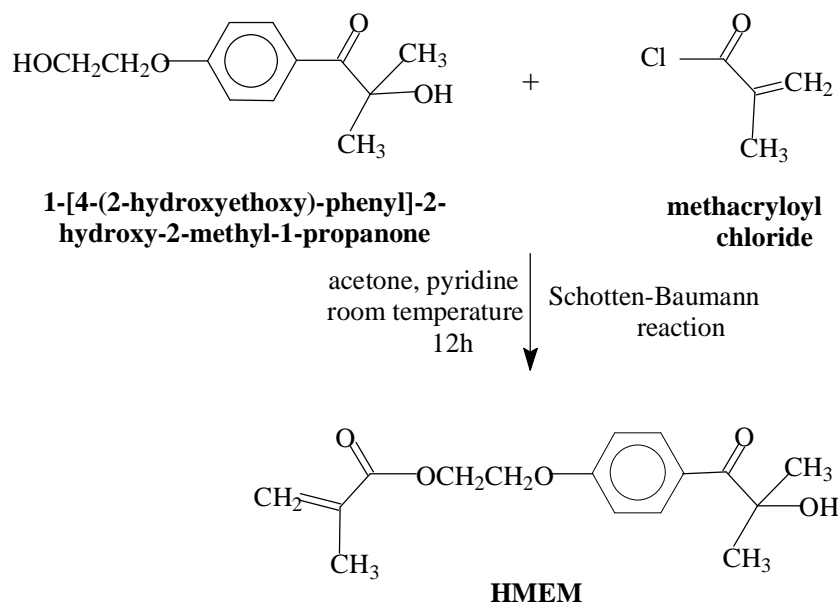


**Figure 2** Synthesis of photoinitiator HMEM by Schotten-Baumann reaction.

**NMR spectrum of HMEM**  $^1\text{H-NMR}$  ( $\text{CD}_3\text{COCD}_3$ ,  $\delta$  in ppm):

$\delta = 1.53$  (s, 6H,  $-\text{C}(\text{CH}_3)_2-\text{OH}$ );  $1.93$  (s, 3H,  $\text{CH}_2=\text{C}(\text{CH}_3)-$ );  $4.45, 4.54$  (t, 4H,  $-\text{O}-\text{CH}_2-\text{CH}_2-\text{O}-$ );  $5.69, 6.10$  (d, 2H,  $\text{CH}_2=\text{C}(\text{CH}_3)-$ );  $7.10, 8.28$  (m, 4H,  $-\text{O}-\text{C}_6\text{H}_4-\text{CO}-$ ).

### 1.3 Synthesis of Anionic PS-co-HMEM Core Latices

The synthesis of anionic core latices was carried out in a 3000 ml double-wall reactor (Büchi) using a conventional emulsion polymerization. The reactor consists of a thermometer, a reflux condenser, a paddle stirrer system (IKA) with an anchor stirrer (Büchi) and a thermostatic system (Lauda R400). In a typical run, 3.14 g SDS was dissolved in 1240 ml deionized water under stirring. When 312 g styrene was added, the reactor was degassed under vacuum and filled by  $\text{N}_2$  afterwards for five times. The emulsion polymerization was started by adding 0.66 g anionic thermal initiator KPS which was dissolved in 20 ml deionized water at the temperature of  $80^\circ\text{C}$ . The reaction lasts for 60 minutes at  $80^\circ\text{C}$  under 300 rpm stirring. Then, the temperature was decreased to  $70^\circ\text{C}$ . Afterwards, 17.52 g HMEM (2 mol% of the used styrene, which can also vary from 0.5 mol% to 3 mol%) dissolved in 20 ml acetone was added using a dosing motor under starved condition (about 0.2 ml/min) at  $70^\circ\text{C}$  to obtain a well-defined thin layer of photoinitiator on the poly(styrene) core.

### 1.4 Synthesis of Modified Anionic PS-co-HMEM Core Latices

To get bigger specific surface area modified anionic PS core latices with smaller core radius were synthesized in the same Büchi reactor by seed polymerization. The seed latex Saat 6772 provided by BASF AG was used as received. At first, 624 g Saat 6772 (PS latex supplied by BASF AG, 33.3% solid content, 23 nm radius), 614 g deionized water and 52g styrene were mixed in the reactor. When air in the reactor and in emulsion was totally replaced by nitrogen, the mixed emulsion was heated to 70 °C under the stirring of 300 rpm. 0.30 g KPS dissolved in 10 ml deionized water was injected to start the reaction. The reaction lasts 60 minutes at 70 °C. Then, modification with a thin layer photoinitiator was carried out under the same conditions as in case of the anionic latices.

### 1.5 Synthesis of Cationic PS-co-HMEM Core Latices

The synthesis of cationic PS-co-HMEM core latices was achieved in the above-mentioned reactor system by conventional emulsion polymerization. In a typical run, 7.98 g CTAB was dissolved in 1240 ml deionized water under stirring. When 312 g styrene was added, the reactor was degassed under vacuum and filled by nitrogen for five times. The emulsion polymerization was started by adding 0.91 g cationic thermal initiator V50 which was dissolved in 20 ml deionized water at the temperature of 65 °C. The reaction lasts for 120 minutes at 65 °C under 300 rpm stirring. Afterwards, 17.52 g HMEM (2 mol% of the used styrene, which can also vary from 0.5 mol% to 3 mol%) dissolved in 20 ml acetone was added using a dosing motor under starved condition (about 0.2 ml/min) at 65 °C to obtain a well-defined thin layer of photoinitiator on the poly(styrene) core. The difference between the synthesis of anionic and cationic PS-co-HMEM core consists in surfactant, initiator, reaction time and temperature.

Reaction temperature and duration for the synthesis of different PS-co-HMEM core latices are summarized as followed in Table 1.

*Table 1 Comparison of preparation of different PS-co-HMEM core latices*

	<b>ani. core</b>	<b>modi. ani. core</b>	<b>cat. core</b>
<b>Recipe</b>	3.14g SDS 1260g water 312g styrene 0.66g KPS 17.52g HMEM	624g Saat 6772 624g water 52g styrene 0.30g KPS 17.52g HMEM	7.98g CTAB 1260g water 312g styrene 0.91g V50 17.52g HMEM
<b>Charge</b>	negative	negative	Positive

<b>Core radius</b>	58 nm	25 nm	45 nm
<b>Reaction duration</b>	260 min.	260 min.	320 min.
<b>Reaction temperature</b>	70~80 °C	70 °C	65 °C
<b>Mixing speed</b>	300 rpm	300 rpm	300 rpm

Saat 6772: Poly(styrene) latex obtained from BASF AG with 23 nm core radius and 33.3% solid content.

### 1.6 Preparation of SPB by Photo Polymerization

The PS core latices modified with a thin layer of HMEM were filled in a UV-reactor (a.c.k GmbH, volume: 2000-3000mL, range of wavelengths: 200-600nm, see Figure 3) and diluted to the weight concentration of 2.5% with water. The total volume of latices was adjusted to about 2500 mL. Then defined amounts of monomer, such as ATAC, VBTMAC or NaSS were added under vigorous stirring. To avoid the disturbance of oxygen dissolved in latices the whole reactor was degassed by repeated degassing and subsequent gas charging of nitrogen for at least 5 times. Photopolymerization was performed by means of UV/Vis-radiation at 15 °C. Strong stirring ensured homogenization of latices in UV-reactor. The photo-emulsion polymerization was finished within 30 minutes. After that, SPB latices were filtered over glass wool to remove possible coagulum.

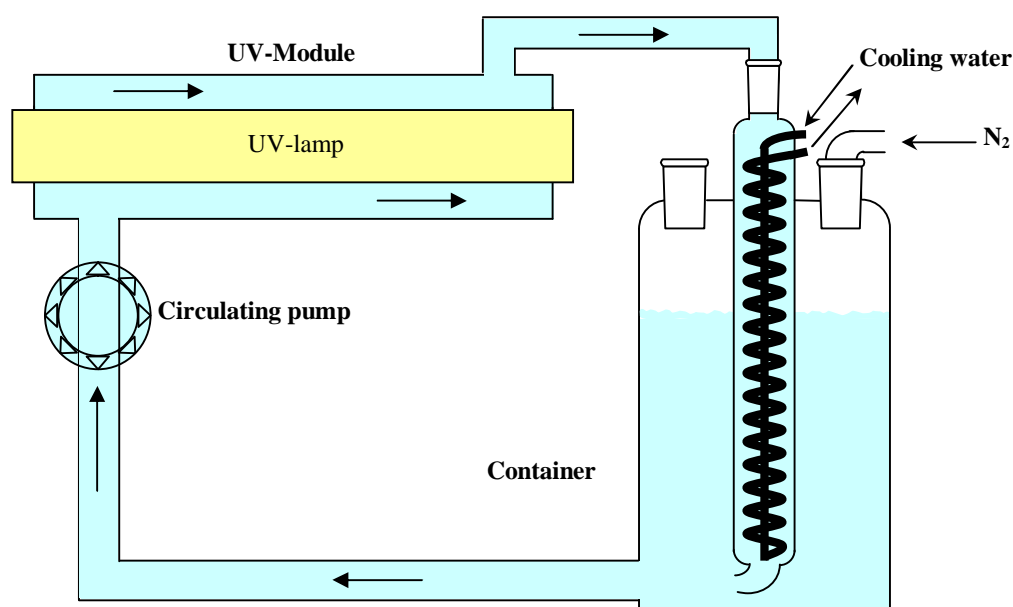


**Figure 3** Schematic diagram of UV-reactor (a.c.k. GmbH), which consists of a Hg UV-lamp, a circulating pump and a container. The reaction volume varies from 1.8-3.0 liters.

Although PS-co-HMEM latex is very turbid, it does not disturb photoinitiation since the UV-light which is not adsorbed by photoinitiator located on surface of latex particles will be scattered further and finally reach another particle to initiate a radical. The strong elastic light scattering in the latex system ensures a high efficiency of UV/Vis-radiation.

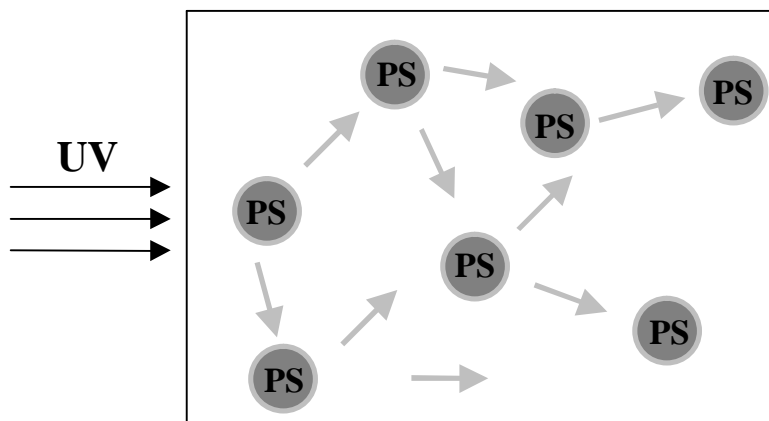


**Figure 4** The strong scattering of UV/Vis light in turbid latex system during photo-emulsion polymerization ensures a high efficiency of UV/Vis-radiation.

Upon UV/Vis-radiation the photoinitiator HMEM is decomposed into two initiating radicals by a cleavage mechanism shown in Figure 5 [2, 3]. Half of the radicals remain on the surface of the PS core, which will initiate polymerization of brush chains; And another half of the radical species enter into the aqueous medium and will initiate polymerization in solution. After UV-reaction, the SPB latices should be completely purified by ultrafiltration against deionized water to remove the polymer chains grown in aqueous medium to avoid the possible disturbance in following analysis.

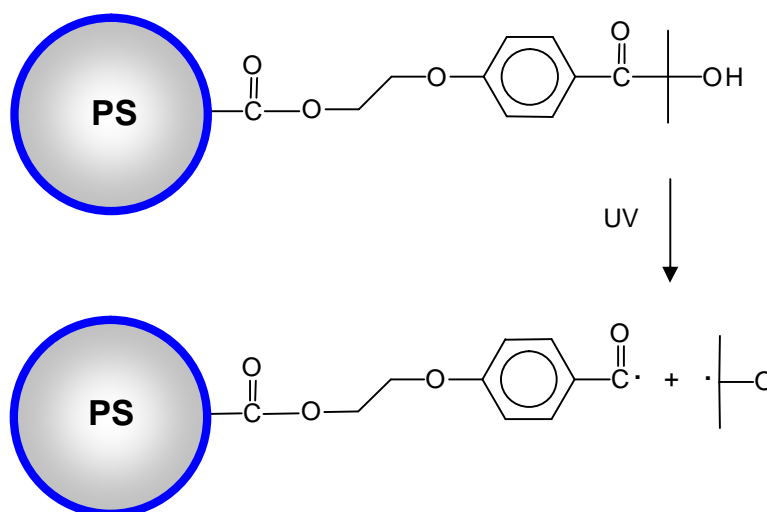


**Figure 5** Decomposition of photoinitiator HMEM into radicals under UV/Vis-radiation. Half of the radicals enter into aqueous medium, another half of the radicals remain on the surface of PS cores.

### 1.7 Purification of Latices

The latices must be cleaned before the characterization and further application in order to remove the impurities dissolved in the latex and thus to avoid potential problems. It is especially important for polyelectrolytes since their behavior is very sensitive to the ionic strength in solution. Normally, two purification methods were used in the experiments: dialysis and serum replacement (Ultrafiltration).

The dialysis uses membranes from Visking (Medicell, molecular size exclusion: 12000-14000 Dalton) to remove dissolved small molecules and ions. The tubing membrane is boiled in water for 2 hours before use, then filled with latices, closed and dipped in a deionized water bath. Hanging on a motor, it rotated continually to obtain an efficient diffusion of small molecules in the latices. The outer water is changed every day until its conductivity becomes constant.

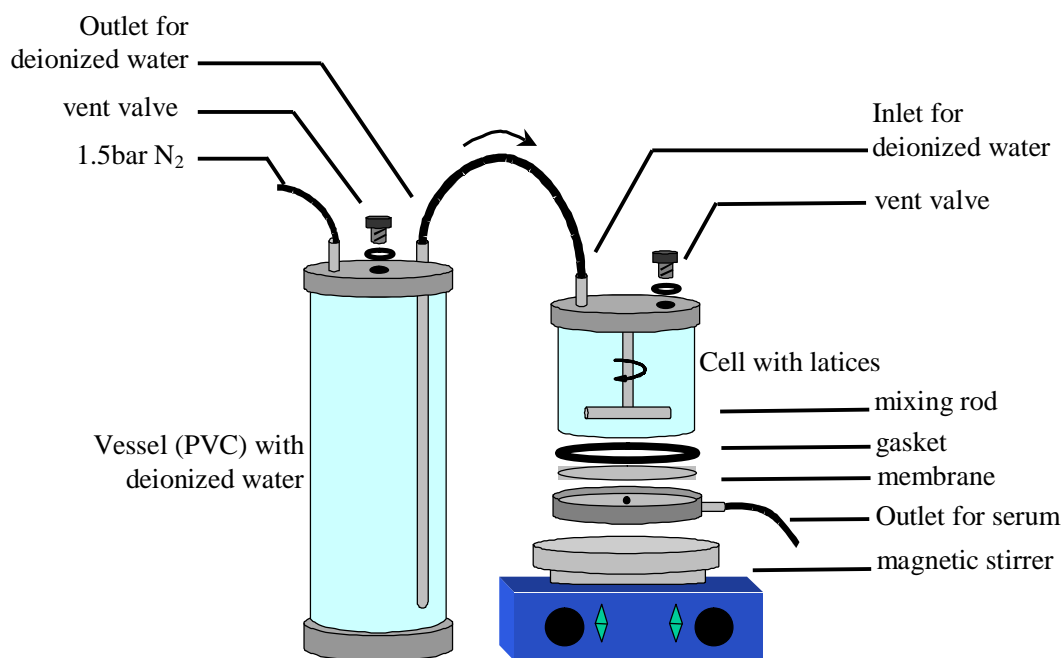


**Figure 6** Schematic diagram of home-made serum replacement equipment.

The serum replacement is the application of pressure to force the solvent and small particles across a membrane while the larger latex particles are retained. The equipment (see figure 6) were made in our institute. The latices are cleaned by serum replacement with membrane filters (Schleicher & Schuell) made from cellulose nitrate

with the pore size of 100 nm or 50 nm, which depends on the core radius of the latex, against pure deionized water until the conductivity of the serum was around 10-15  $\mu\text{S}\cdot\text{cm}^{-1}$ .

Purification of PS core latex was performed by dialysis to avoid potential agglomeration of PS latex under the high pressure during serum replacement; while SPB latex was normally cleaned by serum replacement since polymer chains grown in aqueous medium are out of limit of molecular size exclusion of dialysis membrane, and moreover the efficiency of serum replacement is higher than in case of other methods.

## 2 Characterization of SPB Latices

Polymerization initiated by UV/Vis-radiation was monitored by DLS, figure 7 shows the increase of the brush thickness ( $L$ ) of PATAc as function of reaction time. Small amounts of latices were collected and diluted with deionized water, and measured by DLS. Figure 6 proved that brush thickness can be controlled by adjusting the amount of monomer used for polymerization. This amount is counted as molar percent of styrene used in the core latex preparation. The hydrodynamic radius of the particles increased rapidly, it reached a plateau after circa 20 minutes in each case. The increase of  $L$  as function of reaction time is due to the gradually increased crowding of the chains on the surface and consequently the stretching due to mutual interaction.

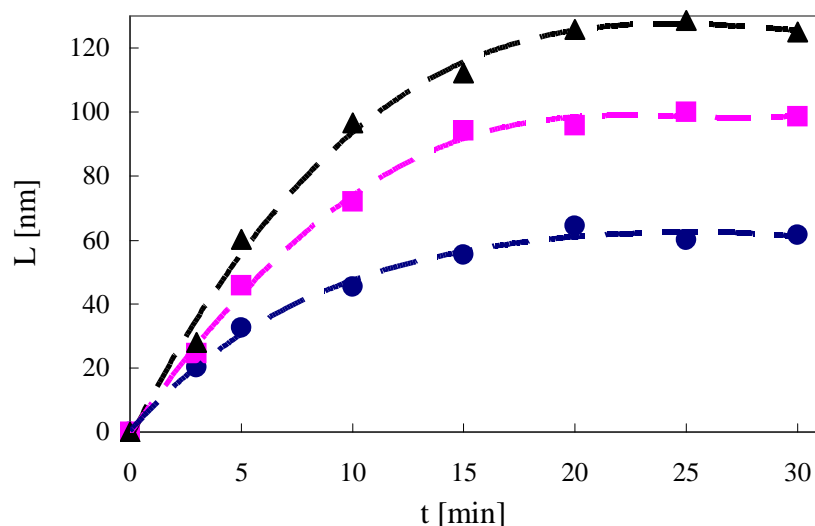


**Figure 7** Brush lengths as function of reaction time. Different amounts of monomers were added to PS core latices with 2.0 mol% photoinitiator HMEM. The dashed lines are guides to eyes. Brush length reaches a maximum after 20 minutes UV/Vis-radiation.

▲: LA3 with 72 mol% ATAC;

■: LA2 with 56 mol% ATAC;

●: LA1 with 40 mol% ATAC.

## 2.1 Determination of Particle Size Distribution of Latices

The images from transmission electron microscopy (TEM) in Figure 8 show that the latex particles have narrow size distribution in all steps of synthesis. Although the photoinitiator shell formed in the second step can hardly be seen since it is only about 2~3 nm thick, no new phase appears. But the brush layer obtained in photo emulsion-polymerization can not be discerned in TEM images since they collapsed into a thin layer on the surface of poly(styrene) core under high vacuum and their contrast is low.

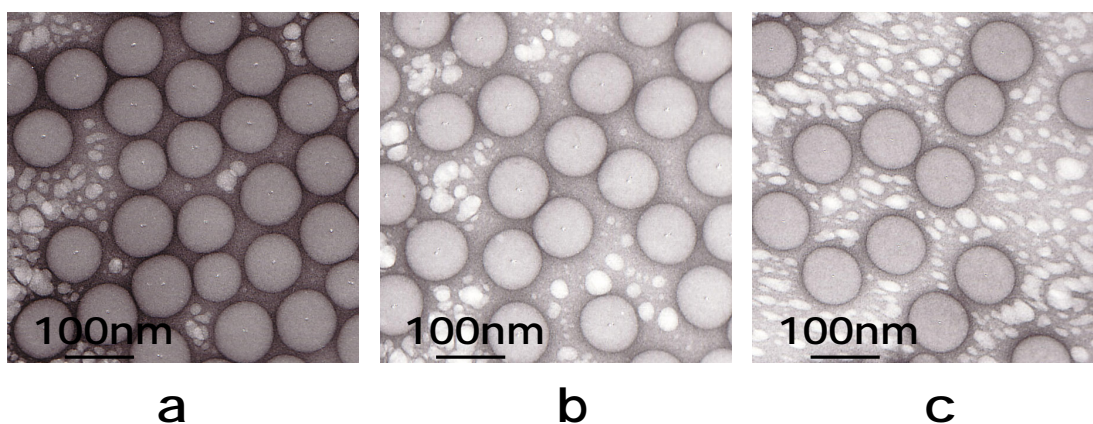


**Figure 8** TEM images of latex particles. All images were taken with 36000 times magnification. The white spots in the images were caused by contrast solution (1% phosphotungstic acid solution).

- Cationic PS core;
- Cationic PS-co-HMEM;
- Cationic SPB with PATAc brushes.

To ensure a narrow particle size distribution, all latices were carefully checked by DCP (Brookhaven BI-DCP) during preparation. Only latices with narrow particle size distribution were chosen and further used. Actually, the particles size distribution of latices was well controlled, as shown in Figure 9. The results from DCP accord with that from TEM.

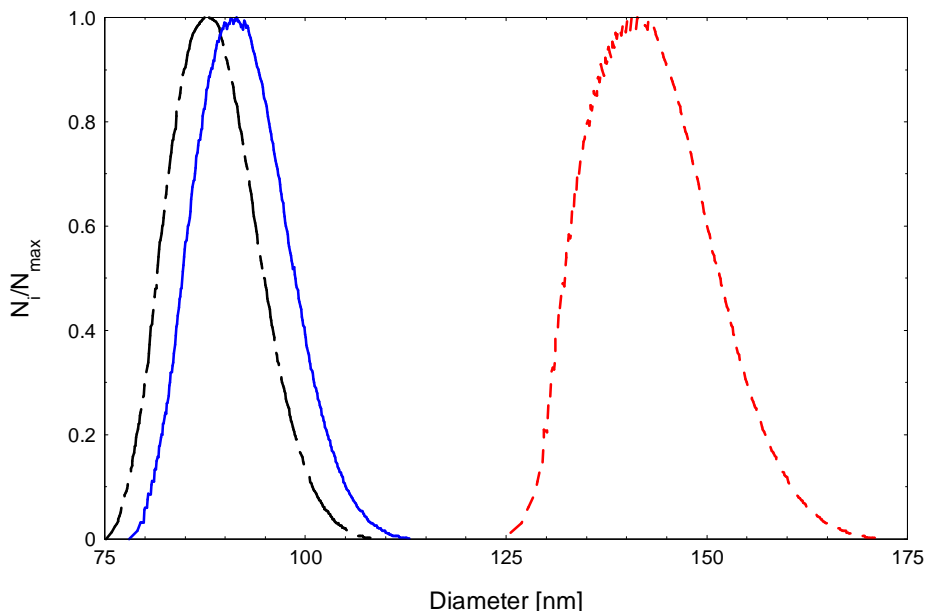


**Figure 9** Size distributions of latex particles in different stages of synthesis.  
 Black long dashed line: PS core latex;  
 Blue real line: PS-co-HMEM latex;  
 Red short dashed line: SPB latex.

## 2.2 Cleavage of Polyelectrolyte Brushes Grafted on PS Cores

150 ml latices which contain about 1.5 g polyelectrolyte brushes were hydrolyzed with 2 mol/l NaOH solution in a 250 ml Teflon flask at 120 °C for 10 days. During the hydrolysis the latices became unstable and coagulated slowly. After hydrolysis, the coagulum was separated from suspension by centrifugation with 20000 rpm/min for 3 hours. The polyelectrolytes remained in supernatant liquid were purified by means of ultrafiltration with regenerated cellulose membrane (Millipore, molecular exclusion size: 5000 Dalton) after neutralization. Deionized water (Millipore,  $\kappa \leq 0.05$   $\mu\text{S}/\text{cm}$ ) was used as replaced serum.

The amount of purified polyelectrolytes was determined by gravimetry after drying. Measurements of the intrinsic viscosity  $[\eta]$  in 0.5 mol/l NaCl at 25 °C by using of Ubblohde capillary viscometer allowed to determine the viscosity average molecular weight of the polyelectrolytes with help of the Mark-Houwink relation:

$$[\eta] = KM_h^\alpha \quad (1)$$

where  $M_h$  is the viscosity-average molecular weight,  $K$  and  $\alpha$  are Mark-Houwink constants depend upon the type of polymer, solvent, and the temperature of the



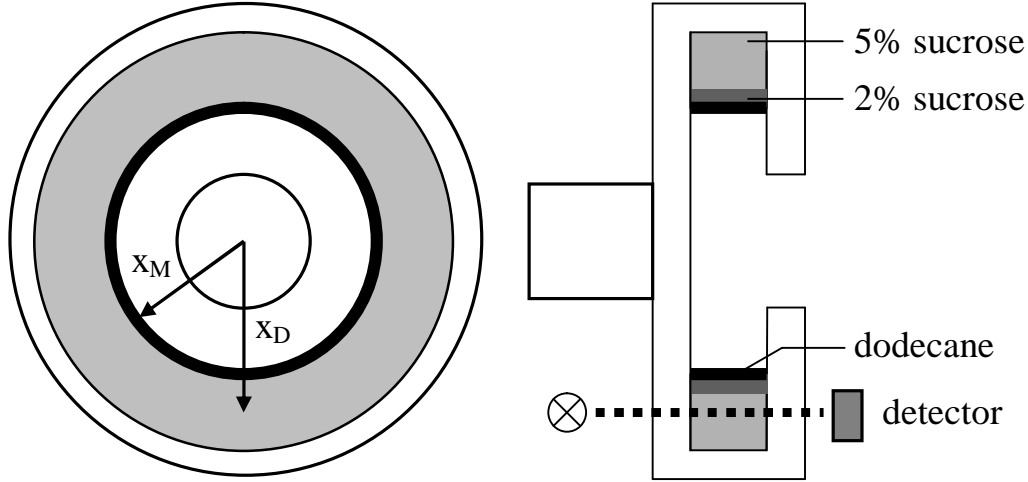


**Figure 11** Schematic diagram of disc  
Centrifuge in frontal view (left) and side view (right).

The sedimentation behavior of particles depends on the particle density and the density and viscosity of the liquid through which the particles sedimentate. The time ( $t$ ) for a spherical particle of diameter ( $d$ ) to travel from the initial radius ( $x_M$ ) at the surface of the spin fluid to the radius at the detector ( $x_D$ ) is given by:

$$t = \frac{18h \cdot \ln(x_D / x_M)}{d^2 \cdot \Delta\rho \cdot \omega^2} \quad (2)$$

$t$ : sedimentation's time

$\eta$ : viscosity of spin-liquid

$x_D$ : radial coordinate of detector

$x_M$ : radial coordinate of start point

$d$ : particle's diameter

$\Delta\rho$ : difference of density between particles and spin-liquid

$\omega$ : angular velocity

Hence, each particle size is related to a sedimentation time, which is proportional to the reciprocal of particle size. Particle population depending on sedimentation time is determined by turbidity of a certain position  $x_D$  of the spin disc: [5]:

$$t(s) \sim \left( \frac{\partial r}{\partial s} \right) \cdot s^3 \cdot \bar{Q}_{sca}(s, m) \quad (3)$$

$t(s)$ : turbidity

$\left( \frac{\partial r}{\partial s} \right) \cdot s^3$ : differential volume distribution

$\bar{Q}_{sca}(S, m)$ : normalized, integrated efficient factor (Ratio between scattering cross section and geometric cross section)

The normalized, integrated efficient factor results from the integration of efficient factor in complete wavelength range [6]. The value of  $\bar{Q}_{sca}(S, m)$  is included in the calibration curve in the analysis software of DCP. Particle size distribution and various mean values of particle size can thus be calculated.

### 3.2 Transmission Electron Microscopy (TEM)

Transmission electron microscopy (TEM) operates on the same basic principles as light microscopy but uses electrons instead of light as “light source”. The much lower wavelength of the electron makes it possible to get a thousand times better resolution than with an optic microscope. By TEM small details in the cell or different materials down to near atomic levels can be studied. The possibility for high magnifications has made TEM a valuable tool in both medical, biological and materials research.

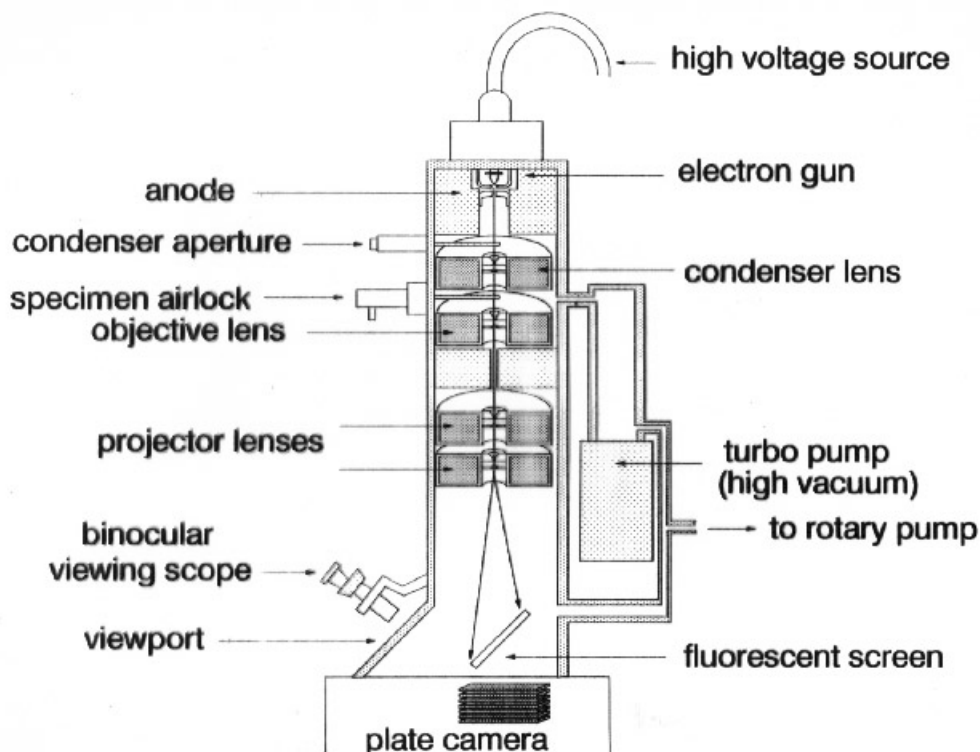


*Figure 12 Schematic construction of Transmission Electron Microscope.*

The instrument is equipped with a medium acceleration voltage of 200 kV, a high brightness electron source, digital image recording, a computer-controlled sample

goniometer, and a geometrically optimized X-ray detector. A “light source” at the top of the microscopy emits the electrons that get through vacuum in the column of the microscopy. Instead of glass lenses focusing the light in the light microscopy, the TEM uses electromagnetic lenses to focus the electrons into a very thin beam. The electron beam then gets through the specimen to be studied. Depending on the density of the material present, some of the electrons are scattered and disappear from the beam. At the bottom of the microscopy the unscattered electrons hit a fluorescent screen, which gives rise to a “shadow image” of the specimen with its different parts displayed in varied darkness according to their density. The image can be studied directly by the operator or photographed with a camera.

In this study Hitachi H-700 TEM was performed to observe the morphology of latex particles with 36000 times magnification. For the sample preparation 1% phosphotungstic acid ( $\text{H}_3[\text{P}(\text{W}_3\text{O}_{10})_4 \cdot x\text{H}_2\text{O}]$ ) solution was used to increase the contrast. TEM images of PS-co-HMEM were counted by a mechanical particle size counter (Carl Zeiss TGZ 3) to determine the particle size distribution.

### **3.3 Field Emission Scanning Electron Microscopy (FESEM)**

Field Emission Scanning Electron Microscopy (FESEM, see Figure 13) is a powerful tool for topographic analysis. It produces clearer, less electrostatically distorted images with generous depth of field and ultra high spatial resolution down to a few nanometers. With special detectors not only topographic information but also compositional information can be obtained. FESEM allows the observation of the surface fibril aggregates.

FESEM consists of two ultra high vacuum-chambers (UHV) containing several surface analysis and sample modification systems. The sample is located in the center of the analysis chamber (about  $10^{-10}$  mbar) in a manipulator. The combination of step motors (step width: 64 nm) and piezo translators serves for an accurate sample movement and positioning. As anodes we use differently shaped tungsten needles (flat anodes with up to 3 mm in diameter and electrolytically etched microanodes with about 20 nm radius of curvature). By means of a fast regulation the applied high voltage (0-35 kV) is reduced so that the field emission current does not exceed a fixed value. This guarantees emitter detection without destroying them by high currents. In another scan mode, using the piezo system the current is kept constant by controlling the distance between the sample and the anode at a constant voltage.

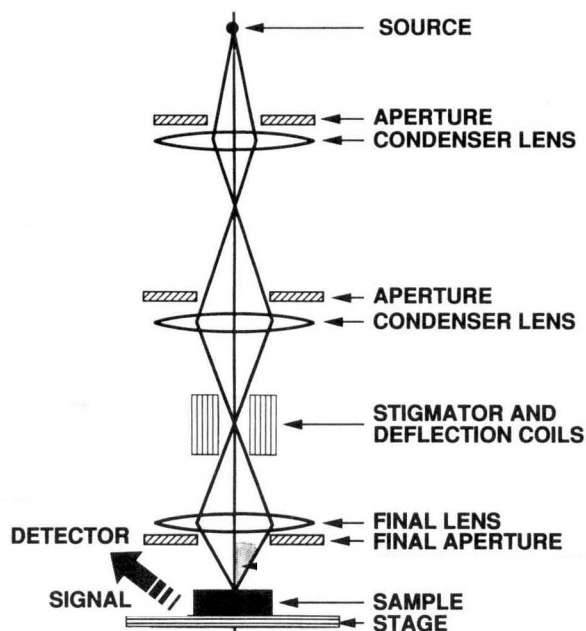


**Figure 13** Schematic construction of Field Emission Scanning Electron Microscope.

The resolution in FESEM is normally smaller than that in transmission electron microscopies, but the depth of focus is several orders of magnitude greater.

All the SEM images in this work were taken by Leo1530 FESEM. The samples on a freshly cleaved mica substrate (white mica, Plano GmbH) were dried in air and coated by a very thin layer (circa 1nm) of platinum before measurements.

### 3.4 Atomic Force Microscopy (AFM / SFM)

The atomic force microscopy (AFM), or scanning force microscopy (SFM) was invented in 1986 by Binnig, Quate and Gerber. Like all other scanning probe microscopies, AFM utilizes a physical probe raster scanning across the sample using piezoelectric ceramics. A feedback loop is used to maintain a constant interaction between the probe and the sample [7, 8]. The position of the probe and the feedback signal are electronically recorded to produce a three dimensional map of the surface or other information depending on the specialty probe used.

Compared with SEM and TEM, AFM can image samples both in air and under liquids, provides extraordinary topographic contrast direct height measurements and unobscured views of surface features. No coating is necessary. Samples will be not defiled or destroyed by coating.

Many AFM modes have appeared for special purposes while the AFM technique is becoming mature. Here the three commonly used techniques were discussed:

### 3.4.1 Contact Mode

In contact mode, the force on the cantilever (and thus the deflection) is kept constant. The distance between tip and sample surface is sufficiently small that the hard-ball repulsion effect is dominant. The force and the deflection of the cantilever are calculated by Hook's law:

$$F = -kd \tag{4}$$

where  $F$  is the force,  $k$  is the spring constant, and  $d$  is the deflection of the cantilever. In most AFM cantilevers,  $k$  is about 0.1 N/m. As the tip rasters across the sample, surface features cause a deflection in the cantilever, which is detected by a split photodiode detector and fed back to the piezo controller; which adjusts the z-position of the sample (or cantilever) to restore the setpoint force and deflection.

Contact mode is capable of generating quite accurate topographies, but is strongly influenced by tip geometry effects as well as potential damaging to the sample or tip.

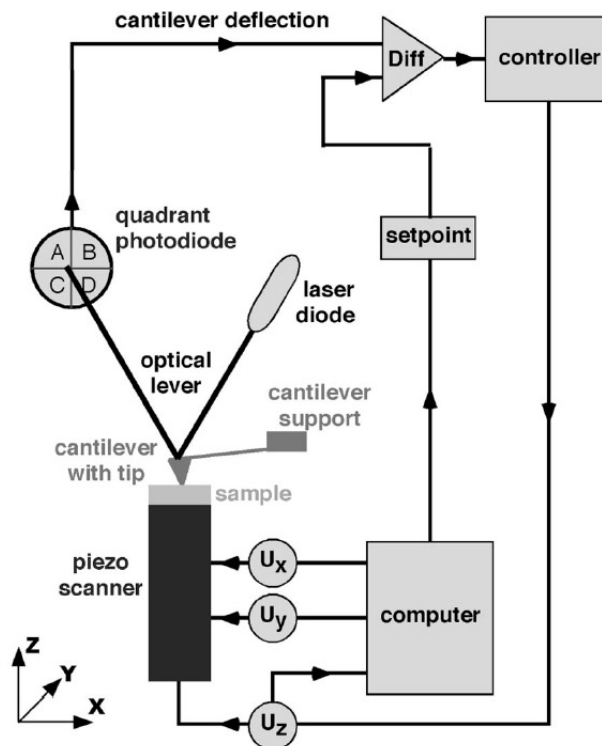


**Figure 14** Schematic diagram of an Atomic Force Microscope [9].

### 3.4.2 Non-Contact Mode

In non-contact mode, the AFM derives topographic images from measurements of attractive forces, the tip never truly comes into contact with the surface [10], as the distance between the tip and surface (1-10 nm) is such that the attractive Van der Waals force is dominant. The cantilever is oscillated at the resonant frequency, defined as:

$$f = \frac{1}{2\pi} \sqrt{\frac{k}{m}} \quad (5)$$

*f*: resonant frequency

*k*: spring constant

*m*: mass

The amplitude and phase of the resonance are measured by the detector, and the amplitude shift that occurs when the tip is in the Van der Waals regime is used to determine the set point. The amplitude set point is then used as the reference for the feedback loop that is used to control the sample positioning with respect to the tip. As the tip does not come into contact with the sample in this mode, damage to the tip and specimen can be avoided. However, because of the lack of contact, the resolution is generally poorer than the contact mode.

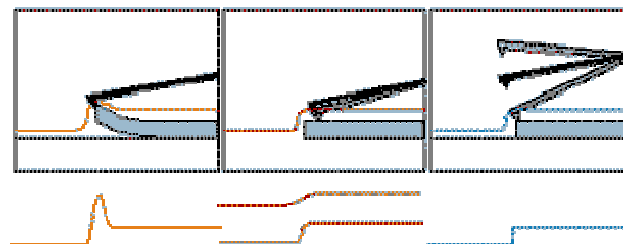


**Figure 15** Three commonly used scanning modes of AFM:  
Contact Mode (left), Non-contact Mode (middle) and Tapping Mode (right).

### 3.4.3 Tapping Mode

Tapping mode is a key advance in AFM. This potent technique allows high resolution topographic imaging of sample surfaces which are easily damaged, loosely hold to their substrate, or difficult to image by other AFM techniques. Since several years, tapping mode became the most popular scanning mode of AFM.

The process consists of allowing the cantilever to reach a resonant frequency (50,000-500,000 Hz), and bringing it close to the sample until contact is made with the sample. As the cantilever bounces up and down, it is resistant to the adhesion and adsorbed meniscus sticking problems that can adversely affect contact mode measurements. Furthermore, as the tapping probe tip comes into contact with the substrate, the high resolution of contact AFM can be achieved while drastically reducing tip or sample damage. The energy loss resulting from tip-sample contact naturally generates an amplitude loss, which is measured and used to identify surface features. The difference in amplitude also varies with different phases in the samples (due to different properties), and the amplitude shift can be used to map phases by amplitude contrast.

AFM can also image the softness of a sample by pressing the cantilever into it at each point in a scan. The piezo-scanner raises the sample or lowers the cantilever to a preset amount, the modulation “amplitude” (usually 1-10 nm). In response, the cantilever deflects an amount dependent on the softness of the sample: the harder the sample, the more the cantilever deflects, as shown in figure 16.

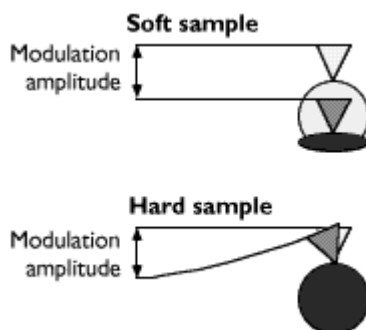


**Figure 16** AFM can image sample elasticity by pressing the tip into the sample and measuring the resulting cantilever deflection.

All the AFM measurements in this work were performed using the NanoScope IIIa (Digital Instruments Inc.). The images were scanned in tapping mode in air using commercial Si cantilevers (Digital Instruments Inc.) with a resonance frequency of 320 kHz or 170 kHz. The images show unfiltered original data. All AFM data in this work show typical structures which are representative for the corresponding sample. For sample preparation, a droplet of 20-40  $\mu\text{l}$  samples was put onto a freshly cleaved mica surface (muscovite white mica, Plano GmbH) and dried in air.

### 3.5 Dynamic Light Scattering (DLS)

#### 3.5.1 Theoretical Fundamentals

DLS is based on the scattering of light by diffusing particles. At any instant the suspended particles will have a particular set of positions within the scattering volume. The particles scatter the radiation (laser light) to the detector, but the relative phase of scattered wavelets differ, due to the differing incident phases which they experience and due to different particle-detector distances. The intensity at the detector is the superposition of all the scattered wavelets and will have a value  $I(t)$  at time  $t$ . At the time  $t+\tau$ , which is a very small time later than  $t$ , the diffusing particles will have new positions and the intensity at the detector will have a value  $I(t+\tau)$ . As time progresses, the intensity at the detector will fluctuate as the Brownian processes in the sample volume continue. Small rapidly diffusing particles will yield fast fluctuations, while larger particles and aggregates generate relatively slow fluctuations.

The rate of the fluctuations can be determined through the technique of autocorrelation analysis [11], the normalized time autocorrelation function of the intensity of the scattered light  $g^{(2)}(\tau)$  for a given delay time  $\tau$  is given by [12]:

$$g^{(2)}(\tau) = \frac{\langle I(t)I(t+\tau) \rangle}{\langle I(t) \rangle^2} \quad (6)$$

where the braces indicate averaging over  $t$ .

In most cases of practical interest of the intensity-intensity time autocorrelation function may also be expressed in terms of the field-field time autocorrelation function  $g^{(1)}(\tau)$  as:

$$g^{(2)}(\tau) = B + b[g^{(1)}]^2 \quad (7)$$

with  $g^{(1)}(\tau)$  given by

$$g^{(1)}(\tau) = \frac{\langle E(t)E^*(t+\tau) \rangle}{\langle E(t)E^*(t) \rangle} \quad (8)$$

where  $E(t)$  and  $E(t+\tau)$  are the scattered electric fields at times  $t$  and  $t+\tau$ , respectively, and  $\beta$  is a factor that depends on the experimental geometry. Equation (7) is known as the Siegert relation [13]. The factor  $B$ , commonly referred to as the baseline, is the long-time value of  $g^{(2)}(\tau)$ .

For monodisperse particles in solution the field-correlation function decays exponentially,  $g^{(1)}(\tau) = \exp(-\Gamma\tau)$ , with a decay rate (the inverse of the correlation time) of  $\Gamma = Dq^2$ , where  $D$  is the diffusion coefficient of the particles and  $q$  is the magnitude of the scattering wave vector. The scattering wave vector  $q$  is defined as the difference between the incident and the scattered wave vectors, and its magnitude  $q$  is given by

$$q = \frac{4\pi n}{\lambda_0} \sin\left(\frac{\theta}{2}\right) \quad (9)$$

$\lambda_0$ : the wavelength of the laser in vacuo;  
 $n$ : refractive index of the solvent;  
 $\theta$ : scattering angle.

The exponent in the above equation yields the mutual diffusion coefficient,  $D_m$ , from which particle sizes can be obtained via the Stokes-Einstein equation:

$$D_m = \frac{k_B T}{6\pi\eta R_{eff}} \quad (10)$$

$D_m$ : mutual diffusion coefficient  
 $k_B$ : Boltzmann constant  
 $T$ : absolute temperature  
 $\eta$ : dynamic viscosity  
 $R_{eff}$ : effective (hydrodynamic) radius

For a polydisperse sample,  $g^{(1)}(\tau)$  can no longer be a single exponential and must be represented as an integral over a distribution of decay rates  $G(\Gamma)$  by:

$$g^{(1)}(t) = \int_0^{\infty} G(\Gamma) \exp(-\Gamma t) d\Gamma \quad (11)$$

### 3.5.2 Method of Cumulants

Finding the precise functional form for the distribution of decay rates  $G(\Gamma)$  is problematic because the correlation function is measured discretely only over an incomplete range of  $\tau$  and there is always noise associated with the data. There are several ways of using DLS data to characterize  $G(\Gamma)$  [13], but one of the simplest is the method of cumulants first proposed by Koppel [14], which is based on two

relations: one between  $g^{(1)}(\tau)$  and the moment-generating function of the distribution, and another one between the logarithm of  $g^{(1)}(\tau)$  and the cumulant-generating function of the distribution. It is appropriate only for use in cases in which  $G(\Gamma)$  is monomodal.

In fact, as was discussed by Koppel [14], the form of  $g^{(1)}(\tau)$  as given in Equation (11) is equivalent to the definition of the moment-generating function  $M(-\tau, \Gamma)$  of the distribution  $G(\Gamma)$ :

$$M(-t, \Gamma) = \int_0^{\infty} G(\Gamma) \exp(-\Gamma t) d\Gamma \equiv g^{(1)}(t) \quad (12)$$

The  $m$ th moment of the distribution  $m_m(\Gamma)$  is given by the  $m$ th derivative of  $M(-\tau, \Gamma)$  with respect to  $\tau$ :

$$\begin{aligned} m_m(\Gamma) &= \left. \frac{d^m M(-t, \Gamma)}{d(-t)^m} \right|_{-t=0} \\ &= \int_0^{\infty} G(\Gamma) \Gamma^m \exp(-\Gamma t) d\Gamma \Big|_{-t=0} \end{aligned} \quad (13)$$

Similarly, the logarithm of the field-correlation function is equivalent to the definition of the cumulant generating function  $K(-\tau, \Gamma)$  [15]

$$K(-t, \Gamma) = \ln[M(-t, \Gamma)] \equiv \ln[g^{(1)}(t)] \quad (14)$$

where the  $m$ th cumulant of the distribution  $\kappa_m(\Gamma)$  is given by the  $m$ th derivative of  $K(-\tau, \Gamma)$ :

$$k_m(\Gamma) = \left. \frac{d^m K(-t, \Gamma)}{d(-t)^m} \right|_{-t=0} \quad (15)$$

The first cumulant describes the average decay rate of the distribution. The second and the third cumulants correspond directly to the appropriate moments about the mean: The second moment corresponds to the variance, and the third moment provides a measure of the skewness or asymmetry of the distribution. The first two cumulants must be positive, but the third cumulant can be positive or negative.

The basis of the cumulant expansion that is usually used in the analysis of DLS

data lies in expanding the logarithm of  $g^{(1)}$  in terms of the cumulants of the distribution. This relation follows from the fact that the  $m$ th cumulant is the coefficient of  $(-\tau)^m/m!$  in the Taylor expansion of  $K(-\tau, \Gamma)$  about  $\tau=0$ , as given by

$$\ln[g^{(1)}(t)] \equiv K(-t, \Gamma) = -\Gamma t + \frac{k_2}{2!} \cdot t^2 - \frac{k_3}{3!} \cdot t^3 + \frac{k_4}{4!} \cdot t^4 \dots \quad (16)$$

To take advantage of this form and use linear least squares methods to fit this function to the data requires that a key assumption be made about the data, the baseline must be assumed to be exactly one. Then a fit can be made to:

$$\ln[g^{(2)}(t) - 1] = \ln \frac{b}{2} - \Gamma t + \frac{k_2 t^2}{2!} - \frac{k_3 t^3}{3!} + \dots \quad (17)$$

Equation (17) is the traditional fitting function that is described in many DLS texts [16, 17].

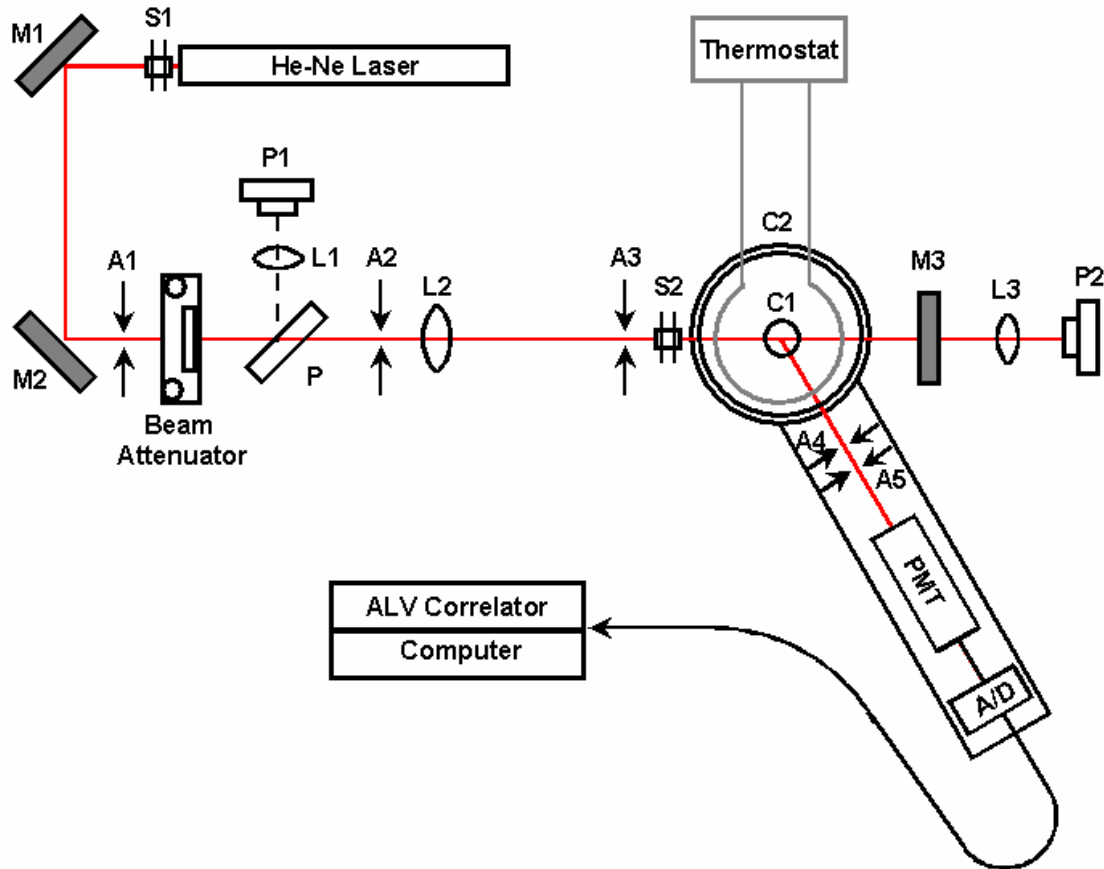


**Figure 17** Schematic constructions of dynamic light scattering apparatus:  
S1-S2: Beam shutter;

*M1-M3: Mirrors;*

*A1-A5: Apertures;*

*P: Beam splitter plate;*

*P1-P2: Reflection quadrant photodiodes;*

*L1-L3: Bispherical lense;*

*C1: Probe holder;*

*C2: Thermostated measurement cell;*

*PMT: Photomultiplier tube;*

*A/D: Analog-digital converter.*

Dynamic light scattering was performed by a Peters ALV 4000 light scattering goniometer, which contains a 50 mV He-Ne-Laser ( $\lambda=632.8$  nm), focus system, optic system, detection system, and a signal processing system which consists of a correlator and a computer. With a moveable goniometer arm, the measurement could be between  $14^\circ$  and  $152^\circ$  realizable. According to the supplier's instruction, the ALV 4000 can measure particles between 1 nm to 1  $\mu\text{m}$  or diffusion coefficient between  $1.0 \times 10^{-6}$  to  $2.5 \times 10^{-9}$   $\text{cm}^2/\text{s}$ .

A thermostat (JULABO F30-C,  $\pm 0.01$   $^\circ\text{C}$ ) was used to control the temperature. Before each measurement the sample was tempered by a thermostat for at least 10 minutes. The measurements were taken at a certain scattering angle of  $90^\circ$ , since there's no influence at different angles when the sample is monodispersed. At first, to be measured sample was diluted into about  $10^{-2}$  g/l with water based dispersion medium, such as deionized water, salt solution or buffer solution etc. With a 0.45 or 1.00  $\mu\text{m}$  Polyester-Membrane filter (membraPure MEMBREX 25 PET), the prepared sample was filtered directly into a quartz glass cuvette, which was pre-washed with THF and deionized water. All of the samples preparation was performed in a clean room workbench (Köttermann, Flowbox 8580).

### **3.6 Dynamic Drainage Jar (DDJ)**

The dynamic drainage jar is a common and reliable tool to evaluate retention and drainage of single or multi-component retention systems under conditions which are quite similar to large-scale papermaking processes. Importantly, the DDJ can simulate the impact of shear as induced e.g. by screens in paper machines [18]. In the present work a DDJ with a 200-mesh bottom screen; and an impeller speed of 400 or 900 rpm was used.

The retention efficiency of each flocculation system is quantified using the so-called first pass retention (FPR) and the corresponding ash retention (AR) defined as follows [19, 20]:

$$FPR = \frac{C_i - C_0}{C_i} \times 100\% \quad (18)$$

$$AR = \frac{A_i - A_0}{A_i} \times 100\% \quad (19)$$

where  $C_i$  and  $C_0$  are the concentration of colloidal particles in the stock before drainage and in the filtrate, respectively.  $C_i$  and  $C_0$  are obtained by filtering the respective suspension using a filter paper and weighing the fully dried filtrate.  $A_i$  and  $A_0$  are the total inorganic (“ash”) content of the stock before drainage and in the filtrate respectively. The latter is determined by incineration the filtrated material at 500 °C for 5 hours.

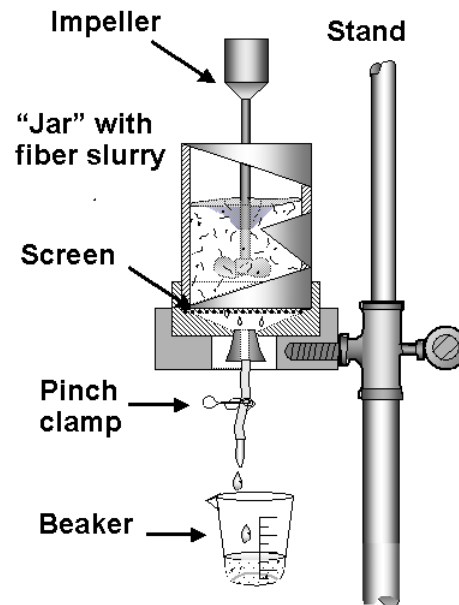


**Figure 18** Schematic diagram of dynamic drainage jar.

In a typical flocculation sequence 0.04% cationic PAM (wt% with respect to solid pulp) was added into the 0.8 wt% paper suspension in order to induce agglomeration of fibers and fillers. Subsequently, shear of 900 rpm was applied for 20 s, inducing partial break-down of the primary flocs. Then, bentonite or SPB was added with a relative amount between 0 and 0.40 wt% (with respect to the solid contents in the primary pulp suspension). During the addition of the SPB (or bentonite) the mixture

was stirred at 400 rpm for 15 s, at which again formation of flocs in the pulp suspension occurred. Stirring continued during the drainage.

### 3.7 Other Instruments and Methods

Nuclear magnetic resonance (NMR) spectra were recorded at room temperature in acetone- $d_6$  using a Bruker AC 400 spectrometer with 400MHz ( $^1\text{H}$ -NMR) and 100MHz ( $^{13}\text{C}$ -NMR). Tetramethylsilane (TMS) served as an internal standard.

PH-value and conductivity were determined using the microprocessor pH meter (WTW, pH 537) and the microprocessor conductivity meter (WTW, LF 537), respectively.

The viscosity-average molecular weight of the attached polymer chains was determined by Ubbelohde capillary viscometer (Schott, Ubbelohde KPG,  $K=0.009534$ ).

## 4 Survey of the Experimental Data

The physical parameters such as grafting density ( $\sigma$ ), distance between two neighboring polymer chains ( $D$ ), cation exchange capacity, viscosity-average molecular weight ( $M_\eta$ ), Kuhn length ( $l_K$ ), contour length ( $L_c$ ) of grafted polyelectrolyte brushes can be determined.

To determine the molecular weight of the grafted polymer chains, they should be cut from surface of PS core. The photoinitiator HMEM used in this study contains an ester bond which connects the initiating group and the PS core. Since the ester bond can be cleaved in a strong alkaline solution, polyelectrolyte chains can be cleaved from the surface of latex particles and analyzed separately. In the case of PATAC polymer brush, it contains an ester bond in each repeat unit, which can also be cleaved in the strong alkaline solution. The sodium salt of PAA is thus obtained after hydrolysis.

All pertinent parameters, namely, the core radius ( $R$ ), the distance of two neighbouring chains ( $D$ ) and contour length ( $L_c$ ) of the attached chains as well as the grafting density ( $\sigma$ ) are known from the analysis or calculation. Table 2 summarizes the characteristic data of the SPB used in this study.

**Table 1** Characterization of SPB lattices

Sample	Charge	Brush	R [nm]	L <sub>c</sub> [nm]	M <sub>η</sub> [g/mol]	σ [nm <sup>-2</sup> ]	D [nm]	L <sub>c</sub> /R
LA1	positive	PATAC	45	84	64900	0.050	5.1	1.87
LA2	positive	PATAC	45	116	89700	0.049	5.1	2.57
LA3	positive	PATAC	49	149	115000	0.052	5.0	3.04
LQ3	negative	PNaSS	68	108	88000	0.039	5.7	1.59
LQ6	negative	PNaSS	68	165	135000	0.027	6.8	2.43
LQ7	negative	PNaSS	54	141	115000	0.031	6.4	2.61
LB1	negative	PNaSS	58	103	84300	0.065	4.4	1.78
LB2	negative	PNaSS	25	141	115800	0.040	5.6	5.64

*R*: core radius;

*M<sub>η</sub>*: molecular weight of grafted chains as determined by viscosimetry;

*L<sub>c</sub>*: contour length of grafted chains determined from *M<sub>η</sub>*;

*σ*: graft density on surface of core particles;

*D*: the average distance between two neighbouring graft points.

The data of the systems LQ3, LQ6 and LQ7 have been taken from reference [Guo et al. 2001].

## 5 References

1. Guo, X.; Weiss, A.; Ballauff, M., *Macromolecules*, **1999**, 32, 6043.
2. Salamone, J.C. ed., *Polymer Materials Encyclopedia*, vol. 7, CRC Press, **1996**.
3. Fouassier, J.P., *Photoinitiation, Photopolymerization, and Photocuring, Fundamentals and Applications*, Hanser Publishers, Munich, **1995**.
4. Brandrup, J.; Immergut, E. H., Eds., *Polymer Handbook*, 3<sup>rd</sup> ed., **1989**, Wiley, New York.
5. Devon, M.; Meyer, E.; Provder, T.; Rudin, A.; Weiner, B., *ACS Symp. Ser.*, **1991**, 472, 155.
6. Oppenheimer, L.E., *J. Colloid Interface Sci.*, **1983**, 92, 350.
7. Binnig, G.; Quate, C.F.; Gerber, C., *Phys. Rev. Lett.*, **1986**, 56(9), 930-933.
8. Pang, G. K. H.; Baba-Kishi, K. Z.; Patel, A., *Ultramicroscopy*, **2000**, 81, 35.
9. Schitter, G.; Menold, P.; Knapp, H. F.; Allgöwer, F.; Stemmer, A., *Rev. Sci. Instrum.*, **2001**, 72(8), 3321.
10. Albrecht, T.R.; Grütter, P.; Horne, D.; Rugar, D., *J. Appl. Phys.*, **1991**, 69(2), 668-673.

11. Abbiss, J.b.; Smart, A.E., *Photon correlation Techniques and Applications*, **1988**, OSA Proceedings.
12. Berne, B.J.; Pecora, R., *Dynamic Light Scattering with Applications to Chemistry, Biology, and Physics*, **2000**, Dover.
13. Brown, W., *Dynamic Light Scattering*, **1993**, Oxford University, Oxford, UK, 76-240.
14. Koppel, D.E., *J. Chem. Phys.*, **1972**, 57, 4814-4820.
15. Stuart, A.; Ord, J. K., *Kendall's Advanced Theory of Statistics*, **1994**, Chap. 4, Wiley, New York.
16. Pecora, R., *Dynamic Light Scattering*, **1985**, Plenum, New York.
17. Chu, B., *Laser Light Scattering: Basic Principles and Practice*, **1991**, Academic, Boston.
18. Mark, R. E.; Habeger, C. C.; Borch, J.; Lyne, M. B., *Handbook of Physical Testing of Paper, Vol. 1, 2nd Ed.*, **2001**, New York.
19. Physical and Chemical Standards Committee, *Ash of paper and paperboard, Technical Section*, **1986**, Canadian Pulp & Paper Association, Montreal.
20. Reid, I.; Ricard, M., *Enzyme and Microbial Technology*, **2000**, 26, 117.

## Glossary

AA	acrylic acid
AC	acryloyl chloride
AFM	atomic force microscopy
AR	ash retention
ATAC	(2-(acryloyloxy)ethyl)trimethylammonium chloride
$B(q)$	the scattering amplitude
$c_a$	ionic strength of the system
$c_s$	local ionic strength inside the brush
CEC	cation exchange capacity
CPAM	cationically modified polyacrylamide
CTAB	cetyltrimethylammonium bromide
D	average distance between two neighboring grafted points
$D_m$	mutual diffusion coefficient
DLS	dynamic light scattering
$e$	elementary charge
$E(t)$	scattered electric fields at time $t$
FPR	first pass retention
$g^{(1)}(\tau)$	temporal time correlation function
$g^{(2)}(\tau)$	normalized time correlation function
$G(\Gamma)$	distribution function of $\Gamma$
GCC	ground calcium carbonate
HMEM	methacrylicacid-[-4-(2-hydroxy-2-methyl-propionyl)-phenoxy]-ethylester
I	ionic strength
$I(q)$	scattering intensity
IR	infrared
Irgacure 2595	1-[4-(2-hydroxyethoxy)-phenyl]-2-hydroxy-2-methyl-1-propanone
$k$	Boltzmann constant or a constant
$k_i$	constants ( $i=0,1,2,\dots$ )
KP 2515	cationically modified polyacrylamide of BASF AG
KPS	potassium persulfate
L	thickness of brush
$l_B$	Bjerrum length
$l_c$	distance between two charged points along the polymer chain

$L_c$	contour length of a grafted polymer chain
$l_k$	Kuhn length
$l_{k,0}$	intrinsic Kuhn length
$l_{k,e}$	electrostatic Kuhn length
$l_p$	persistence length
$l_{p,0}$	intrinsic persistence length
$l_{p,e}$	electrostatic persistence length
$m$	scaling exponent
$M_\eta$	viscosity average molecular weight
MC	methacryloyl chloride
N	the number of monomer segments in a polymer chain
$N_A$	the Avogadro's number
NaSS	4-vinylbenzenesulfonic acid sodium salt
$n_i$	molar concentration of the species $i$
NMR	nuclear magnetic resonance
NB	neutral brush regime
OB	osmotic brush regime
PATAC	poly(2-(acryloyloxy)ethyltrimethylammonium chloride)
PDADMAC	poly(diallyldimethylammonium chloride)
PEI	poly(ethylenimine)
PEO	poly(ethylene oxide)
PNaSS	poly (sodium styrenesulfonate)
PPB	planar polyelectrolyte brush
PS	poly(styrene)
$q$	scattering vector
$\langle R^2 \rangle$	mean square end-to-end distance of polymer coil
$R_g$	radius of gyration
$R_h$	hydrodynamic radius
S	singlet state
SAMs	self-assembled monolayers
$S(q)$	the structure factor
SB	salted brush regime
SDS	sodium dodecylsulfate
SPB	spherical polyelectrolyte brush
FESEM	field emission scanning electron microscopy
T	triplet state or temperature
TEM	transmission electron microscopy
UV	Ultraviolet

## Appendix: Glossary

---

V50	2,2'-azobis(2-amidinopropane)dihydrochloride
V	Volume
v	excluded volume parameter
VBTMAC	(ar-Vinylbenzyl)-trimethylammonium chloride
$z_i$	valency of the species i

## Greek

$G$	the relaxation rate
$\epsilon_0, \epsilon$	dielectric constant of the solvent and the solution respectively
$h$	viscosity
$[h]$	intrinsic viscosity
$j$	mean electrostatic potential
$k^{-1}$	Debye length
$l$	wavelength
$q$	scattering angle
$\bar{r}_f$	volume-averaged fixed charge density in the brush
$s$	average grafting density of brush
$t$	correlation time
$x$	size of blobs in blob model

## Publications

*“High Catalytic Activity of Platinum Nanoparticles Immobilized on Spherical Polyelectrolyte Brushes”*

Yu Mei, Geeta Sharma, Yan Lu, Matthias Ballauff, Markus Drechsler, Thorsten Irrgang, Rhett Kempe, *Langmuir*, (2005), accepted.

*“Thermosensitive Core-Shell Particles as Carriers for Ag nanoparticles: Modulating the Catalytic Activity by the Volume Transition in Networks”*

Yan Lu, Yu Mei, Markus Drechsler, Matthias Ballauff, *Angewandte Chemie*, (2005), accepted.

*“Interaction of spherical polyelectrolyte brushes with CaCO<sub>3</sub> and cellulose fibers. Mechanistic studies and their application in papermaking”*

Y. Mei, C. Abetz, O. Birkert, V. Schädler, R. J. Leyrer, M. Ballauff, *Journal of applied polymer science*, (2005), accepted.

*“Effect of counterions on the swelling of spherical polyelectrolyte brushes”*

Y. Mei, M. Ballauff, *Eur. Phys. J. E*, 16, 341-349 (2005).

*“Engineering the Interaction of Latex Spheres with Charged Surfaces: AFM Investigation of Spherical Polyelectrolyte Brushes on Mica”*

Y. Mei, A. Wittemann, G. Sharma, M. Ballauff, Th. Koch, H. Gliemann, J. Horbach, Th. Schimmel, *Macromolecules*, 36, 3452-3456, (2003).

*“The Ratio of Error Propagation and its Application in Multivariate Calibration Titration”*

Y. Mei, Z. Zhu, T. Li, *Jisuanji yu Yingyong Huaxue (Computers and Applied Chemistry)*, (1-2), 117-118, (2000), (in Chinese).

*“Application of factor analysis in struction of analytical chemistry”*

Z. Zhu, Y. Mei, J. Zhang, T. Li, *Daxue Huaxue, (University Chemistry)*, 15(6), 17-19, (2000), (in Chinese).

*“Optimizing Residual Standard Deviation-Rank Annihilation (ORS-D-RA) in analysis of electrolytic kinetic process of phenol”*

J. Zhang, Y. Mei, Z. Zhu, *Huaxue Shijie (Chemical World)*, 41(10), 146, (2000), (in Chinese).

*“Application of Rate Constant-Rank Analysis in the Process Analysis of Chemical Reaction”*

Z. Zhu, L. Yu, W. Song, Y. Mei, T. Li, *Gaodeng Xuexiao Huaxue Tongbao (Chemical Journal of Chinese Universities)*, 22, (5), 734-738, (2001), (in Chinese).

## Curriculum Vitae

### zur Person

Name: Yu Mei

Anschrift: Richard-Wagner-Straße 73a, 95444 Bayreuth

Geschlecht: männlich

Geburtsort: Hunan Provinz, VR China

Geburtsdatum: 28. Sep. 1976

### Schulbildung

Sep.1982-Juli 1987      1. Grundschule der Stadt Linxiang

Sep.1987-Juli 1990      1. Mittelschule der Stadt Linxiang

Sep.1990-Juli 1993      1. Mittelschule der Stadt Changsha

### Studium

Sep.1993-Juli 1998      Fakultät für Chemie, Universität Tongji, Shanghai

Abschluss: „*Bachelor of Science*“

Thema: „*Synthesis and characterization of MCM-41*“

Sep.1998-März 2001      Fakultät für Chemie, Universität Tongji, Shanghai

Abschluss: „*Master of Science*“

Thema: „*The application of ORSD-RA method in the process analysis of chemical reactions* “

### Promotion

Juli 2001-Dez.2003      Polymer-Institut, Universität Karlsruhe(TH)

Arbeitskreis Prof. Dr. M. Ballauff

Seit Jan. 2004

Lehrstuhl für Physikalische Chemie I, Universität Bayreuth

Arbeitskreis Prof. Dr. M. Ballauff

Thema: „*Synthesis and characterization of cationic spherical polyelectrolyte brushes*“

## Danksagung

Herrn Prof. Dr. M. Ballauff danke ich für die interessante Aufgabenstellung, sein Interesse an meiner Arbeit, viele Anregungen und seine stetige Diskussionsbereitschaft. Vielen Dank auch für die Unterstützung bei den Publikationen.

Bei allen Mitgliedern und Ehemaligen des Polymerinstituts möchte ich mich herzlich für das angenehme Arbeitsklima, die gute Zusammenarbeit sowie die Hilfsbereitschaft bei Fragen aller Art bedanken. An dieser Stelle möchte ich insbesondere Sabine Rosenfeldt, Alexander Wittemann, Arben Jusufi, Li Li, Mushtaq Patel, Geeta Sharma und Jerome Crassous erwähnen, welche zahlreiche Aufgaben zur Aufrechterhaltung eines intakten Laborbetriebs übernahmen. Björn Haupt danke ich für die enge Zusammenarbeit, die Aufnahme der TEM-Bilder, die Hilfe bei Computerproblemen.

Mein besonderer Dank gilt der BASF AG für die finanzielle Unterstützung. Herrn Dr. Dieter Distler, Dr. Reinhold J. Leyrer und Frau Dr. Lian Ma möchte ich herzlich danken für die interessante Projektstellung. Herrn Dr. Volker Schädler, Dr. Axel Weiss, Dr. Oliver Birkert, Dr. Oliver Koch, Dr. Martin Reif und Herrn Reinhard Barthel möchte ich mich herzlich bedanken für die gute Kooperation und zahlreiche Hilfe bei der Arbeit und den Messungen.

Unseren Sekretärinnen Frau Manuela Winkler und Ilona Deger sowie Christine Thunig danke ich herzlich für ihr großes Engagement, die Abwicklung der Personalbelange sowie den reibungslosen Ablauf der Dienstgeschäfte. Herrn Kühn danke ich für seinen unermüdlichen Einsatz bei der Verbesserung und der Konstruktion neuer Ultrafiltrationsapparaturen, ohne die diese Arbeit in dieser Form nicht möglich gewesen wäre.

Eine besondere Bereicherung waren die externen Kooperationen während meiner Arbeit. Insbesondere möchte ich mich bei Hartmut Gliemann und Thomas Koch aus der Arbeitsgruppe von Prof. Dr. T. Schimmel am Institut für Nanotechnologie (INT) des Forschungszentrums Karlsruhe für die Durchführung der AFM-Messungen bedanken. Dr. Hartmut Gliemann danke ich insbesondere für die ausgiebigen und interessanten Fachdiskussionen und Erklärungen. Weiterhin gilt mein Dank Frau Clarissa Abetz am Bayreuther Institut für Makromolekülforschung für die geschickten Messungen von Rasterelektronenmikroskopie, Herrn Markus Hund von der Physikalischen Chemie II für die geduldige und ausführliche Einführung in die AFM.

## Danksagung

---

Schließlich möchte ich mich ganz herzlich bei meiner Frau und meinen Eltern bedanken, die mich immer vielseitig unterstützt haben, so daß ich mich immer auf die Arbeit konzentrieren konnte.

## **Erklärung**

Hiermit erkläre ich, dass ich die Arbeit selbständig verfasst und keine anderen als die angegebenen Quellen und Hilfsmittel benutzt habe.

Ferner erkläre ich, dass ich nicht anderweitig mit oder ohne Erfolg versucht habe, eine Dissertation einzureichen oder mich einer Doktorprüfung zu unterziehen.

\_\_\_\_\_ (Yu Mei)

Bayreuth, den 06.06.2005